國立臺灣大學生物資源暨農學院生物環境系統工程學系

碩士論文

Graduate Institute of Bioenvironmental Systems Engineering

College of Bioresources and Agriculture

National Taiwan University

Master Thesis

台灣山區扁柏林地可感熱、潛熱及二氧化碳通量特性之研究

Characteristics of Heat, Water Vapor and CO_2 Fluxes Above a Mountainous Cypress Forest in Taiwan

蕭軒梅

Hsuan-Mei Hsiao

指導教授：謝正義 博士

Advisor: Cheng-I Hsieh, Ph. D.

中華民國九十八年六月

June, 2009

國立臺灣大學碩士學位論文
口試委員會審定書

台灣山區扁柏林地可感熱、潛熱

及二氧化碳通量特性之研究

Characteristics of Heat, Water Vapor and CO_2 Fluxes

Above a Mountainous Cypress Forest in Taiwan

本論文係蕭軒梅君（R96622009）在國立臺灣大學生物環境系統工程學系、所完成之碩士學位論文，於民國 98 年 6 月 19 日承下列考試委員審查通過及口試及格，特此證明

口試委員：謝正義 （簽名）

（指導教授）朱佳仁

張倉榮

陳明志

系主任、所長 黃宗誠 （簽名）

Acknowledgement

一如我每次做事一樣，總是要搞到最後一刻才大致上完成，論文也不例外。碩士班這兩年過的很快，卻也經歷了不少轉折。從發現自己原來不是對所有東西都很好奇，到直接的面對了做研究根本就不是好奇這種動力就可以支持到最後的事實。到現在我還是說不出為甚麼要讀研究所，但心裡面清楚的知道這兩年學到很多和研究相關的事，而研究之外的，卻又更多了。

謝謝朱佳仁老師、陳明志老師，及張倉榮老師百忙中抽空幫我口試，提供我研究上的寶貴意見。謝謝我的指導老師，從進到這間研究室以來，我老是在出包，好像沒有一次把事情搞對。老師在人力上的小本經營再加上昂貴又常常壞掉的儀器，有時候看著老師還真的不知道老師做研究的熱情從哪裡來的，不過我知道我們沒出狀況的時候，老師都很開心。或許這就是做研究的人需要的東西吧，我還在學習和體會。

謝謝研究室的成員，丞瑋、阿苗和詩惘，還有曾經帶給我短暫歡樂的凱名、柏儒和 Fancy。不管怎麼樣不同的價值觀和處事態度，謝謝你們包容我亂七八糟還到處侵占的物品，有你們讓這條路順利許多。也感謝東華大學夏老師的研究團隊，特別是侯森，提供測量數據和實地實驗相關資料和經驗。

謝謝我親愛的各式各樣可愛、溫馨或白目的朋友和師長們，感謝你們的關愛，趕論文這陣子其實是我身體上最不舒服，心靈上卻最滿足的時光。你們的存在給我一種力量，去找尋自己的意義，去創造不同的價值。

最後，感謝我親愛的家人，關心我身體和情緒遠大於我論文進度的爸媽，那些不斷地安慰和陪伴，說就算我延畢也會養我的舉動，還有說就算做出來的是垃圾也很有價值的哥哥，謝謝你們，沒有你們我真的走不到這裡。我想我還是不夠好，儘管跌跌撞撞的，因為有你們，我會笑著，不害怕。

謝謝你們，我愛你們！

Abstract

Second-order turbulence moments of wind velocities, temperature, water vapor, and CO_2 observed with an eddy covariance system over a mountainous cypress forest are used to investigate the transportation of momentum and scalars between the atmosphere and the ecosystem.

In this site, vertical wind velocity was found to follow the Monin-Obukhov similarity functions after separating the measurements with the uphill and downhill flow directions. We also found that temperature similarity characteristic constant consists with previous studies with a near unity value, while water vapor and CO_2 require a Bowen ratio filtering procedure to get more reasonable values.

The characteristic constants found were checked over with the flux-variance method, and fair to good results were noticed. For sensible heat flux, the general flux-variance equation works well. And For water vapor and CO_2 fluxes, the representative relative transport efficiencies are preferred, while the characteristic constants found with Bowen ratio filtering method can also provide a fair estimation.

Methods for the relation between relative transport efficiency and its correlation coefficient are also explored for water vapor and CO_2 against temperature. A blurred relation is found for water vapor due to the complicated humidity field over the site, and a -0.5 power relation is introduced for CO_2 when Bowen ratio is higher than unity.

Keywords: flux-variance relation, complex topography, relative transport efficiency

Contents

List of Figures

List of Tables

Chapter 1 Introduction

To understand atmosphere-forest interactions, evapotranspiration and CO_2 assimilation are important parameters. These two parameters are complicated in estimating, leading to numerous studies with different instruments and techniques. If water and CO_2 transfer dynamics are clearly known, the water and carbon circulation in the ecosystem can be found.

High frequency time series data for wind velocity, temperature, water vapor, and CO_2 are collected on a micro-meteorological tower over a temperate humid cypress forest in I-lan, Taiwan, from March 2005 to May 2009. The results are used to investigate the turbulent transport processes within the context of the flux-variance relation. Compared with most previous researches, this complex study site in topography, has a high frequency cloud coverage and experiences long period daily torographic fog.

The existing theory which operates smoothly over ideal and near ideal terrains could not fit well at this experimental site. Several sites which encountered likewise difficulties emphasized the influences done by these non-ideal conditions. Since this flux-variance relation is the only well developed way in understanding the turbulent transport in the surface boundary layer, filtering methods were introduced to eliminate the theoretically undesired records.

In this study, we first investigate the vertical and horizontal wind velocity behavior in assurance of site measurement quality. Then discuss the temperature flux-variance relation. Water vapor and CO_2 characteristics are analyzed with revised filtering methods from previous studies. The relative transport efficiencies between temperature, water vapor, CO_2, and its scalar correlation coefficients are also investigated. The similarity constants are found with records from March 2005 to March 2009, and verified with records from April and May 2009.

Chapter 2 Theory and literature review

Based on Monin-Obukhov similarity theory (MOST), the normalized standard deviations of wind velocities and scalars can be presented as a function of the thermal stability:

$$\sigma_{u,w}/u_* = f(\zeta) \quad (1)$$

$$\sigma_x/x_* = f(\zeta) \quad (2)$$

where $\sigma_{u,w}$ is the standard deviation of horizontal or vertical wind velocity, u_* is the friction velocity defined as $u_* = \left(\overline{u'w'}^2 + \overline{v'w'}^2\right)^{1/4}$, x is the scalar term, and ζ is the thermal stability defined as $\zeta = (z-d)/L$, where z is the measurement height, d is the zero displacement ($\approx 0.65h_c$; h_c is the canopy height, Campbell and Norman, 1998), and L is the Obukhov length defined as $L = -Tu_*^3/kg\overline{w'T'}$; in which T is the air temperature, k (=0.4) is the von Karman constant, g is the gravitational acceleration, and $\overline{w'T'}$ is the vertical temperature flux.

The similarity functions of wind velocities were determined by fitting numerous previous studies, and suggested forms are raised as:

for $\zeta < 0$, $\sigma_{u,w}/u_* = A_1(1 - B_1\zeta)^{1/3}$ (3)

for $\zeta > 0$, $\sigma_{u,w}/u_* = A_2 + B_2\zeta$ (4)

for $\zeta \to 0$, $\sigma_{u,w}/u_* = D$ (5)

where A_1, A_2, B_1, B_2, and D are constants estimated with measured records. Previous results of wind velocity similarity functions are listed in Table 1, and the site descriptions are listed in Appendix A.

For vertical wind velocity, previous studies agreed in the similarity function with slightly different characteristic functions over varies landscapes: flat and homogeneous (e.g. Beljaars et al., 1983; De Bruin et al., 1993; Choi et al., 2004), tall canopy covering (e.g., Asanuma and Brutsert, 1999; Katul et al., 1995), and complex

topography or vegetation type (e.g., Marques et al., 2008).

For horizontal wind velocity, most studies observed no obedience in flux-variance similarity as in De Bruin et al. (1993) over a flat and homogeneous grass site, while some are still found following the similarity function as in Andreas et al. (1998) over a patchy vegetation flat terrain.

As for scalar similarity under unstable condition, a $-1/3$ power function is raised:

$$\text{for } \zeta < 0, \qquad \sigma_x / x_* = C_1 (1 - C_2 \zeta)^{-1/3} \tag{6}$$

and simplified under free convection (Cava et al., 2008) condition to

$$\text{for } \zeta < -5, \qquad \sigma_x / x_* = C_x (-\zeta)^{-1/3} \tag{7}$$

where σ_x is the standard deviation of scalar x, x_* is defined as $x_* = \overline{w'x'}/u_*$, and C_1, C_2, C_x are the similarity characteristic constants, which is claimed in Panofsky and Dutton (1984) to be universal.

Temperature characteristic constants (C_T) found by regression of equation (7) follow the similarity with a near unity value over ideal terrains (e.g., Tillman, 1972; Ohtaki, 1984; Weaver, 1990; De Bruin et al., 1993; Albertson et al., 1995; Andreas et al., 1998; Choi et al., 2004) and with a slightly larger value over complex ones (e.g., Kustas et al., 1994; Wesson et al., 2001; Cava et al., 2008; Hsieh et al., 2008; Marques et al., 2008).

Though little differences exit in C_T between landscape types, the overall assumption is that C_T is independent with surface identities, and serves as a standard value in similarity comparison against other scalars.

Since water vapor is thought to be a passive factor which depends on temperature, the similarity characteristic constants should be equal. But this is only for some cases, such as Högström and Smedman-Högström (1974) over flat mixed agricultural site,

Beljaars et al. (1983) over a flat terrain, and Ohtaki (1985) over a flat wheat field. More studies unfulfilling the similarity theory are found over varies landscapes (e.g., De Bruin et al., 1993; Katul et al., 1995; Andreas et al., 1998; Assanuma and Brutsaert. 1999; Detto et al., 2008;). This dissimilarity is also observed in the CO_2 similarity characteristic constant (C_c) in Cava et al. (2008) and Detto et al. (2008).

As listed in Table 2, C_q ranges from 1 to 1.34 (Högström et al., 1974; Ohtaki, 1984; Wesely, 1988; Andreas et al., 1998; Choi et al., 2004; Hsieh et al., 2008; Marques et al., 2008) and C_c ranges from 0.95 to 1.25 (Ohtaki, 1984; Wesely, 1988; Hsieh et al., 2008) over flat terrain with low canopy, implying that in near ideal conditions the water vapor and CO_2 source and sink partly follow the similarity. But when encountering tall canopies or complex terrains, scatters appeared and much larger values are observed: a range from 1.3 to 1.61 for C_q (Asanuma, 1999; Lamaud and Irvine, 2006; Cava et al., 2008; Hsieh et al., 2008; 袁一夫, 2008); 1.32 and 1.7 for C_c (Cava et al., 2008; Hsieh et al., 2008).

Several studies discussed this dissimilarity behavior and suggested the causing reasons as the following: terrain complexity, source heterogeneity, active role of temperature in the turbulent kinetic energy budget, outer-layer effects, entrainment effects, and advection (e.g., Roth and Oke, 1995; Lamaud and Irvine, 2006; Cava et al., 2008). The dissimilarity affects the precision of flux-variance method, as found in Detto et al. (2008) over a Mediterranean area.

It was claimed in Andreas et al. (1998) that Monin-Obukhov similarity theory is the only conceptual framework for treating near-surface turbulence. Intending to understand the transports over heterogeneous surfaces, an overcome process must be introduced. To deal with these scattering records which lead to regression bias, filtering processes were brought about by Cava et al. (2008) and Detto et al. (2008).

In Cava et al. (2008), the anomalous records are picked out through two processes. With two sets of eddy covariance systems, one in the canopy and one on

top of the canopy, the respiration events from the forest floor can be picked out by comparing the two measurements at different heights. And by observing the normalized time series of T', q', and c', the outer-layer effect can be found with a sharp decrease or increase in the time series graph.

In Detto et al. (2008), a two year measurement is done over a Mediterranean area, where vegetation changes seasonally. Close consideration of effects on scattering records is assumed as Cava et al. (2008), but a rather subjective filtering method is used. Detto gave strict ranges for the acceptable records for the similarity analysis (see Table 3), and with these data filtering thresholds, the records collected reduced to 17.8% of the possible collection.

With a single height measurement, a four year long-term data set, and unclear site characteristics, the above two filtering methods are not suitable for this study. A much more simple way in eliminating anomalous records is implied in Lamaud and Irvine (2006), where water vapor during a dry-to-wet transition period over a pine forest is analyzed.

With the Bowen ratio ($Bo = H/LE$, where H is the sensible heat flux and LE is the latent heat flux) as a classifying factor, Lamaud and Irvine separates scattered records with those who follow the $-1/3$ power law: the acceptable range is $0.5 \le Bo \le 2$ (see Figure 1(a)). This Bo dependent relation consists with an early observation in Weaver (1990), where a one-dimensional eddy covariance system measures over a tall grass prairie. In Weaver's case, when $Bo = 1$, C_q is around 0.98, and when $Bo = 5$, C_q rises to a higher value, 2.5.

For the checking of the consistency of C_T, C_q and C_c, the flux variance method suggested in Hsieh et al. (2008) is listed below.

$$H = \rho C_p \overline{w'T'} = \rho C_p \left(\frac{\sigma_T}{C_T} \right)^{3/2} \left(\frac{kg(z-d)}{T} \right)^{1/2} \tag{8}$$

$$LE = L_v \overline{w'q'} = L_v \frac{\sigma_q}{C_q} \left(\frac{kg(z-d)}{\rho C_p T} H \right)^{1/2} \tag{9}$$

$$F_{CO_2} = \overline{w'c'} = -\frac{\sigma_c}{C_c} \left(\frac{kg(z-d)}{\rho C_p T} H \right)^{1/2} \tag{10}$$

where ρ (≈ 1.192 kg m^{-3}) is the mean air density, C_p (≈ 1.017 J g^{-1} K^{-1}) is the specific heat capacity of air, and L_v (≈ 2450 J g^{-1}) is the latent heat of vaporization.

For understanding the role of the relative transport efficiencies between scalars, the term λ is introduced. It could be written as following:

$$\lambda_{Tq} = \frac{R_{wT}}{R_{wq}} = \frac{\overline{w'T'}/\sigma_w\sigma_T}{\overline{w'q'}/\sigma_w\sigma_q} = \frac{\overline{w'T'}}{\overline{w'q'}} \frac{\sigma_q}{\sigma_T} \tag{11}$$

$$\lambda_{Tc} = \frac{R_{wT}}{R_{wc}} = \frac{\overline{w'T'}/\sigma_w\sigma_T}{\overline{w'c'}/\sigma_w\sigma_c} = \frac{\overline{w'T'}}{\overline{w'c'}} \frac{\sigma_c}{\sigma_T} \tag{12}$$

$$\lambda_{qc} = \frac{R_{wq}}{R_{wc}} = \frac{\overline{w'q'}/\sigma_w\sigma_q}{\overline{w'c'}/\sigma_w\sigma_c} = \frac{\overline{w'q'}}{\overline{w'c'}} \frac{\sigma_c}{\sigma_q} \tag{13}$$

where R_{xy} is the correlation coefficient between x and y.

Theoretically, for the scalar characteristic constants to approach unity as assumed for ideal conditions, the correlation coefficients between the vertical wind velocity and the scalars should equal, as $R_{wT} = R_{wq} = R_{wc}$, and the relative transport efficiencies should value around unity. It is introduced in Asanuma and Brutsaert (1999) that if we substitute equation (7) into equation (11), (12) and (13), respectively, we get the following:

$$\lambda_{Tq} = C_q / C_T \tag{14}$$

$$\lambda_{Tc} = C_c / C_T \tag{15}$$

$$\lambda_{qc} = C_c / C_q \tag{16}$$

It is obvious that if $\lambda_{Tq} > 1$ or $C_q > C_T$, the transport efficiency of temperature is higher than water vapor. The same explanation for equation (15) and (16) is derived.

$\lambda_{Tq} \geq 1$ and $\lambda_{Tc} \geq 1$ are found in most of the recent studies, which means that the temperature usually transports more efficiently than water vapor and CO_2. Moriwaki (2006) addressed that both the active role of temperature and the heterogeneous source distribution of scalars were the cause of this phenomenon. This value consists with the declaration given above, $C_T < C_q$ and $C_T < C_c$. With this equal relation and the relative transport efficiency value, another FV method function is generalized as below:

$$LE = L_v \frac{R_{wq}}{R_{wT}} \frac{\sigma_q}{\sigma_T} \overline{w'T'} \tag{17}$$

$$F_{CO_2} = \frac{R_{wc}}{R_{wT}} \frac{\sigma_c}{\sigma_T} \overline{w'T'} \tag{18}$$

And good results are showed for water vapor in Choi et al. (2004).

Wesely (1988) claimed that to use $\overline{w'x'} / \overline{w'y'}$ on turbulent flux estimation, as in equation (17) and (18), the correlation coefficient between x and y must be near unity. And so the analysis of correlation coefficients between scalars (R_{Tq}, R_{Tc}, and R_{qc}) is add into the discussion by Katul et al. (1995). These values represent the dynamic relation between the two scalars, which helps in finding the motive powers of scalar transport in the ecosystem.

The different behaviors of R_{xy} in wet and dry conditions were analyzed in different ways. Detto et al. (2008) found that when water supply was sufficient, R_{Tq} and $-R_{Tc}$ would have a near unity centralized value. And through dry conditions, the correlation coefficients would be scattered and R_{Tq} appears lower than $-R_{Tc}$. The

dissimilar reason aimed on the land cover heterogeneity in water vapor.

With statistical approach and a near unity R_{Tq} value, Bink and Meesters (1997) stated that the relative transport efficiency λ_{Tq} could be approximated by R_{Tq} when $\lambda_{Tq} < 1$ (usually found in dry periods) and by $1/R_{Tq}$ when $\lambda_{Tq} > 1$ (usually found in wet periods). It is then claimed that for R_{Tq} far from unity, instead of assuming that this behavior exists, the flux-variance method could be improved if R_{Tq} is used as an estimate for the ratio of the transfer efficiencies.

It is then obvious that between clearly wet and dry conditions, a blurred zone exits. Lamaud and Irvine (2006) constructed the relationship in this zone as a function of the Bowen ratio:

$$\lambda_{Tq} = R_{Tq}^{\ k} \tag{19}$$

where $k = -1 - 2\log(Bo)$ when $0.1 \le Bo \le 1$ (see Figure 1(b)). Moriwaki and Kanda (2006) tried this relation on CO_2, and found a similar linear relation between λ_{Tc}^{-1} and R_{Tc} presented with a ratio as $\lambda_{Tc}^{-1} = 0.6R_{Tc}$.

Chapter 3 Experimental site

This experiment site is located in the Chi-Lan Mountain area, Ilan, northeastern Taiwan (see Figure 2(a)). The measurement tower location is 24°35'25.03"N, 121°24'55.46"E; 1650 m above sea level. Research area ranges in altitude from 1400 to 1800 m with a average slope around 15° in valley direction (NW-SE). It is close to the Yuan Yang Lake natural preserver, always from any major industrial or urban impacts (see Figure 2(b)).

As detailed in Klemm et al. (2006), the dominant species of this cypress forest is the *Chamaecyparis formosensis* and the *chamaecyparis obtusa var. formosana* (together over 82%). The investigated vegetation distribution is shown in Figure 2(c). The mixed cypress forest areas are in the original forest composition with different tree ages and life stages, and the new cypress forest area was a 40-year-old *chamaecyparis obtusa var. formosana* plantation (planted between 1961 and 1978). The other areas were shared by 32 broad-leaved tree species. Tree heights vary between 10 to 13 m above ground with a closed tree-crown and extraordinary uniformity.

The climate is classified as humid-temperate. Annual air temperature is around 14°C with the highest monthly average occurring in July (20°C) and the lowest occurring between December and February (7°C). The monthly averaged relative humidity is higher than 80% through the whole year. Fog duration per day is up to 13 hours in winter time and lowered to about 3 hours in summer time. The annual precipitation is larger than 4000 mm with rainfall mostly occurring in the summer and early autumn. High frequency of rainfall, cloud and fog coverage reduces solar radiation income, which is an important influence factor at on biophysical reaction.

As described in Klemm et al. (2006), this site has a typical wind direction behavior; valley winds mostly come from south-east during day-time, and mountain winds mostly come from north-west during night-time, as showed in Figure 3. The valley winds brings advection with warm and moist air masses leading to foggy conditions, and the mountain winds brings advection with cool and dry air masses dissipating the fogs.

The instrumental tower (see Figure 4) is equipped with a fast response EC system and several low frequency climate record instruments. The equipments and its location in this study are listed in Table 4. Since the operation begin in March 2005, several instrument repairing and changing occurred, as listed in Table 5.

The EC system was set at 23.8 m above ground surface, and data collection is set at 10 Hz. A sonic anemometer and a gas analyzer form the system, and the time lag between instrument collections are captured and corrected when data-logging.

The climate instruments are more stable than the EC system in performance. CRN-1 radiometer is placed at 22.5 m, quantum sensor collecting the photosynthetic active radiation is places at 23.6 m, air temperature and humidity were measured at 23.6 m with shield covering, and canopy-top visibility is tracked for fog existence. These low responding instruments are connected to a data-logger (CR23X before 2006/9 and CR5000 after 2006/9) with collection at 1 Hz and a 10 min interval output. All instruments are powered by a series of 12 VDC batteries.

Data collection began on March 2005, and the analyzed period extends to May 2009. High quality records from March 2005 to March 2009 were picked out for similarity characteristic constants regressions, and records within reliable thresholds from April to May 2009 were used to check these constants with flux variance methods.

Raw data were first checked for amount and time series continuity, and then unit

conversion and two repeats of spike removal with $\pm 4\sigma$ acceptable range are held for each 30 minutes. Maximum correlations between vertical wind velocity and scalars are calculated to insure time lag between instrument outputs.

Steady state test is provided (see Appendix B), and we use the test from Foken and Wichura (1996) in our study. Data with $RN_{\mathrm{cov}} > 10$ are eliminated before coordinate rotation (see Appendix C). Planar fit method is brought up in two ranges of wind directions: 0-200 degree and 200-360 degree. After the coordinate rotation, Webb-Pearman-Leuning correction (Webb et al., 1980) and scalar density correction (Detto and Katul, 2007) are done. Manual check on reasonable ranges and relations between flux and climatic data are done. Data with $RN_{\mathrm{cov}} < 0.3$ are applied for the characteristic examinations. Fetch examination with footprint model from Hsieh et al. (2000) is done for source area investigation. The same steps were followed for records from April to May 2009, but with $RN_{\mathrm{cov}} < 0.75$ as the reliable threshold.

Chapter 4 Results and Discussions

In this section, we discuss the wind velocity, temperature, water vapor, and CO_2 characteristics with the flux-variance method, both in normalized standard deviation and relative transport efficiency. The characteristic constants and representative relative transport efficiency are checked for consistency. Also the parameterization of the relation between relative transport efficiency and its correlation coefficient is examined.

4.1 Wind velocity characteristics

In spite of the complexity of our study site, a good result is found for vertical wind velocity under unstable condition. As showed in Figure 5(a), the uphill direction wind follows closely with the suggested function, $\sigma_w/u_* = C_1(1-C_2\zeta)^{1/3}$, resulting in $C_1 = 1.2$ and $C_2 = 1.9$ at RMSE=0.43. For the downhill direction showed in Figure 5(b), a similar result with slightly larger value is found with $C_1 = 1.3$ and $C_2 = 1.21$ at RMSE=0.64. With this result we conclude that vertical wind velocity similarity is obeyed even over a complex terrain, which matches with the declaration in Detto et al. (2008) over a seasonally changing Mediterranean ecosystem.

For the horizontal wind velocity (see Figure 6), a fair performance is found with function $\sigma_u/u_* = C_1(1-C_2\zeta)^{1/3}$ in the uphill wind direction: $C_1 = 2.18$ and $C_2 = 0.69$ at RMSE=1.13. Scatters are found in the downhill wind direction, which is thought to be caused by the separated bubbles appearing when air flows down a steep hill. Comparing with the uphill direction, a shift up regression line with $C_1 = 2.81$ and $C_2 = 0.49$ at RMSE=1.77 is determined.

In downhill wind direction results (Figure 5(b) and 6(b)), the scattered σ_u/u_* and a well performed σ_w/u_* suggests that the planar fit method works well in the

wind-field-planar search over this complex terrain, which rotated the coordinate system parallel with the mean stream line to provide acceptable vertical transport calculations.

A comparison with suggested wind velocity functions from previous studies is showed in Figure 7. It is then concluded that the vertical wind similarity functions are close to each other over different land covers, while the horizontal wind similarity functions varies, especially under very stable states.

For records under stable conditions collected in night-time, scatters exist in both horizontal and vertical wind velocities while it roughly follows the suggested function, $\sigma_{u,w}/u_* = C_1 + C_2\zeta$. As Marques et al. (2008) inspected, self-correlation effect under stable condition is large, which leads to errors in similarity estimations. Also that long fetches ranging from 1000 m to 9 km are found in our records, which includes undesired source area. We do not discuss the behavior under stable condition in this study.

Due to the short transition periods and the large errors during transition time over this site, records under neutral or near neutral condition are rare and scattered. Thus we determine the approached constant values of σ_u/u_* and σ_w/u_* with records under unstable and stable conditions. Though differences between the two-side-approach exist, comparing with previous studies, the values are in acceptable ranges: σ_u/u_* from 1.93 to 3.03 and σ_w/u_* from 1.1 to 1.37.

Details of the similarity constants are listed in Table 6.

4.2 Scalar characteristics

The scalar characteristic constants in function $\sigma_x/x_* = C_x(-\zeta)^{-1/3}$ are estimated with records under free convection ($-\zeta > 5$ from Cava et al., 2008). Results are showed in Table 7 and Figure 8, 9 and 10. An over all fair relation is found in the

following of the similarity functions with different C_x values obtained.

The temperature characteristic constants are found near unity with $C_T = 1.17$ in uphill wind direction and a higher value of 1.29 with downhill wind direction. This implies that the temperature field is more uniform in the downhill side (single species forest) than the uphill side (natural mixed forest) forest, which matches with the assumption that the leaf shading identities dominate the temperature field over closed forest sites.

For water vapor characteristic constants, the filtering method introduced in Lamaud and Irvine (2006) is used. The Bowen ratio in our study has a much smaller range than the conspicuously dry-to-wet pine forest site in Lamaud and Irvine (2006) (ranging from 0.2 to 9), so a shrinkage in the acceptable Bowen ratio range is set to be $0.8 \le Bo \le 1.25$. Records in classification of the three Bowen ratio ranges are showed in Figure 8, and good filtering of scattered points are observed for both uphill and downhill wind directions. The constants (1.57 and 1.77) are much higher than the temperature ones, matching with the heterogeneity observed over a coniferous forest sites in Cava et al. (2008).

The Bowen ratio filtering method is also placed on CO_2, with the hypothesis that water vapor and CO_2 are both biophysically powered. With the classification, most scatters were filtered out, leaving some obvious outliers for manually pick-out. The characteristic constants found for the uphill and downhill wind directions are 1.45 and 1.49, which is lower in value and also more concert than the water vapor constants with RMSE values 0.12 and 0.138 against 0.215 and 0.269. This lower behavior also matches the finding in Cava et al. (2008).

Choi et al. (2004) claimed that the value of C_T is universal and independent on surface conditions, while C_q seems to be dependent. Hsieh et al. (2008) suggested the roughness length as a positive factor of the characteristic constant values, where C_q

and C_c increases as z_0 increases. We examined the characteristic constants against roughness length in the studies list in Table 2, result is showed in Figure 11. A log form trend is found for C_q, while second order polynomials are observed for C_T and C_c. This result can only be viewed as a reference, because of the different procedures in the determinations of the constants.

4.3 Correlation coefficients and relative transport efficiencies

The correlation coefficients of vertical wind velocity with temperature (R_{wT}), water vapor (R_{wq}), and CO_2 (R_{wc}) are showed against thermal stability in Figure 12, 13, and 14. It is observed that these correlation coefficients have different values at the same stability, which matches with the observed results in Beljaars et al. (1983) and Moriwaki and Kanda (2006) over complex terrains. Not much difference is found between downhill and uphill wind direction results.

With the probability distribution function analysis, maximum occurrence values are estimated for temperature, water vapor, and CO_2: in uphill wind direction 0.61, 0.46, and -0.49, respectively, and in downhill wind direction 0.59, 0.48, and -0.48, respectively (listed in Table 9). It is obvious that temperature has a better correlation with vertical wind velocity than water vapor and CO_2, just as found in previous studies, while water vapor and CO_2 are at the same magnitude of correlation.

Observing the R_{wT} records in Figure 12, we surmise that the values begin at zero under neutral condition and increase roughly to its maximum when $-\zeta = 1$, then smoothly decreases as the $-\zeta$ gets higher. This same behavior is expected on water vapor and CO_2 with records lower in magnitude and more dispersed as found in Lamaud in Irvine (2006).

The correlation coefficients are than plotted against Bowen ratio, as in Figure 15, 16, and 17. Clear triangle shaped relation are found in temperature and CO_2, with

near zero values at $Bo \to 0$, highest values around $Bo = 0.5$, and approaching constant when $Bo \geq 2$. Water vapor shows a scattered relation, partly independent to the Bowen ratio. We conclude that temperature and CO_2 over a highly humid forest are most active when latent heat flux dominates the energy transport. While for water vapor, the high humidity interrupts the transport reaction and behaviors independent with Bowen ratio are found.

Relative transport efficiencies between the scalars are showed in Figure 18, 19, and 20. By operating the probability distribution analysis, values of λ_{Tq}, λ_{Tc}, and λ_{qc} are found as 1.105, -1.095, and -0.95 in uphill wind direction and 1.125, -1.075, -0.88 in downhill wind direction, respectively (see Table 8). With these values, we conclude that temperature has the highest transport efficiency which is then followed by CO_2 and lastly the water vapor. This result matches with the observations in Cava et al. (2008) over a coniferous forest. Not much difference is found between the two wind directions.

When only leaf stomata control the mass transfer, the relative transport efficiency of water vapor and CO_2 should approach -1 and the inequalities may be used to access respiratory contributions (Cava et al., 2008). Katul et al. (1995) and Andreas et al. (1998) claimed that relative transport efficiency of temperature and water vapor should be close to unity when approaching neutral stability, then scattering out as the stability goes more unstable. Same as results over a suburban area in Moriwaki and Kanda (2006), the claimed stability dependent relation is not found in our study. Values under unity are found for near neutral stabilities, implying that water vapor and CO_2 transport more efficiently than temperature under these conditions.

The relation of relative transport efficiencies against Bowen ratio are showed in Figure 21, 22, and 23. A clear relation as found in Lamaud and Irvine (2006) is observed for both λ_{Tq} and λ_{Tc}. The values approach zero when $Bo \to 0$ and scatter out with values higher than unity. No relation to Bowen ratio is found in λ_{qc},

showing that energy partitioning differences do not influence the transport ratio of these two photosynthetic scalars, which implies that biophysical reaction dominates over this site.

With the characteristic constants and relative transport efficiencies collected (listed in Table 7 and 8), we check over these results with records collected in April and May, 2009. The measured and calculated values of sensible heat flux, latent heat flux and CO_2 flux and results are listed in Table 9.

A 0.91 slope is found in sensible heat flux with r-square values at 0.74 (see Figure 24). With all the day-time records involving, this result is assumed to be good. For latent heat and CO_2 fluxes, the Bowen ratio filtering method rise the estimation accuracy in the FV functions from Hsieh et al. (2008) around 10%, with r-square value increasing from 0.48 to 0.59 for latent heat flux, and 0.43 to 0.62 for CO_2 flux (see Figure 25(a) and 26(a)). Cava et al. (2008) claimed that after the filtering methods, values of C_q and C_c are not identical to the similarity theory functions, even though they follow the scaling. With the improved estimation given, we still assume the constants after filtering as a good tool for gap filling.

While the relative transport efficiency is presented with its median or mean, the peak value found by the probability distribution function gives a good shot when we observe the prediction functions from Choi et al. (2004). Slopes with value of 1.07 and 0.81 are found for water vapor and CO_2 flux, with r-square at 0.62 and 0.7. This estimation result is clearly better than the characteristic constants (see Figure 25(b) and 26(b)). A FV method choice is then suggested: when relative transport efficiencies have a well shaped bell like distribution, the most occurred value found by the probability distribution function is assumed a good way in estimating; and when relative transport efficiencies are scattered or not available, Bowen ratio filtering method on the normalized standard deviation function can also give a fair estimation.

The results of correlation coefficients between scalars (R_{Tq}, R_{Tc}, and R_{qc}) are showed in Figure 27, 28 and 29. Unlike the highly concentrated value found in Cava et al. (2008), scattered points are observed, indicating that the scalar fields in this study are mostly independent to thermal stabilities, especially for water vapor against temperature or CO_2.

In Scanlon and Sahu (2008), day-time correlation coefficients between water vapor and CO_2 are close to -1 during dry conditions, and degrade in magnitude during wet conditions. This degrading is assumed to be caused by large-scale eddy convections (Roth and Oke, 1995). With previous studies focusing on areas with obviously dry or wet conditions, our scattering result imply that over high humidity and biophysically dominated areas the complexity in water vapor transfer exits and the saying provided fails.

We then examine the relationship of these scalar correlation coefficients against Bowen ratio (see Figure 30, 31, and 32), and the suggested steep rising pattern from Lamaud and Irvine (2006) is only found in R_{Tc}, supporting the further complexity saying of water vapor behavior. Further analysis over high humidity zones is needed.

4.4 Parameterization of $\lambda - R$ relationship

The k power method in Lamaud and Irvine (2006) is examined on water vapor as showed in Figure 33. Different to the results found in Lamaud and Irvine (2006), k did not approach -1 for water vapor when $Bo \geq 1$; it instead follows the same relation as the records with $0.1 \leq Bo \leq 1$, where functions of $k = -0.44 \ln Bo - 0.64$ and $k = -0.5 \ln Bo - 0.64$ are found in uphill and downhill wind direction, respectively. These k values are checked with records from April and May in 2009, and results with undesired r-square values show that the k power method is not suitable for water vapor. But clearly some kind of relationship determined by Bo exists.

By examining Figure 34, we see the relation between λ_{Tq}^{-1} and R_{Tq} falls in the range of $\lambda_{Tq}^{-1} = R_{Tq}$ and $\lambda_{Tq}^{-1} = 1$, and the slopes found with -1 power regression get steeper as the Bowen ratios get higher. With this observation we produce a relation function as $R_{Tq} = a\lambda_{Tq}^{-1} + b$, where a and b are linear functions of Bo.

As showed in Figure 35, records with $Bo \le 0.4$ are rare and scattered, so regression is only done for records with $0.4 \le Bo \le 5$. Six selected ranges and their regression results are listed in Table 10(a). Plotting the results in Figure 34, we can obviously see that the relation functions between Bo and a or b could be classified into two zones: $Bo \le 1$ and $Bo \ge 1$. When $Bo \le 1$, a negative linear relation is found for a and a positive one found for b; while when $Bo \ge 1$, no relation is observed. Placing the regressed values back to the produced function, we get the new relation between λ_{Tq}^{-1} and R_{Tq} as listed in Table 10(b).

Assuming biophysics dominating, the same procedures are placed on CO_2. Comparing with water vapor, a rather different result is showed in Figure 36. When $Bo \ge 1$, an independent relation between k and Bowen ratio is found, suggesting -0.55 and -0.5 as k values for the uphill and downhill wind directions. The same calculation procedure on a and b are also done and results are showed in Figure 37 and 38 with values listed in Table 11.

Lamaud and Irvine (2006) claimed that the scattering in the k regression is anticipated and acceptable, and the intermediate relations stand still in the behavior estimation. With records from April and May in 2009 as a checking in the fitting of k and $R_{Tx} = a\lambda_{Tx}^{-1} + b$, acceptable results are found for $0.4 \le Bo \le 1$ and rather good results for $1 \le Bo \le 4$ (see Figure 39 and Table 10 and 11).

Chapter 5 Conclusions

With measurements separated into uphill and downhill directions, the vertical wind velocity was found to follow the Monin-Obukhov similarity relation over a mountainous terrain. Temperature also follows the similarity function well with a characteristic constant higher than unity value, and through Bowen ratio filtering method, reasonable characteristic constants can be found for water vapor and CO_2.

Over high humidity forests with long-term fog duration and no water coverage and sufficient radiation input, the water vapor transport characteristics are complicated, while temperature and CO_2 characteristics behave more actively in conditions with low Bowen ratios. Water use efficiency which could separate stomata transport with non-stomata ones would be an important future work for these kinds of ecosystems.

For application of FV method in gap filling, the representative value of relative transport efficiencies between temperature, water vapor and CO_2 are suggested with functions in Choi et al. (2004). While the FV functions in Hsieh et al. (2008) together with filtering thresholds in Bowen ratio could obtain fair results.

The relation functions between relative transport efficiency and scalar correlation coefficients are investigated for water vapor and CO_2 over this site. A -1 power law with parameters in linear functions of Bowen ratio is raised when $0.4 \le Bo \le 1$ for water vapor and CO_2, and a -0.5 power law is introduced when $1 \le Bo \le 4$ for CO_2.

Appendix

Appendix A. Brief site descriptions of previous studies cited

study	brief site description
Tillman (1972) (a)	Homogeneous and flat grass terrain at south Dartmouth, Mass; land covering: grass; measured at 40 m. Fair weather periods used; sampling at 1.2 sec and averaged at 60-75 min; instruments: bivane, platinum resistance temperature transducer, dual-channel microwave refractometer.
Tillman (1972) (b)	Bonneville salt flats near Wendocer, Utah; land covering: crystalline salt; measured at 0.55, 2, and 8 m. Sampling at 12.5 Hz and averaged at 40 min; instruments: channel platinum temperature transducer, sonic anemometer.
Högström et al. (1974)	Agricultural site covered with different kinds of crops and scattered groups of houses and trees at Marsta, Sweden; covered with different crops and scattered houses and trees. Measurement height at 3 and 12 m; data collecting at 30-50 Hz, averaging period 30 min.
Beljaars et al. (1983)	In the center of the Netherlands; flat grassland interrupted by trees; measurement height 3.5 m and 22.5 m; 10 min linear trend removal; averaged at 30 min. instrument: Kaijo-Denki DAT300, Lymanalfa humidity sensor, thermocouple.
Ohtaki (1984) (a & b)	The first and second experiment: Wheat covered Kurashiki site; canopy height 0.4 and 0.65 m and measured at 1.1 m. Record collected on 3/29 and 4/20, 1982; instruments: special designed IRGA, sonic anemometer, thermocouple thermometer.
Ohtaki (1984) (c)	The third experiment: Wheat covered Hachihama site; canopy height 0.85 m and measured at 1.8 m. Record collected on 5/2, 1983.
Weaver (1990)	Tall grass prairie and desert-shrub; averaged in 5 &15 min; sampling at 10 Hz; cup anemometer, fasr-response Young 03001, wet-bulb psychrometers and Krypton open-path hygrometers, fine-wire thermocouples.
De Bruin et al. (1993)	Horizontal uniform plain of La Crau, South of France; grasses and herbs covered; data collected during dry sunny periods, June 1987; sampling at 0.7 Hz and averaged in 10 min;

	measurement at 11.3 m; instruments: sonic anemometer (Kayo Denki IC-05D), fast temperature sensor (KNMI) and Lyman-α hygrometer (BLR).
Padro (1993)	Fully leaved deciduous forest, leafless deciduous forest, a wetland region; summer time; northern Ontario, Canada. Canadian Forces Based Camp Borden; 44°19'N, 80°56'W; July & August 1988; canopy height 18 m; measurement height 33.4 m; 30 min averaged.
Kustas et al. (1994)	Fairly complex surface in the Walnut Gulch experimental watershed; mildly hilly terrain with homogeneous vegetation; measurement height 2 m; 8 sites.
Albertson et al. (1995)	Dry owens Lake bed in Owens Valley, southeastern California; during late June and early July, 1993. Measurement height 2.5 m; Instrument: Gill-1012R2; sampling at 10 Hz and averaging in 13.6 min.
Hsieh and Katul (1996)	Non-uniform Alta Fescue grass covered forest in Durham, North Carolina; elevation 163 m; measurement height 1.54 m; instrument: Gill triaxial, sonic anemometer; canopy height 0.23 m; Measured on 7/26.27 (21Hz, 26 min) and 8/10 (56 Hz, 19.5 min).
Andreas et al. (1998)	McKenzie Flats in Sevilleta National Wildlife Refuge; 106°41'9.47''W, 34°21'5.15''N; homogeneous (in large scale) grassland (38% vegetation covered); black grama (*Bouteloua eripoda*, 18%) dominated with height 0.05 m. Record collected on 4-16 August, 1991 during rainy days; Kaimal sonic/thermometer mounted at 4 m; data collected at 10 Hz, averaging period 50 min.
Asanuma et al. (1999)	Flat Landes forest; land covering: maritime pine stands (65%) and agricultural crops and clearings (35%). Pine height 10-20 m. Variable surface over 150 km flight measurement; block averaged over 10 km. During HAPEX-Mobilhy in 1986, in southwestern France.
Choi et al. (2004)	Short grass prairie (BJ site on Tibetan Plateau) near Naqu, Tibet, China; 92.04°E, 31.29°N; 4580 m above sea level; soil type: sandy silt loam; canopy height 0.05 m and measured at 2.85 m; homogeneous and flat terrain. Record collected during late May and mid September, 1998 (wet and dry season transit at late June); sampling at 20 Hz and averaged at 30 min;

	stationary test and WPL correction provided; instruments: CSAT3, KH20, thermocouple.
Lamaud and Irvine (2006)	30 year old maritime pine stand in Landes forest, La Bray, France; main species: *Pinus pinaster Ait*; sequentially rainfall and drought; canopy height 19 m and measured at 40 m. Record collection during 7/28-10/24, 1999 at local time 1000-1400 used; sampling at 20 Hz and averaged at 30 min; instruments: Grill R3 and E009.
Moriwaki and Kanda (2006)	Low storied residential area in Kugahara, Tokyo, Japan; 34°34'N, 139°41'E; land covering: house (33%); house height 7.3 m and measured at 29 m; flat and uniform with 5.7° at one direction. Record collection in July 2001 at local time 0900-1600 under fair weather periods; sampling at 8 Hz and averaged at 60 min; double rotation method provided; WPL correction provided; instruments: USA1, LI7500.
Cava et al. (2008)	Uneven-aged mixed coniferous forest at Lavarone, Italy; 45.96°N, 11.28°E; 1300 m above sea level; main species: *Abies alba* (70%); maximum LAI: 9.6; canopy height 28-30 m and measured at 32 m. Record collection during 8/10-9/8, 2000 at local time 0900-1500 under cloud free periods; towered situated on gently rolling plateau; sampling at 20 Hz and average at 30 min; double rotation method provided; stationary test, WPL and Detto-Katul correction provided; instruments: Gill R3, LI7500.
Detto et al. (2008)	Mediterranean ecosystem at Orroili, Sardinia, Italy; 39°41'N, 9°6'E; 500 m above sea level; land covering: soil and grass (70%); LAI: 3.5-4.5; maximum canopy height 5 m and measured at 10 m. Record collection during April 2003 and October 2005 at day-time under fair weather periods; sampling at 10 Hz and averaged at 30 min; planar fit method provided; WPL and Detto-Katul correction provided; instruments: CSAT3, LI7500.
Hsieh et al. (2008) (a)	Temperate humid grassland at Crook County, Ireland; 52°8'N, 8°39'E; 200 m above sea level; canopy height 0.1-0.45 m and measured at 10 m; flat terrain. Record collection during 1/1-12/31 2002 under unstable condition; sampling at 10 Hz and averaged at 30 min; double rotation and planar fit method provided; WPL and Detto-Katul correction provided;

	instruments: Young 81000, LI7500.
Hsieh et al. (2008) (b)	Subtropical monsoon irrigated paddy rice field at An-Kang, Taipei, Taiwan; 24°57'N, 121°31'E; <20 m above sea level; canopy height 0.5-0.8 m and measured at 2 m; flat terrain. Record collection during 9/26, 2006 to 5/18, 2007 under unstable condition; sampling at 10 Hz and averaged at 30 min; double rotation and planar fit method provided; WPL and Detto-Katul correction provided; instruments: CSAT3, LI7500.
Hsieh et al. (2008) (c)	Warm temperate yellow cypress forest at Chi-Lan mountain, Ilan, Taiwan; 24°35'N, 121°30'E; 1650-2432 m above sea level; canopy height 10.3 m and measured at 24 m; sloppy with 15° at one direction. Record collection during April 2005 to December 2006; sampling at 10 Hz and averaged at 30 min; double rotation and planar fit method provided; WPL and Detto-Katul correction provided; instruments: Young 81000v, LI7500.
Marques et al. (2008)	Pantanl wetland Arboreal savanna at Mato Grosso do Sul, Brazil; 19°34'S, 57°1'W; 80 m above sea level; measured at 25 m. Record collection during April and May 1998 (wet and dry transition) under rain-free periods; sampling at 21 Hz and averaged at 60 min; instruments: Gill-Solent.
袁一夫 (2008)	台灣南投縣魚池鄉蓮華池試驗林區第五號集水區；北緯 23 度 55 分、東經 120 度 53 分；平均坡度百分之四十；海拔 720 至 800 公尺。資料於晴朗天氣收集，乾季 45 天，濕季 13 天；30 分鐘計算區間；樹高 17 公尺，於 25 公尺量測；儀器為 Young 81000 和 KH20。

Appendix B. Steady state tests

Under steady state conditions as assumed in the empirical equations, all statistical parameters do not vary with time. Non-stationary conditions occur when changes were made during time, such as changing in meteorological variables and weather patterns. Let out the expectation, it was nearly impossible for wind or scalars to perform ideally steady state behavior, which then leads to acceptable ranges of non-stationary rate.

Two different steady state tests were widely used nowadays in order to test the uniformity in the averaging periods: one is based on block average difference as in Foken and Wichura (1996) and Rebmann et al. (2005), and the other based on the difference divergence as in Mahrt (1998).

Foken and Wichura (1996) proposed the non-stationary ratio (NR) based on developments of Russian scientist, comparing the statistical parameters through the whole averaging time with short interval averages divided from the total interval.

The time series in one basic averaging interval is separated into M short intervals, which leads to N number of data within each. The covariance $\overline{x'w'}$ is calculated for the total interval and each sub-intervals, where w is the vertical wind component and x could be the horizontal wind component or scalars.

Each sub-interval flux is calculated as $\left(\overline{x'w'}\right)_i = \frac{1}{N-1}\left[\sum_j x_j w_j - \frac{1}{N}\sum_j x_j \sum_j w_j\right]$, where i represents 1 to M, and j represents 1 to N. In order to calculate the non-stationary ratio, the sub-intervals are averaged to get one flux value, $\overline{x'w'} = \frac{1}{M}\sum_i \left(\overline{x'w'}\right)_i$. The overall covariance $\left(\overline{x'w'}\right)_o$ is calculated as

$$\left(\overline{x'w'}\right)_o = \frac{1}{M(N-1)}\left[\sum_i\left(\sum_j x_j w_j\right)_i - \frac{1}{MN}\sum_i\left(\sum_j x_j \sum_j w_j\right)_i\right],$$

and the ratio of non-stationarity, NR_{cov}, is presented as $NR_{\mathrm{cov}} = \left| \frac{\left(\overline{x'w'}\right) - \left(\overline{x'w'}\right)_o}{\left(\overline{x'w'}\right)_o} \right|$.

In Foken et al. (2004), with an averaging period of 30 minutes, $M = 6$ and $N = 3000$, the single averaged period is assumed steady state if $RN_{\mathrm{cov}} < 30\%$. As for Aubinet et al. (2000), all data with differences $NR_{\mathrm{cov}} < 30\%$ were of high quality and those with differences between 30% and 60% have an acceptable quality. Concluding with several different flagging ranges produced, the strict standard of stationary limit for characteristic analysis is suggested to be 0.3. Arranged flagging qualities are showed in Table A1.

In Mahrt (1998), basing on the fact that for stationary conditions, the standard error of the record mean due to random variability within the record predicts the variability between record means, the deviation against this status forms NR. First we separate the total averaging interval to I records, and then divide each record into J sub-record segments as showed in Figure A1(a).

The within-record standard deviation of the flux for the ith record is calculated as $\sigma_{wi}(i) = \sqrt{\frac{1}{J-1}\sum_{j=1}^{J}\left[F(i,j) - \overline{F}(i)\right]^2}$, where $F(i,j)$ is the flux of the jth segment of the ith record and $\overline{F}(i)$ is the average flux of the segment fluxes within the ith record. The random error was then determined by $RE = \sigma_{wi}/\sqrt{J}$. The between-record standard deviation was calculated as $\sigma_{btw} = \sqrt{\frac{1}{I-1}\sum_{i=1}^{I}\left(\overline{F}(i) - \overline{F}\right)^2}$, where $\overline{F}$ is the average flux measured in the total interval.

By comparing the value of the within-record and between-record standard deviation defines the non-stationary ratio, $NR \equiv \sigma_{btw}/RE$, and for stationary conditions NR is approximately unity. The standard limits of NR for steady state record limitation is obtained by the relation between NR and SER (scaled energy residual) as showed in Figure A1(b).

In Figure A1(b), the transition point of the SER value is around $NR = 2$, and so value 2 is suggested in that study. This value should be obtained independently for each site, in order to avoid bias in the 'climatology of the data'. This procedure also implies that eliminating the non-stationary records leads to a better energy closure performance.

Appendix C: Coordinate rotation

Errors in correlations of vertical velocity between wind components and scalars occur if the instruments were not leveled or the mean streamline was not perfectly horizontal. To apply the governing equations of EC method under these conditions encounters the problem of non-homogeneous in horizontal items. Two solving choices arise against this condition: aligning all instruments to the local direction of the axis, or allow the flow to set the coordinate system.

The further is difficult when there are many instruments mounted on the tower, so the latter one is widely used. Three typical coordinate rotation methods are presented in previous studies: double rotation method, triple rotation method, and planar fit method. All three with the applicability for the rotation of velocity into the streamline coordinate system.

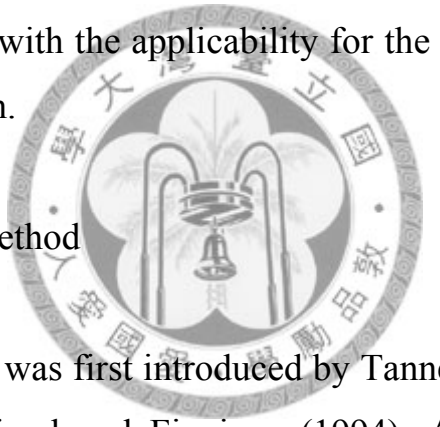

Double and triple rotation method

Double rotation method was first introduced by Tanner and Thurtell in 1969, and described in details by Kaimal and Finnigan (1994). A triple rotation method is addressed in McMillen (1987) for over-land usage.

This rotation is usually performed after each 30 minute period collection; the rotation angle is determined by the mean wind velocity measured by the original coordinate system. The first rotation with angle $\alpha = \tan^{-1}(v/u)$ sets x_{new} to the projection of the mean wind direction on the original $x-y$ plane. The second rotation then aligns x_{new} with the mean wind velocity direction, with rotating angle $\theta = \tan^{-1}\left(w/\sqrt{(u^2+v^2)}\right)$. After these two rotations, $\overline{v}_{new}$ and $\overline{w}_{new}$ are forced to zero.

The third rotation gives three different choices: rotate to let $w-u$ plane tangent to the geo-potential vertical, rotate to let $w-u$ plane perpendicular to the ground surface, or rotate to let $\overline{w'u'}=0$. This third rotation was later assumed unnecessary

because it results in creating unrealistic values and over rotating.

In double rotation methods, each averaging period was treated independently, which is not the real fact in natural. It was then widely criticized in using over complex terrains, because single events which have nothing to do with the coordinate system could contribute significant rotation for particular averaging intervals. This phenomenon is discussed and concluded that the third rotation should be avoided in Finnigan (2004).

The traditional way in doing the double or triple rotation needed angle determination ahead of time, which contains several steps in quadrant estimating. A vector-crossing-dotting procedure for the first two rotations is suggested. First we cross product vector $(0,0,1)$ with $(\overline{u},\overline{v},0)$ and get the new Y axis vector in unit form; then we cross product vector $(\overline{u},\overline{v},\overline{w})$ with (y_1,y_2,y_3) and get the new Z axis vector in unit form. Dot product was put to use in determination of the new wind velocity values with the unit form of the three new axis vectors are $u_{new}=\{u_i,v_i,w_i\}\bullet\{\overline{u},\overline{v},\overline{w}\}$, $v_{new}=\{u_i,v_i,w_i\}\bullet\{y_1,y_2,y_3\}$, and $w_{new}=\{u_i,v_i,w_i\}\bullet\{z_1,z_2,z_3\}$.

Disadvantages of the double and triple rotation methods are discussed in Wilczak et al. (2001). For double rotation method, the tilt angle estimation bias leads to a sampling error in the mean vertical velocity. And without correction in the lateral tilt component, a large mean bias in cross-stream stress appears. As for triple rotation method, large sampling error in the measured lateral stress increases the run-to-run noise in the longitudinal stress component.

Planar fit method

With the calculation errors possibly caused by the double and triple rotation methods, Wilczak et al. (2001) proposed a new coordinate rotation method called the planar fit method, and demonstrated in its study that it reduces the run-to-run stress

errors due to sampling effects. As shown in Figure A2, planar fit assumes that the wind velocities of an individual site falls on a plane dependent on the topography.

The desired unit vector is $\{\vec{i},\vec{j},\vec{k}\}$, where $\vec{i}$, $\vec{j}$, and $\vec{k}$ are parallel to its x, y, and z, respectively. Thus the new vertical velocity could be written as $\overline{w} = \vec{k} \bullet \vec{\overline{u}} = \{k_1, k_2, k_3\} \bullet \{\overline{u}_1, \overline{v}_1, \overline{w}_1 - b_0\}$, where $\overline{u}$ is the mean velocity and b_0 is the instrument offset in the vertical velocity. Rearranging the equation, we get $\overline{w}_1 = b_0 + b_1\overline{u}_1 + b_2\overline{v}_2 + \overline{w}/k_3$, where $b_1 = -k_1/k_3$ and $b_2 = -k_2/k_3$.

By collecting long-term wind velocity values, regression procedure is employed to get b_0, b_1, and b_2 with $\overline{w} = 0$. Then with b_0, b_1, and b_2, we get vertical direction unit vector $\vec{k}$, and the horizontal unit vectors $\vec{j}$ and $\vec{i}$ are calculated through formulas $\vec{j} = \left(\vec{k} \times \vec{\overline{u}}\right) \Big/ \left|\vec{k} \times \vec{\overline{u}}\right|$ and $\vec{i} = \vec{j} \times \vec{k}$. The three unit vector then provides a dot product procedure to examine the true value of flux exchange.

Planar fit method has the advantages that tilt angles where computed with large amount of data which lowers the sampling error, and also the accurate lateral component could be found. The one disadvantage of this method is that based on long-term regression, it could not be applied in real time.

Excluding extreme values of wind speed helps the regression of usual local wind field, which was suggested a threshold of 5 ms^{-1} for agricultural low land sites in Central Europe (Mauder and Foken, 2004).

In Kaimal and Finnigan (1994), evaluating the flow over a steep hill encounters different conditions in up-hill and down-hill wind directions. The real stream lines from up-hill wind flow is assumed to be parallel to the hill surface with a deceleration to the crest, while the down-hill wind flow develops a wake region and also have an opportunity to form separation bubble where flow reverses its direction. The critical downwind hill slope limit with high roughness surfaces to shape separation is suggested to be about 10˚, which indicates that this study site has the opportunity in

forming separated bubbles.

It was concluded in Finnigan (2004) that all three coordinate rotations can not perform well when flow separation exits. Even though errors of planar fit method still exits, it is suggested that a better accuracy could be obtained for steep terrain when making use of it. A separation of the wind directions into down-hill and up-hill ones when fitting the plane might reduces this influence on the total flux estimation.

References

袁一夫. 2008. 應用通量變異法與渦流相關法推估地表通量. 碩士論文. 國立中央大學, 桃園.

褚侯森. 2008. 複雜地形中的通量量測--以棲蘭山台灣扁柏森林樣區為例. 碩士論文. 國立東華大學, 花蓮.

Albertson, J. D., M. B. Parlange, G. G. Katul, C. R. Chu, and H. Stricker: 1995, Sensible heat-flux from arid regions---a simple flux-variance method. *Water Resources Research*, Vol. 31, pp. 969-973.

Andreas, E. L., R. J. Hill, J. R. Gosz, D. I. Moore, W. D. Otto, and A. D. Sarma: 1998, Statistics of surface-layer turbulence over terrain with metre-scale heterogeneity. *Boundary-Layer Meteorology*, Vol. 86, pp. 379-408.

Asanuma, J. and W. Brutsaert: 1999, Turbulence variance characteristics of temperature and humidity in the unstable atmospheric surface layer above a variable pine forest. Water Resources Research, Vol. 35, pp. 515-521.

Aubinet, M., A. Grelle, A. Ibrom, Ü. Rannik, J. Moncrieff, T. Foken, A. S. Kowalski, P. H. Martin, P. Berbigier, C. Bernhofer, R. Clement, J. Elbers, A. Granier, T. Grünwald, K. Pilegaard, C. Rebmann, W. Snijders, R. Valentini, and T. Vesala: 2000, Estimates of the annual net carbon and water exchange of forests: The EUROFLUX methodology, *Advances in Ecological Research*, Vol. 30, pp. 113-175.

Beljaars, A. C. M., P. Schotanus, and F. T. M. Nieuwstadt: 1983, Surface layer similarity under non-uniform fetch conditions. Journal of Climate and Applied Meteorology, Vol. 22, pp. 1800-1810.

Bink, N. J. and A. G. C. A. Meesters: 1997, Comment on 'Estimation of surface heat and momentum fluxes using the flux-variance method above uniform and non-uniform terrain' by Katul et al. (1995). *Boundary-Layer Meteorology*, Vol. 84, pp. 497-502.

Cava, D., G. G. Katul, A. M. Sempreviva, U. Giostra, and A. Scrimieri: 2008, On the anomalous behaviour of scalar flux-variance similarity functions within the canopy sub-layer of a dense alpine forest. *Boundary-Layer Meteorology*, Vol. 128, pp. 33-57.

Campbell, G. S. and J. M. Norman: 1998, An introduction to environmental biophysics (2nd edition). Springer, New York, pp. 286.

Choi, T., J. Hong, J. Kim, H. Lee, J. Asanuma, H. Ishikawa, O. Tsukamoto, G. Zhiqiu, Y. Ma, K. Ueno, J. Wang, T. Koike, and T. Yasunari: 2004, Turbulent exchange of heat, water vapor, and momentum over a Tibetan prairie by eddy covariance and flux variance measurements. *Journal of Geophysical Research*, Vol. 109, D21106.

De Bruin, H. A. R., W. Kohsiek, and J. J. M. van den Hurk: 1993, A verification of some methods to determine the fluxes of momentum, sensible heat, and water vapour using standard deviation and structure parameter of scalar meteorological quantities. *Boundary-Layer Meteorology*, Vol. 63, pp. 231-257.

Detto, M. and G. G. Katul: 2007, Simplified expressions for adjusting higher-order turbulent statistics obtained from open path gas analyzers. *Boundary-Layer Meteorology*, Vol. 122, pp. 205-216.

Detto, M., G. Katul, M. Mancini, N. Montaldo, and J. D. Albertson: 2008, Surface heterogeneity and its signature in higher-order scalar similarity relationships. *Agricultural and Forest Meteorology*, Vol. 148, pp. 902-916.

Finnigan, J. J.: 2004, A re-evaluation of long-term flux measurement techniques Part II: Coordinate systems. *Boundary-Layer Meteorology*, Vol. 113, pp. 1-41.

Foken, T. and B. Wichura: 1996, Tools for quality assessment of surface-based flux measurements. *Agricultural and Forest Meteorology*, Vol. 78, pp. 83-105.

Foken, T., M. Göckede, M. Mauder, L. Mahrt, B. Amiro, W. Munger: 2004, Post-field data quality control. Pages 181-208 in: X. Lee, W. Massman, B.

Law (Eds). Handbook of micrometeorology: A guide for surface flux measurement and analysis. Kluwer Academic, New York.

Foken, T.: 2006, 50 years of the Monin-Obukhov similarity theory. *Boundary-Layer Meteorology*, Vol. 119, pp. 431-447.

Högström, U. and A. S. Smedman-Högström: 1974, Turbulence mechanisms at an agricultural site. *Boundary-Layer Meteorology*, Vol. 7, pp. 373-389.

Hsieh, C. I. and G. G. Katul: 1996, Estimation of momentum and heat fluxes using dissipation and flux-variance methods in the unstable surface layer. *Water Resources Research*, Vol. 32, No. 8, pp. 2453-2462.

Hsieh, C. I., G. Katul, and T. Chi: 2000, An approximate analytical model for footprint estimation of scalar fluxes in thermally stratified atmospheric flows. *Advances in Water Resources*, Vol. 23, pp. 765-772.

Hsieh, C. I., M. C. Lai, Y. J. Hsia, and T. J. Chang: 2008, Estimation of sensible heat, water vapor, and CO_2 fluxes using the flux-variance method. *International Journal of Biometeorology*, Vol. 52, pp. 521-533.

Kaimal, J. C. and J. J. Finnigan: 1994, Atmospheric boundary layer flows: Their structure and measurement. Oxford University, New York, pp. 289.

Katul, G., S. M. Goltz, C. I. Hsieh, Y. Cheng, F. Mowry, and J. Sigmon: 1995, Estimation of surface heat and momentum fluxes using the flux-variance method above uniform and non-uniform terrain. *Boundary-Layer Meteorology*, Vol. 74, pp. 237-260.

Klemm, O., S. C. Chang, and Y. J. Hsia: 2006, Energy fluxes at a subtropical mountain cloud forest. *Forest Ecology and Management*, Vol. 224, pp. 5-10.

Kustas, W. P., J. H. Blanford, D. I. Stannard, C. S. T., Daughtry, W. D. Nichols, and M. A. Weltz: 1994, Local energy flux estimates for unstable conditions using variance data in semiarid rangelands. *Water Resources Research*, Vol. 30, pp. 1351-1361.

Lamaud, E. and M. Irvine: 2006, Temperature-humidity dissimilarity and

heat-to-water-vapour transport efficiency above and within a pine forest canopy: The role of the Bowen ratio. *Boundary-Layer Meteorology*, Vol. 120, pp. 87-109.

Mahrt, L.: 1998, Flux sampling errors for aircraft and towers. *Journal of Atmospheric and Oceanic Technology*, Vol. 15, pp. 416-429.

Marques Filho, E. P., L. D. A. Sá, H. A. Karam, R. C. S. Alvalá, A. Souza, and M. M. R. Pereirá: 2008, Atmospheric surface layer characteristics of turbulence above the Pantanal wetland regarding the similarity theory. *Agricultural and Forest Meteorology*, Vol. 148, pp. 883-892.

Mauder, M. and T. Foken: 2004, Documentation and instruction manual of the eddy covariance software package TK2. Arbeitsergebnisse Nr. 26, Bayreuth.

McMillen, R. T.: 1987, An eddy correlation technique with extended applicability to non-simple terrain. *Boundary-Layer Meteorology*, Vol. 43, pp. 231-245.

Moriwaki, R. and M. Kanda: Local and global similarity in turbulent transfer of heat, water vapour, and CO_2 in the dynamic convective sublayer over a suburban area. *Boundary-Layer Meteorology*, Vol. 120, pp. 163-179.

Ohtaki Eiji: 1984, On the similarity in atmospheric fluctuations of carbon dioxide, water vapor and temperature over vegetated fields. *Boundary-Layer Meteorology*, Vol. 32, pp. 25-37.

Padro, J.: 1993, An investigation of flux-variance methods and universal functions applied to three land-use types in unstable conditions. *Boundary-Layer Meteorology*, Vol. 66, pp. 413-425.

Panofsky, H. A. and J. A. Dutton: 1984, Atmospheric turbulence: Models and methods for engineering applications. John Wiley & Sons, New York, pp. 397.

Paw U, K. T., D. Baldocchi, T. P. Meyers, K. B. Wilson: 2000, Correction of eddy-covariance measurements incorporating both advective effects and density fluxes. Boundary-Layer Meteorology, Vol. 97, pp. 487-511.

Rebmann, C., M. Göckede, T. Foken, M. Aubinet, M. Aurela, P. Berbigier, C. Bernhofer, N. Buchmann, A. Carrara, A. Cescatti, R. Ceulemans, R. Clement, J. A. Elbers, A. Granier, T. Grünwald, D. Guyon, K. Havránková, B. Heinesch, A. Knohl, T. Laurila, B. Longdoz, B. Marcolla, T. Markkannen, F. Miglietta, J. Moncrieff, L. Montagnani, E. Moors, M. Nardino, J.-M. Ourcival, S. Rambal, Ü. Rannik, E. Rotenberg, P. Sedlak, G. Unterhuber, T. Vesala, and D. Yakir: 2005, Quality analysis applied on eddy covariance measurements at complex forest sites using footprint modelling. *Theoretical and Applied Climatology*, Vol. 80, pp. 121-141.

Roth, M. and T. R. Oke: 1995, Relative efficiencies of turbulent transfer of heat, mass, and momentum over a patchy urban surface. *Journal of the Atmospheric Sciences*, Vol. 52, No. 11, pp. 1863-1874.

Scanlon, T. M. and P. Sahu: 2008, On the correlation structure of water vapor and carbon dioxide in the atmospheric surface layer: A basis for flux partitioning. *Water Resource Research*, Vol. 44, W10418, pp. 15.

Tillman, J. E.: 1972, The indirect determination of stability, heat and momentum fluxes in the atmospheric boundary layer from simple scalar variables during dry unstable conditions. *Journal of Applied Meteorology*, Vol. 11, pp. 783-792.

Weaver, H. L.: 1990, Temperature and humidity flux-variance relations determined by one-dimensional eddy correlation. *Boundary-Layer Meteorology*, Vol. 53, pp. 77-91.

Webb, E. K., G. I. Pearman, and R. Leuning: 1980, Correction of flux measurements for density effects due to heat and water transfer. *Quarterly Journal of the Royal Meteorological Society*, Vol. 106, pp. 85-100.

Wesely, M. L.: 1987, Use of variance techniques to measure dry air-surface exchange rates. *Boundary-Layer Meteorology*, Vol. 44, pp. 13-31.

Wesson, K. H., G. Katul, and C. T. Lai: 2001, Sensible heat flux estimation by flux

variance and half-order time derivative methods. *Water Resources Research*, Vol. 37, pp. 2333-2343.

Wilczak, J. M., S. P. Oncley, and S. A. Stage: 2001, Sonic anemometer tilt correction algorithms. *Boundary-Layer Meteorology*, Vol. 99, pp. 127-150.

Table 1. Wind velocity characteristics presented in previous studies: (a) under unstable condition ($\zeta < 0$), (b) under stable condition ($\zeta > 0$), and (c) under neutral condition ($\zeta \to 0$) (revised from Table 1 of Marques et al. 2008).

(a)

study	description	z	h	σ_u/u_*	σ_w/u_*
Panofsky et al. (1984)				$2.29(1-0.04\zeta)^{1/3}$	$1.25(1-3\zeta)^{1/3}$
Wesely (1988)	bare soil	7.7			$1.3(1-2\zeta)^{1/3}$
De Bruin et al. (1993)	plain	11.3		$2.2(1-3\zeta)^{1/3}$	
Andreas et al. (1998)	flat grass land	4	0.25		$1.07(1-4.29\zeta)^{1/3}$
Choi et al. (2004)	Tibetan prairie	2.85	0.05	$3.13(1-8\zeta)^{1/3}$	$1.12(1-2.8\zeta)^{1/3}$
Detto et al. (2008)	Mediterranean	10	5		$1.2(1-2\zeta)^{1/3}$
Marques et al. (2008)	wetland	25	7		$1.17(1-2.44\zeta)^{1/3}$

(b)

study	z	h	σ_u/u_*	σ_w/u_*
Kaimal and Finnigan (1994)				$1.25+0.25\zeta$
Marques et al. (2008)	25	7	$1.74+0.36\zeta$	$1.16+0.12\zeta$

(c)

study	σ_w/u_*	σ_u/u_*
Pantanal region	1.33 ± 0.02	2.21 ± 0.03
Moraes et al. (2005)	1.20	2.40
Krishnan and Kunhikrishnan (2002)	1.37	2.32 ± 0.39
Pahlow et al. (2001)	1.10	2.30
Andreas et al. (1998)	1.20	2.55
Högström (1990)	---	2.78 ± 0.25
Kader and Yaglom (1990)	1.25	2.70
Panofsky and Dutton (1984)	1.25 ± 0.03	2.39 ± 0.03
Merry and Panofsky (1976)	1.30	---
Monin and Yaglom (1971)	1.25	2.30

Table 2. Scalar characteristic constants presented in previous studies; z_0, z, and h are in unit of meters.

study	site description	z_0	z	h	C_T	C_q	C_c
Tillman (1972) (a)	flat grass terrain		40		0.95		
Tillman (1972) (b)	salt flats		8		0.92		
Högström et al. (1974)	agricultural site		3		0.92	1.04	
Ohtaki (1984)	wheat field		*1.33	*0.63	0.95	1.1	1.1
Wesely (1988)	grass / bar soil		7.7		^1.25	^1.25	^1.25
Weaver (1990)	prairie	0.03			1.0		
De Bruin et al. (1993)	plain		11.3		0.95		
Kustas et al. (1994)	shrub	0.03			1.1		
Albertson et al. (1995)	Owens lake bed		2.5	0	0.97		
Hsieh and Katul (1996)	grass	0.065			1.1		
Andreas et al. (1998)	flat grass land	0.04			1.05	1.34	
Asanuma (1999)	flat pine forest	1.2			0.92	1.42	
Wesson et al. (2001)	pine forest		14.5	14	1.3		
	bare soil	0.01			0.99		
Choi et al. (2004)	Tibetan prairie		2.85	0.05	1.1	1.1	
Lamaud and Irvine (2006)	Maritime pine		40	19	0.95	1.3	
Cava et al. (2008)	coniferous forest		32	29	1.09	1.61	1.32
Detto et al. (2008)	Mediterranean		10	5	(1.18)	(1.18)	(1.18)
Hsieh et al. (2008) (a)	grassland		10	0.45	1.1	1.1	0.95
Hsieh et al. (2008) (b)	rice paddy		2	0.65	1.0	1.0	1.0
Hsieh et al. (2008) (c)	cypress forest		23.8	10.3	1.25	1.5	1.7
Marques et al. (2008)	wetland		25	7	1.15		
袁一夫 (2008)	蓮華池林地(dry)		25	17	1.19	1.55	
	蓮華池林地(wet)		25	17	1.09	1.37	

* Average of the three days selected

( ) Determined with very strict filtering ranges

^ Finding the same value

Table 3. Data filtering thresholds in Detto et al. (2008) (quoted from Table 1 of Detto et al., 2008).

Variable	Unit	Range	Number of runs
$\overline{w'T'}$	K m s^{-1}	0.03 to 0.39	9863
u_*	m s^{-1}	0.05 to 2	25311
$\overline{u}$	m s^{-1}	>1	32399
$\overline{w}$	m s^{-1}	-0.12 to 0.12	25526
$\overline{w'q'}$	g m^{-2} s^{-1}	0.02 to 0.2	8225
$\overline{w'c'}$	mg m^{-2} s^{-1}	-0.02 to -1.5	11684
$\overline{q'^2}$	g^2	<1.5	25164
$\overline{c'^2}$	g^2	<30	23267

Table 4. Instrument locations and brief instructions (quoted from Appendix 8.1 of 褚侯森, 2008).

Instrument	Unit	Observation parameter	Location
Net radiatiometer CNR-1, Kipp & Zonen	W m^{-2}	upward/downward short-wave radiation (0.3-3 μm) upward/downward long-wave radiation (5-42 μm)	tower 22.5 m
Quantum sensor LI-190, LICOR	μmole m^{-2} s^{-1}	photo-synthetically active radiation quantum flux (0.4-0.7 μm)	tower 23.6 m
MIRA visibility sensor 3544, Aanderaa	m	visibility	tower 22.0 m
Aspirated radiation shield 43408 & relative humidity / air temperature sensor 41382, R. M. Young	°C %	air temperature relative humidity	tower 23.6 m
Rain intensity recorder TIC-1, Takeda	mm	precipitation	nearby clearance
Barometric pressure sensor 61202V, R. M. Young	mb	atmosphere pressure	tower 2 m
Soil temperature sensor, Mingguan	℃	Soil temperature	soil 0.1 m depth
Soil heat flux sensor HFP01, Hukseflux	W m^{-2}	Soil heat flux	soil 0.1 m depth

Table 5. EC system operation periods (personal contact with 褚侯森, 2008).

period	Sonic Anemometer	Infrared Gas Analyzer
2005/03/05 - 2005/12/05	Young81000v(-)	LI7500(-)
2005/12/06 – 2006/05/16	Young81000v(1564)	LI7500(0951)
2006/05/17 – 2006/06/30	Young81000v(1564)	LI7500(0598)
2006/07/01 – 2006/09/27	Gill R3-50(367)	OP-II
2006/09/28 – 2006/12/14	Gill R3-50(367)	LI7500(0598)
2006/12/15 – 2007/06/21	Gill R3-50(367)	LI7500(0951)
2007/06/23 – 2009/03/27	CSAT3(-)	LI7500(-)

( ) Instrument model type

Table 6. Wind velocity similarity characteristic analysis results: (a) under unstable condition, (b) under stable condition, and (c) under unstable condition.

(a) $\sigma_{u,w}/u_* = C_1(1 - C_2\zeta)^{1/3}$.

Term	wind direction	amount	C_1	C_2	RMSE	residual test mean	residual test stdev
σ_u/u_*	uphill	2306	2.18	0.69	1.129	0.0016	1.129
	downhill	1733	2.81	0.49	1.774	0.0119	1.774
σ_w/u_*	uphill	2306	1.20	1.90	0.428	-0.0071	0.428
	downhill	1733	1.30	1.21	0.643	0.0168	0.643

(b) $\sigma_{u,w}/u_* = C_1 + C_2\zeta$.

term	wind direction	amount	C_1	C_2	R^2
σ_u/u_*	uphill	446	2.542	0.502	0.234
	downhill	3913	2.471	0.674	0.299
σ_w/u_*	uphill	446	1.242	0.292	0.277
	downhill	3913	1.155	0.324	0.383

(c) Approached to constants when $|\zeta| \to 0$.

term	wind direction	$\zeta > 0$	$\zeta < 0$
σ_u/u_*	uphill	2.54	2.18
	downhill	2.47	2.81
σ_w/u_*	uphill	1.24	1.2
	downhill	1.16	1.3

Table 7. Similarity scalar characteristic constants under unstable conditions with function $\sigma_x / x_* = C_x (-\zeta)^{-1/3}$.

term	wind direction	amount	C_x	RMSE	residual test mean	residual test stdev
σ_T / T_*	uphill	2163	1.166	0.060	-0.0004	0.060
	downhill	1040	1.293	0.132	0.0019	0.132
σ_q / q_*	uphill	3757	1.725	1.110	-0.0139	1.101
	downhill	2127	2.031	2.988	0.0429	2.988
σ_q / q_* 2	uphill	337	1.572	0.215	0.0044	0.215
	downhill	159	1.772	0.269	0.0070	0.270
σ_c / c_*	uphill	4534	1.605	2.301	-0.5977	2.223
	downhill	2533	1.937	2.967	-0.4712	2.929
σ_c / c_* 2	uphill	401	1.452	0.120	0.0031	0.121
	downhill	204	1.492	0.138	0.0008	0.139

2: filtered with Bowen ratio range

Table 8. Probability distribution function analysis for maximum occurrence values of the correlation coefficients and relative transport efficiencies in this study.

study	R_{wT}	R_{wq}	$-R_{wc}$	λ_{Tq}	$-\lambda_{Tc}$	λ_{qc}
uphill wind direction	0.61	0.46	0.49	1.11	1.1	0.95
downhill wind direction	0.59	0.48	0.48	1.13	1.08	0.88

Table 9. Flux variance method checked with records from April and May, 2009.

term	number	slope	intercept	R^2
H *	1165	0.91	58.26	0.74
LE a		0.67	36.11	0.48
LE a2	829	0.75	26.43	0.59
LE b2		1.07	18.80	0.62
F_{CO_2} a		0.49	-4.35	0.43
F_{CO_2} a2	862	0.60	-3.73	0.62
F_{CO_2} b2		0.81	-3.04	0.70

*: FV method from Katul et al. (1995)

a: FV method from Hsieh et al. (2008)

b: FV method from Choi et al. (2004)

2: filtered with Bowen ratio range

Table 10. Determine factors of relationship between λ_{Tq} and R_{Tq}: (a) a and b values and (b) regression result of a and b with measured data correlation test.

(a) $R_{Tq} = a\lambda_{Tq}^{-1} + b$

Bowen ratio	uphill wind direction		downhill wind direction	
	a	b	a	b
0.4-0.6	3.9683	-2.8289	2.9709	-2.0048
0.6-0.8	2.3987	-1.3336	2.1523	-3.1339
0.8-1.0	1.9596	-0.9124	1.9516	-0.9167
1-2	1.5858	-0.5482	1.5489	-0.5062
2-3	1.3543	-0.3095	1.4806	-0.3841
3-4	1.1252	-0.1196	1.0290	-0.0269

(b)

Bowen ratio	relation function	wind direction	check slope / R^2
$0.4 < Bo < 1$	$R_{Tq} = (-5.02Bo + 6.29)\lambda_{Tq}^{-1} + 4.79Bo - 5.05$	uphill	1.1312
	$R_{Tq} = (-2.55Bo + 4.14)\lambda_{Tq}^{-1} + 2.72Bo - 3.25$	downhill	0.0496
$1 < Bo < 4$	$R_{Tq} = 0.9116\lambda_{Tq}^{-1}$	uphill	0.9989
	$R_{Tq} = 0.9239\lambda_{Tq}^{-1}$	downhill	0.2241

Table 11. Determine factors of relationship between λ_{Tc} and R_{Tc}: (a) a and b values, (b) regression result of a and b with measured data correlation test.

(a) $R_{Tc} = a\lambda_{Tc}^{-1} + b$

Bowen ratio	uphill wind direction		downhill wind direction	
	a	b	a	b
0.4-0.6	1.8116	0.8590	1.7009	-0.8382
0.6-0.8	1.4928	0.5747	1.4832	-0.6201
0.8-1.0	1.1481	0.2617	1.4327	-0.5642
1-2	1.1617	0.2601	1.2994	-0.4036
2-3	1.3891	0.4456	1.4520	-0.5034
3-4	1.5733	0.6015	1.5878	-0.6186

(b)

Bowen ratio	relation function	wind direction	check slope / R^2
$0.4 < Bo < 1$	$R_{Tc} = (-1.66Bo + 2.65)\lambda_{Tq}^{-1} - 1.5Bo + 1.61$	uphill	0.9651
	$R_{Tc} = (-0.67Bo + 2.01)\lambda_{Tc}^{-1} - 0.69Bo + 1.15$	downhill	0.1221
$1 < Bo < 5$	$R_{Tc} = 0.8445\lambda_{Tc}^{-1}$	uphill	0.9586
	$R_{Tc} = 0.8193\lambda_{Tc}^{-1}$	downhill	0.3078
$1 < Bo$	$R_{Tc} = \lambda_{Tc}^{-0.55}$	uphill	0.9319
	$R_{Tc} = \lambda_{Tc}^{-0.5}$	downhill	0.4894

Table A1. Classification of ratio of non-stationarity.

Class	NR_{cov} range
1	0-15%
2	16-30%
3	31-50%
4	51-75%
5	76-100%
6	101-250%
7	251-500%
8	501-1000%
9	>1000%

Classes 1 to 3 can be used for fundamental research, such as the development of parameterizations, and classes 4 to 6 are available for general use of continuously running systems of long-term measurement programs. Classes 7 and 8 are only for orientation. Sometimes it is better to use such data instead of a gap filling procedure, but then these data should not differ significantly from the data before and after these data in the time series. Data of class 9 should be excluded under all circumstances.

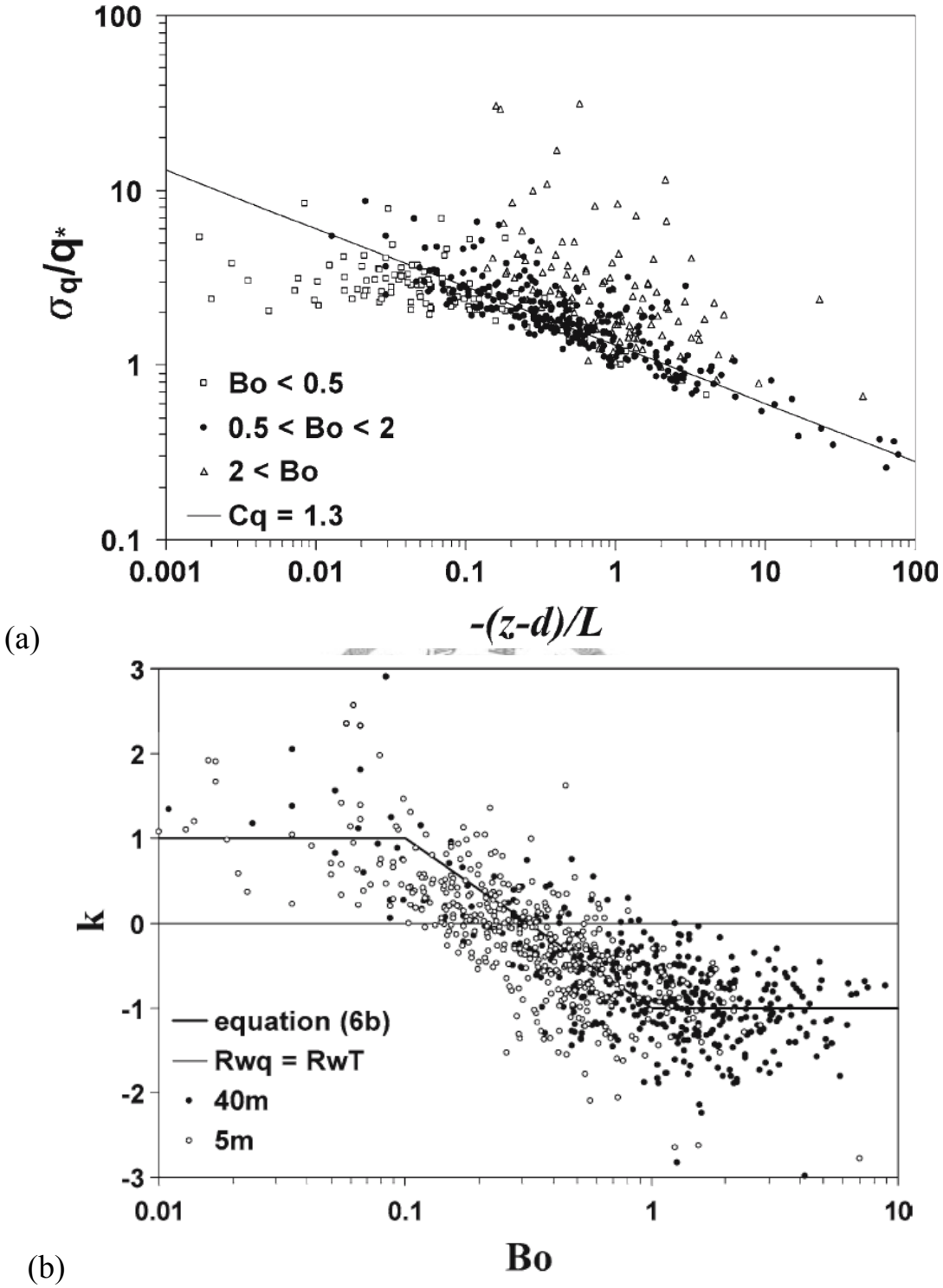

Figure 1. Water vapor similarity characteristics analysis done by Lamaud and Irvine over a dry and wet transitional period; (a) the relation between -1/3 power function and Bowen ratio (quoted from Figure 2 of Lamaud and Irvine, 2006), and (b) the relation between $k = \log(\lambda)/\log(R_{Tq})$ and Bowen ratio (quoted from Figure 7 of Lamaud and Irvine, 2006).

(a)

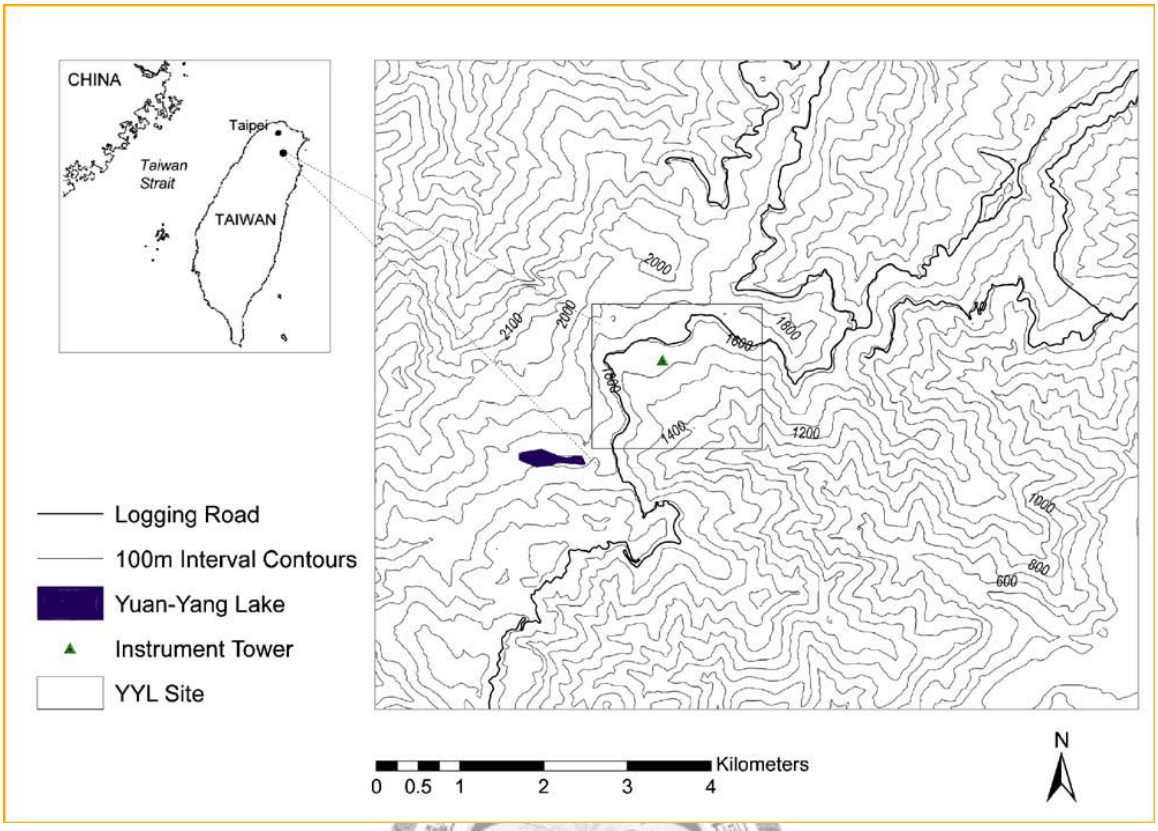
CHINA
Taipei
Taiwan Strait
TAIWAN
Logging Road
100m Interval Contours
Yuan-Yang Lake
Instrument Tower
YYL Site
2000
2100
2000
1800
1600
1400
1200
1000
800
600
0 0.5 1 2 3 4
Kilometers
N

(b)


CLM site
#120 Station
#130 Station
Yuan-Yang Lake
N

(c)

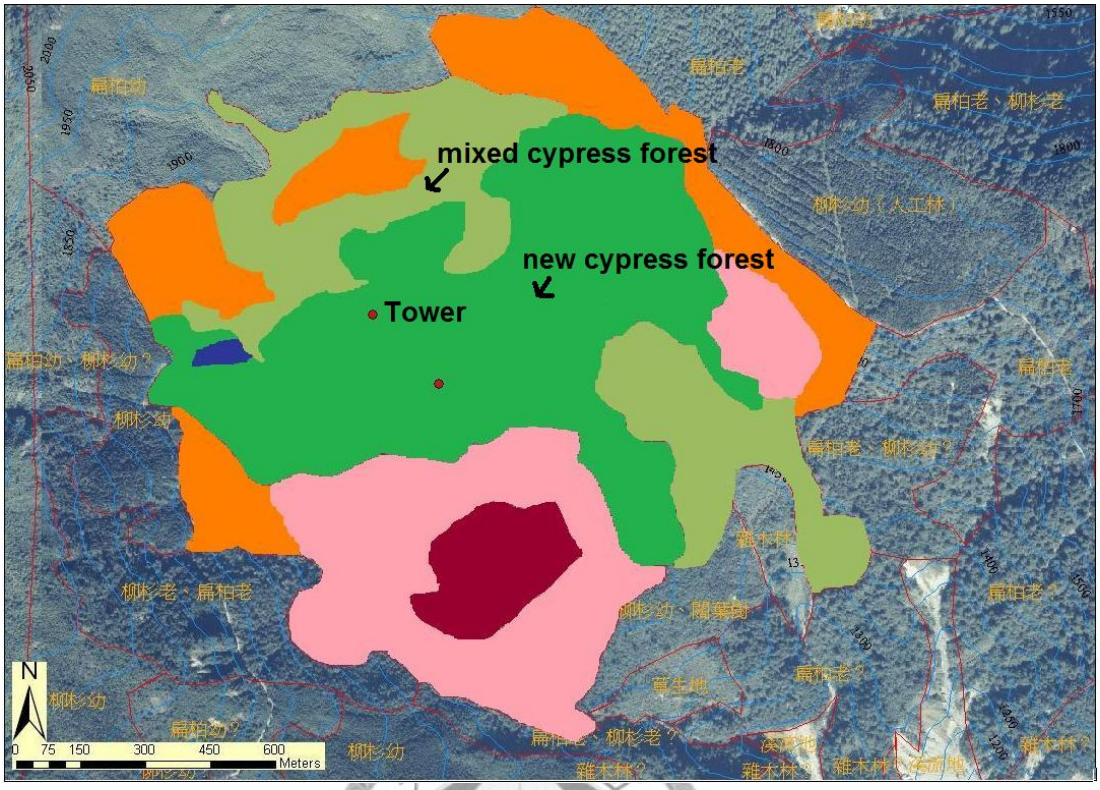

Figure 2. Map of the experiment site in Chi-Lan Mountain area, Ilan, Taiwan: (a) a zoom in look with contour lines (the green triangle is the measurement tower, quoted from Fig. 1 of Klemm et al., 2006), (b) a valley-toward-hilltop view from Google Earth (CLM site is the measurement tower), and (c) the vegetation coverage investigation results (the red circle with Tower aside is the measurement tower, revised from Fig. 12 of 褚侯森, 2008).

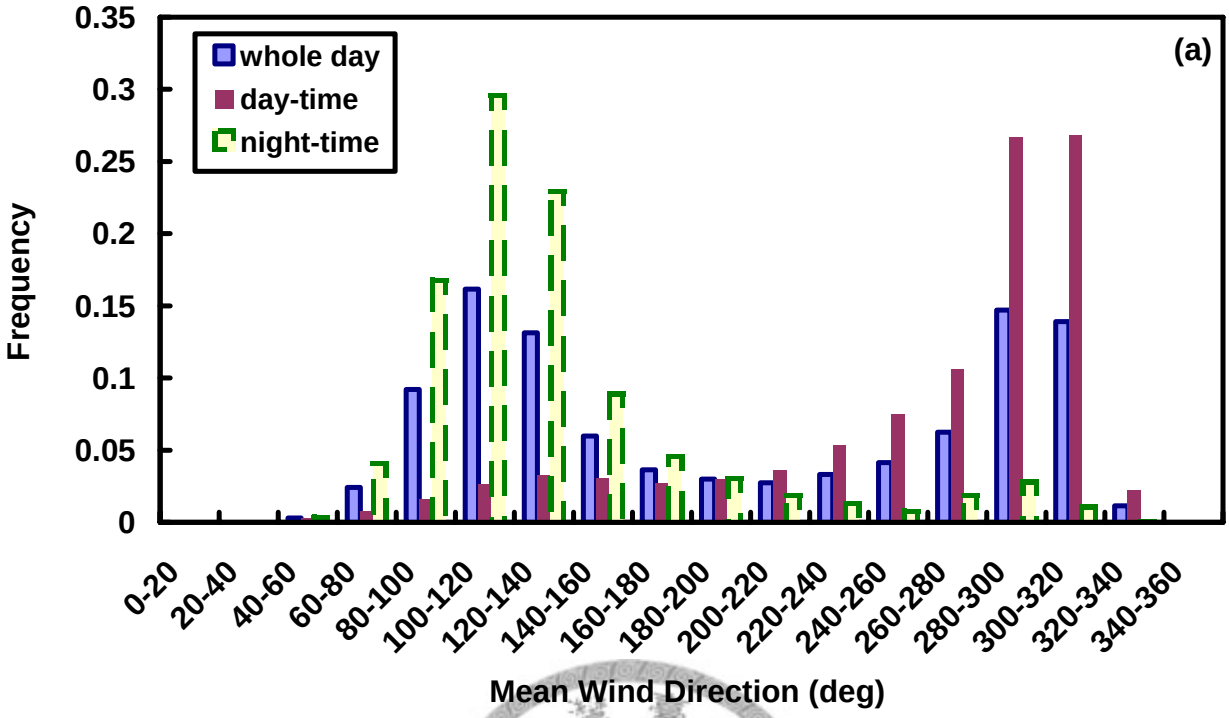

Figure 3. Mean wind direction frequency graph with data from 2005 for example; showed in classification of whole day, day-time, and night-time periods.

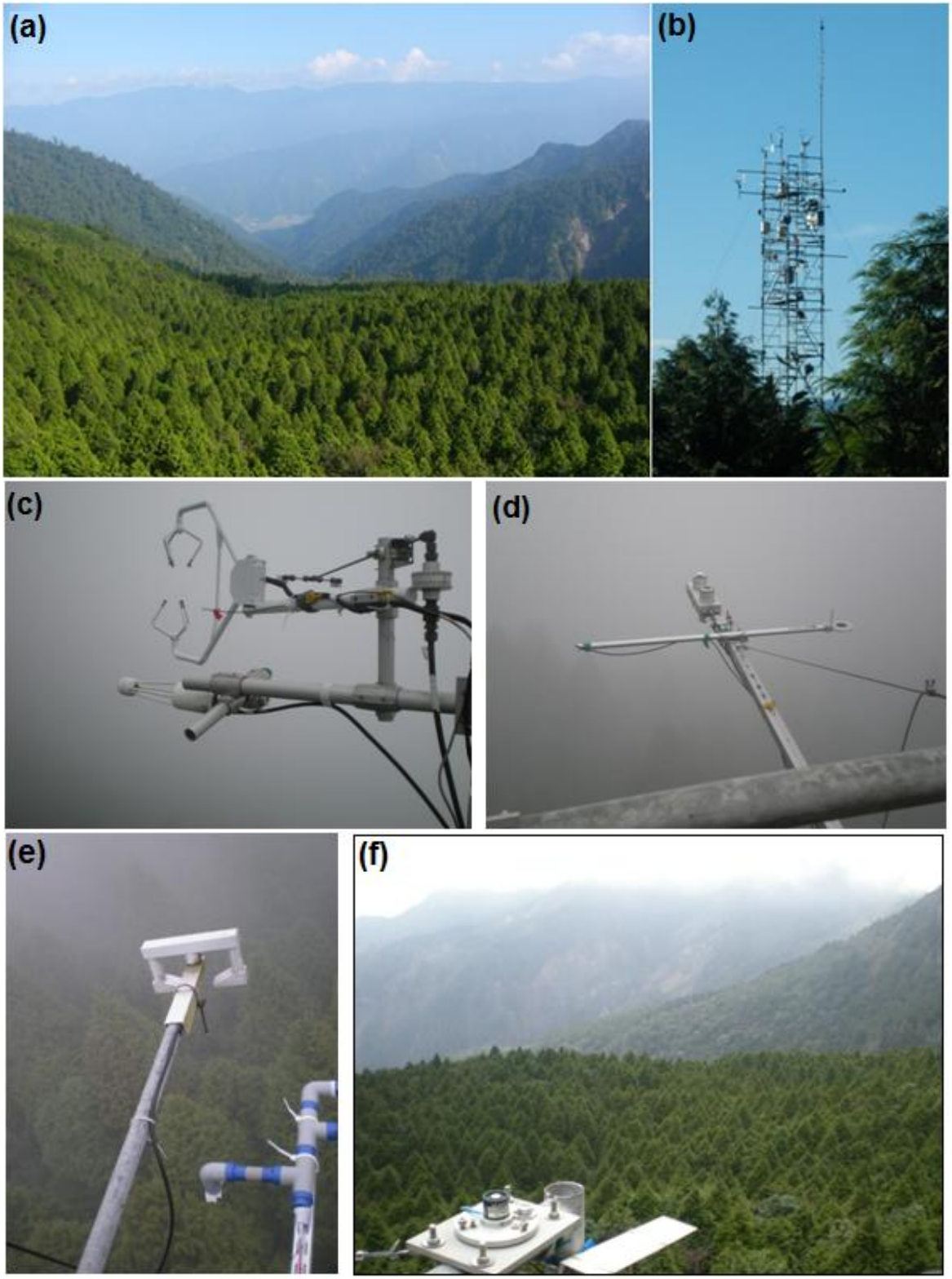

Figure 4. Photos of the experimental site: (a) down-hill direction view on top of the measurement tower, (b) side view of the measurement tower, (c) EC system mounted at 23.8 m (2009/3), (d) CNR-1 mounted at 22.5 m (2009/3), (e) MIRA visibility sensor mounted at 22 m (2009/3), and (f) LI-190 mounted at 23.5 m (2009/3).

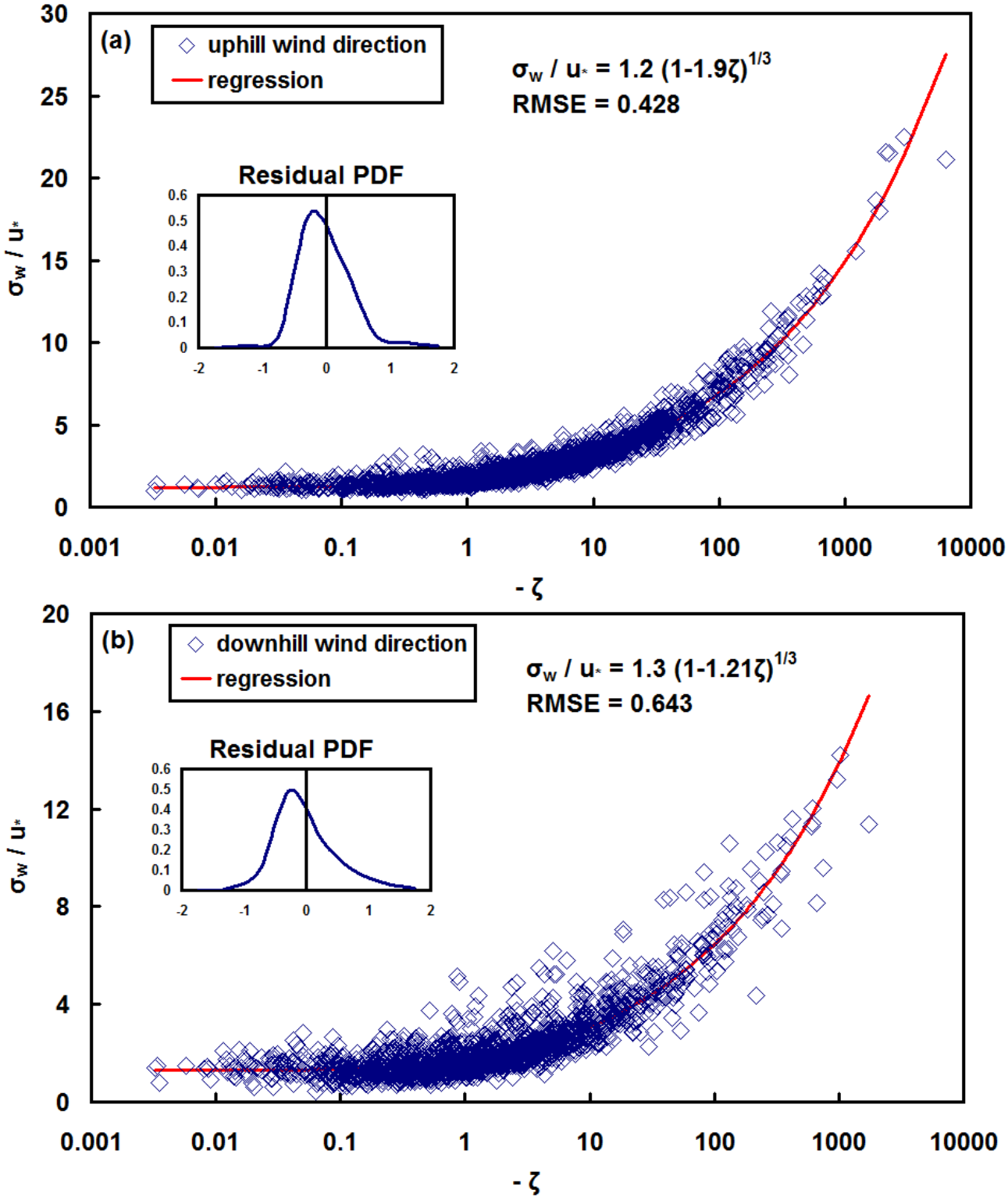

Figure 5. MOST similarity test on vertical wind velocity (σ_w/u_*) plotted against thermal stability with wind direction: (a) uphill and (b) downhill. The residual PDF graph is the residual probability density function of the red regression line and the blue open square measured record.

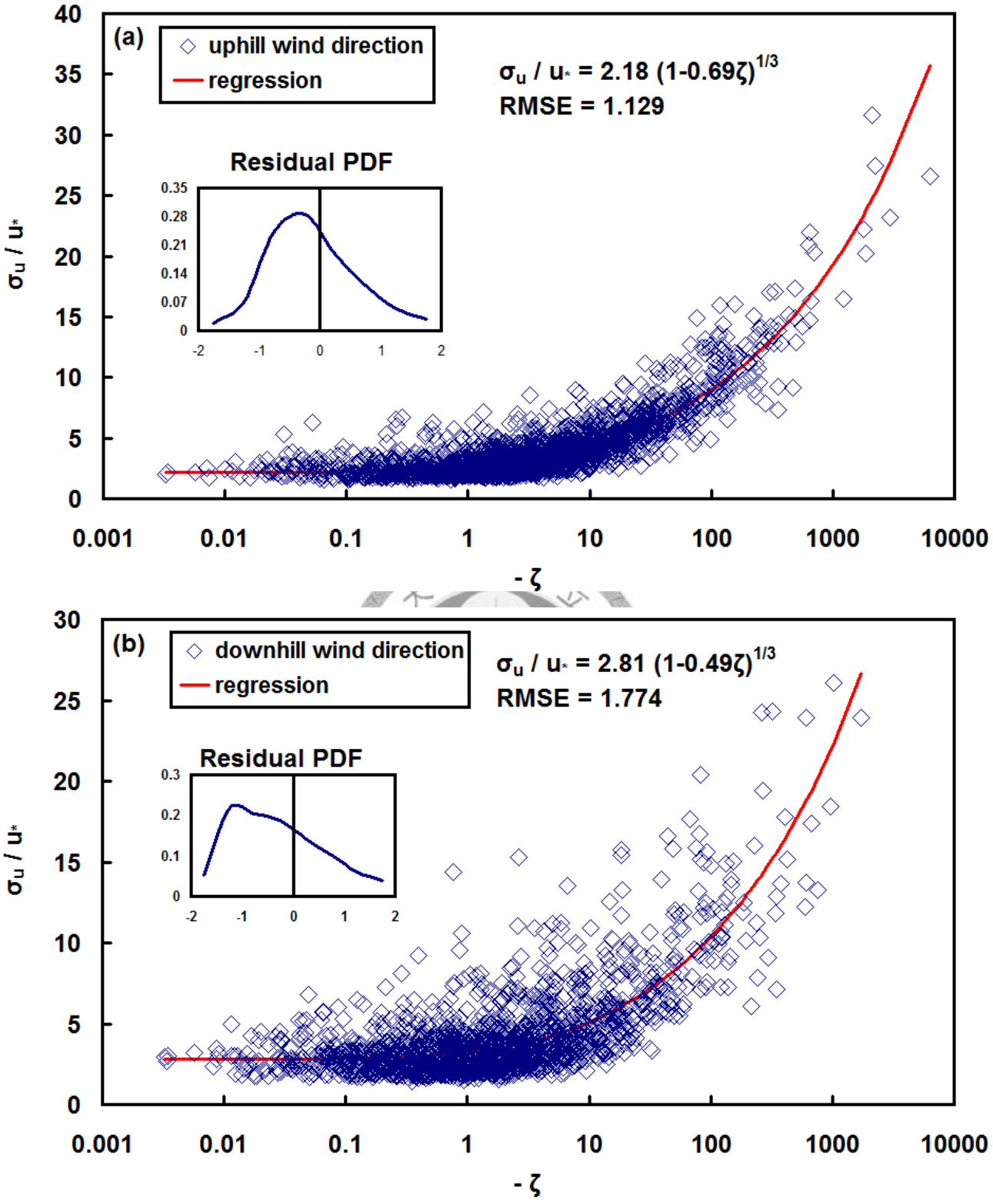

Figure 6. MOST similarity test on horizontal wind velocity (σ_u/u_*) plotted against thermal stability with wind direction: (a) uphill and (b) downhill. With residual PDF graphs same as in Figure 7.

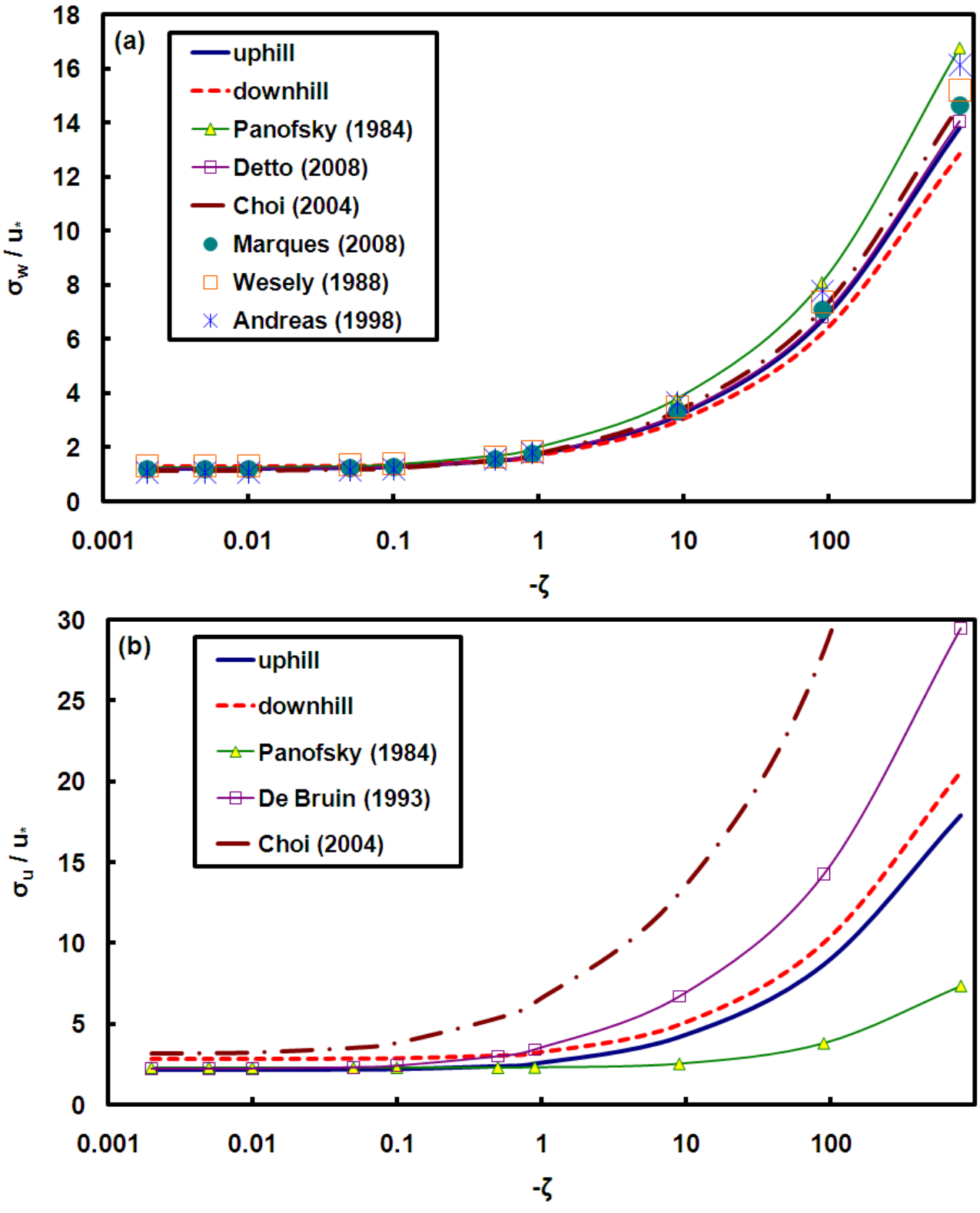

Figure 7. Regression results in MOST wind velocity similarity functions from previous studies in compare with this study: (a) vertical wind velocity and (b) horizontal wind velocity.

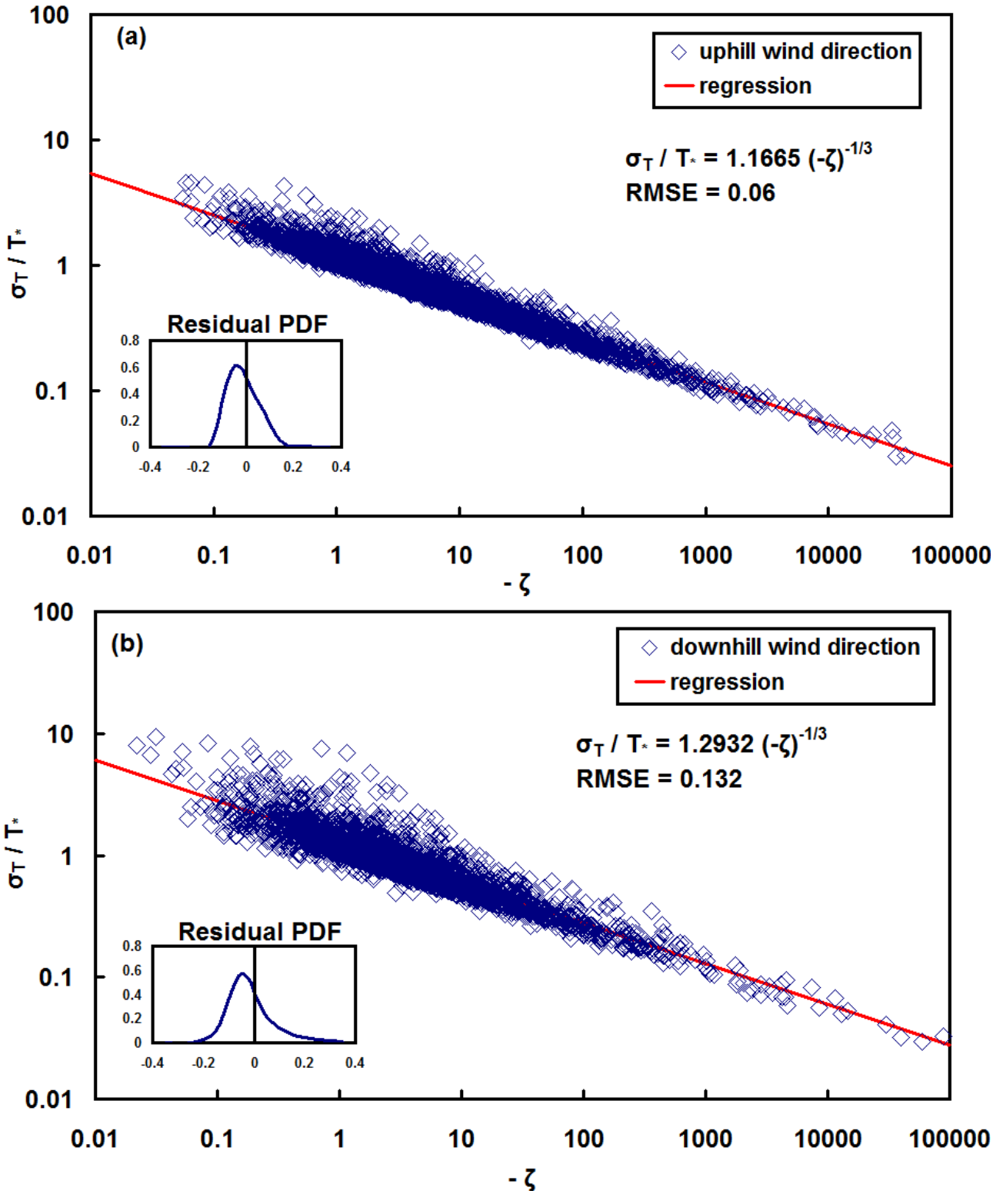

Figure 8. MOST similarity test on temperature (σ_T / T_*) under unstable condition plotted against thermal stability with wind direction: (a) uphill and (b) downhill. With residual PDF graphs same as in Figure 7.

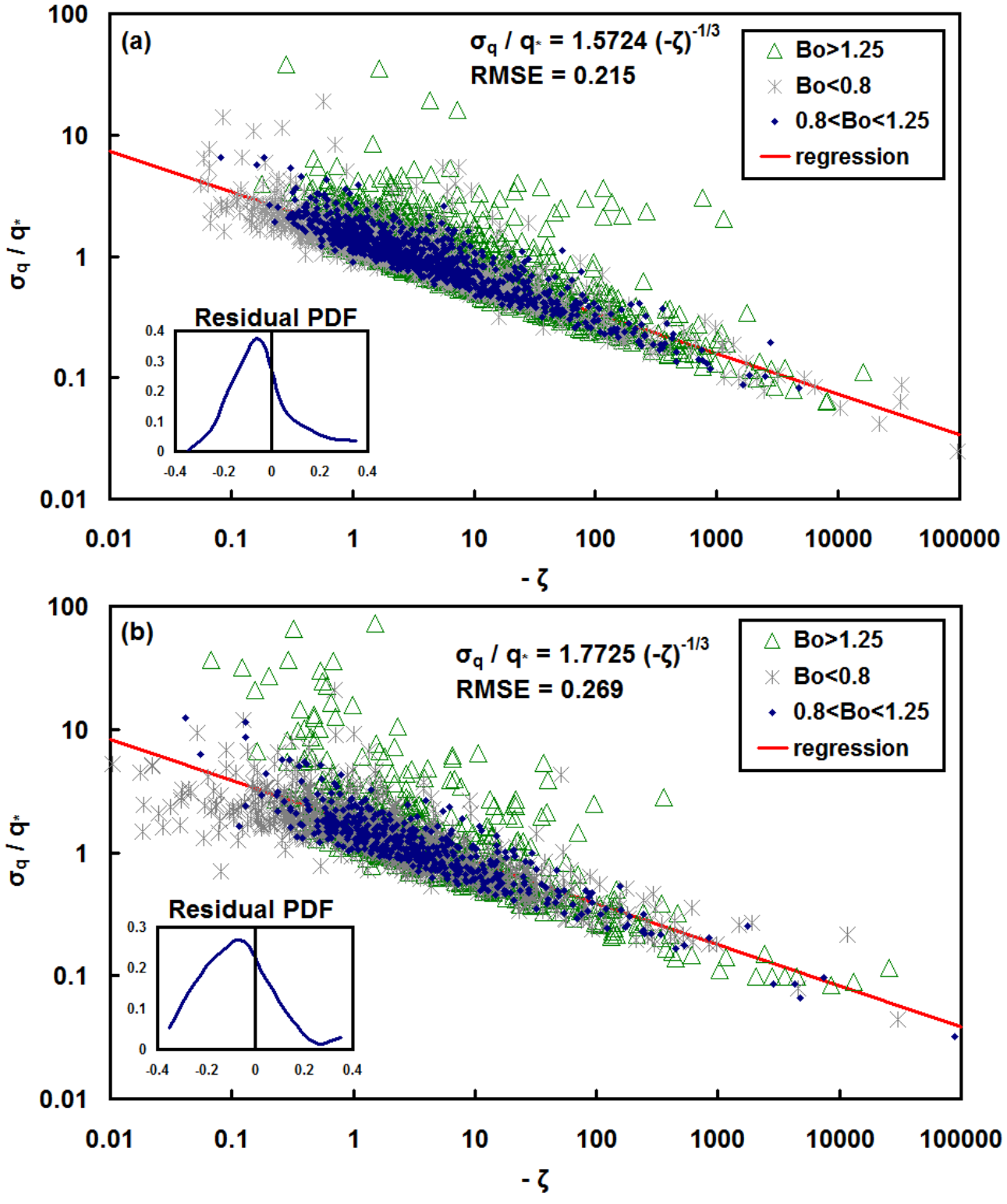

Figure 9. MOST similarity test on water vapor (σ_q/q_*) under unstable condition plotted against thermal stability with wind direction: (a) uphill and (b) downhill. Red lines are regression with records in the range of $0.8 \le Bo \le 1.25$. With residual PDF graphs same as in Figure 7.

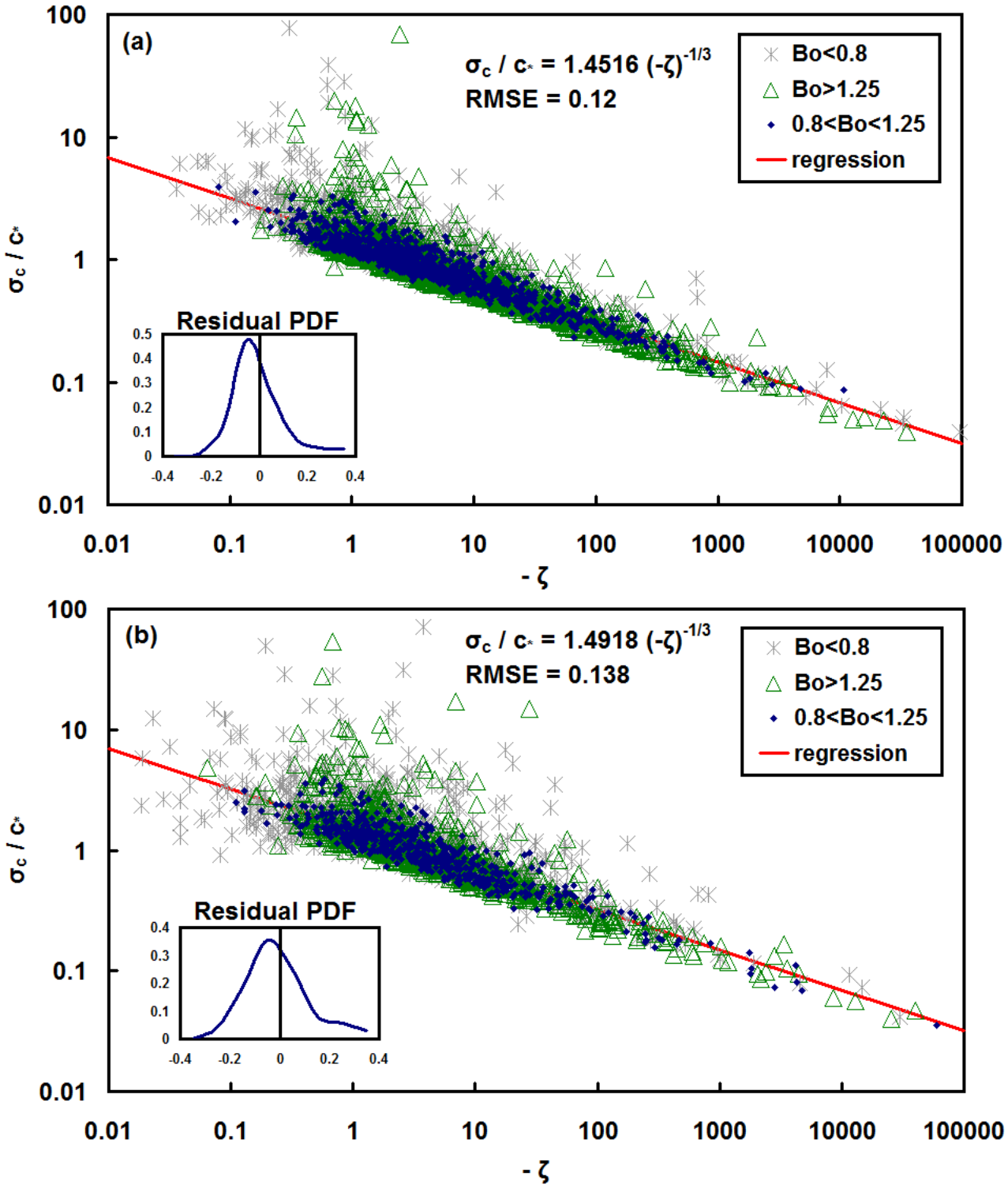

Figure 10. MOST similarity test on CO_2 (σ_c/c_*) under unstable condition plotted against thermal stability with wind direction: (a) uphill and (b) downhill. Red lines are regression with records in the range of $0.8 \le Bo \le 1.25$. With residual PDF graphs same as in Figure 7.

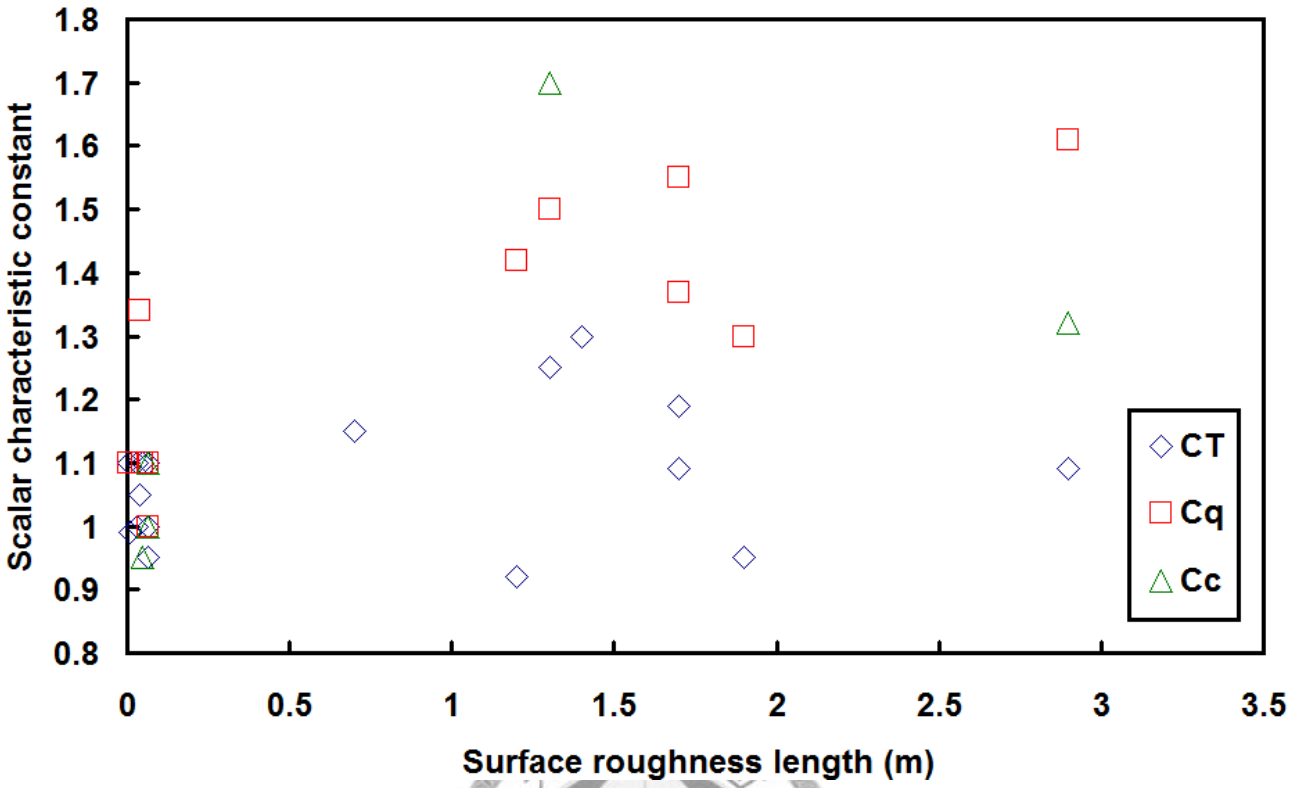

Figure 11. Scalar characteristic constants found in previous studies and this study plotted against the roughness length.

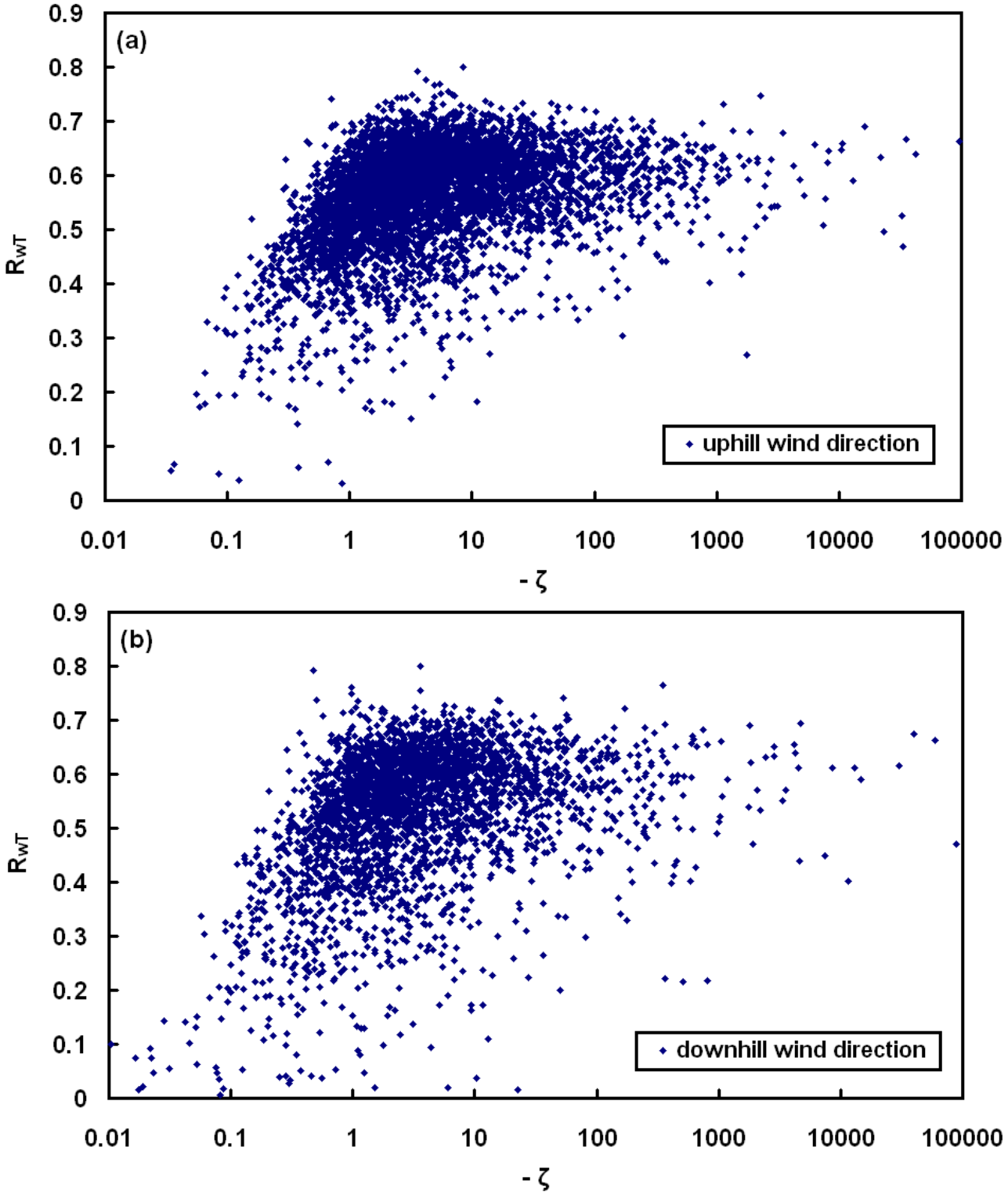

Figure 12. Correlation coefficients of vertical wind velocity and temperature (R_{wT}) plotted against thermal stability in wind direction: (a) uphill and (b) downhill.

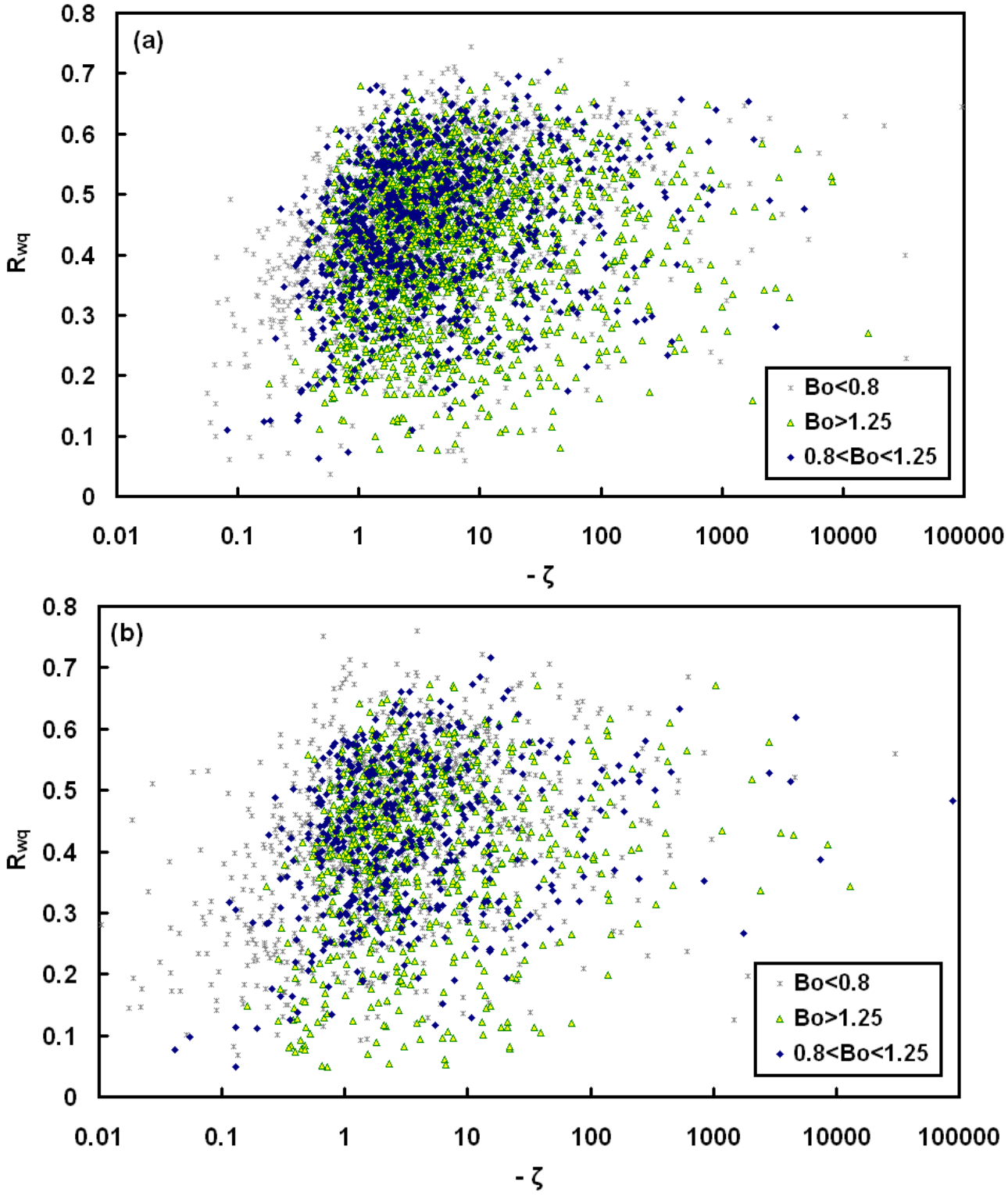

Figure 13. Correlation coefficients of vertical wind velocity and water vapor (R_{wq}) plotted against thermal stability in wind direction: (a) uphill and (b) downhill.

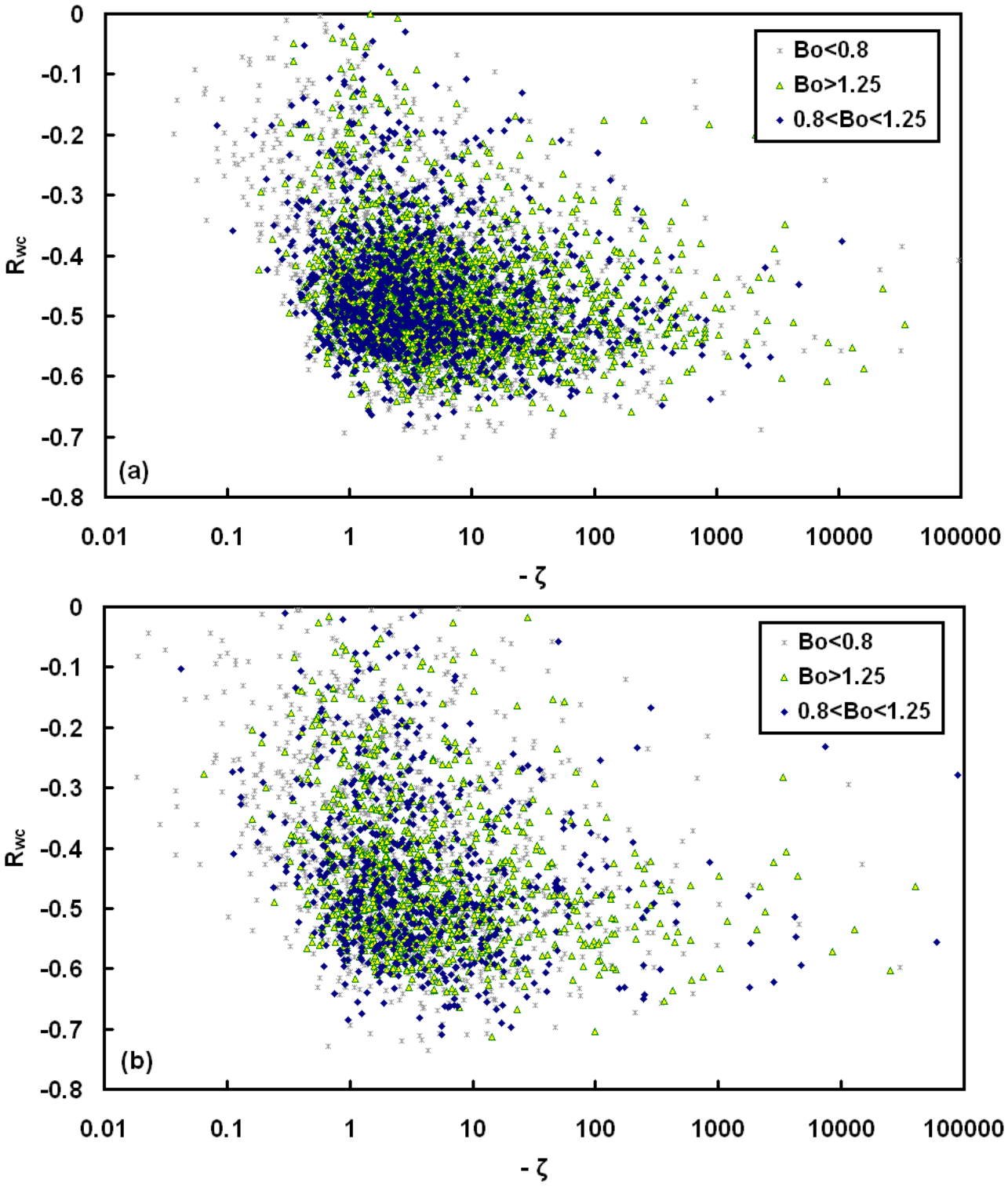

Figure 14. Correlation coefficients of vertical wind velocity and CO_2 (R_{wc}) plotted against thermal stability in wind direction: (a) uphill and (b) downhill.

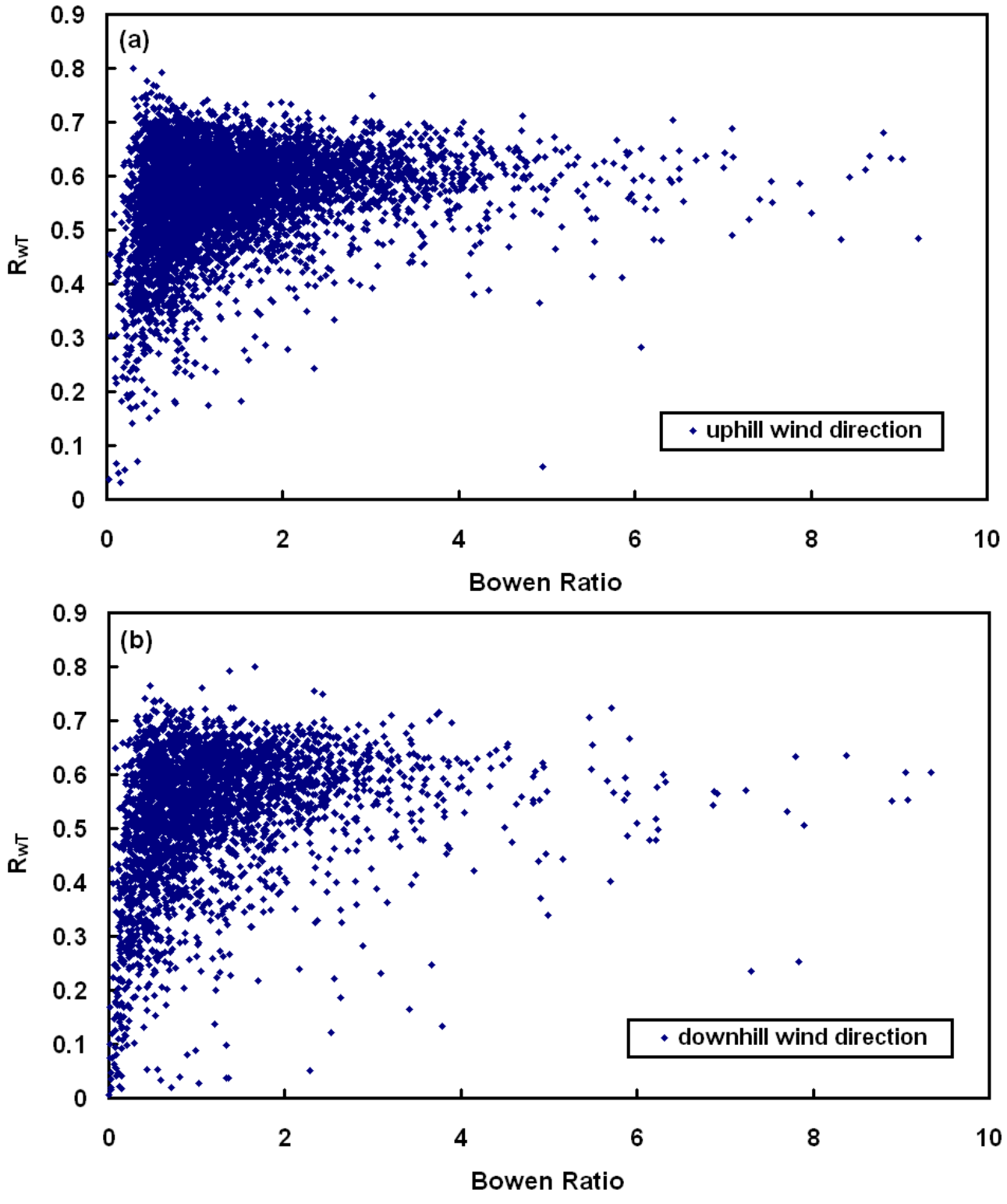

Figure 15. Correlation coefficients of vertical wind velocity and temperature (R_{wT}) plotted against Bowen Ratio in wind direction: (a) uphill and (b) downhill.

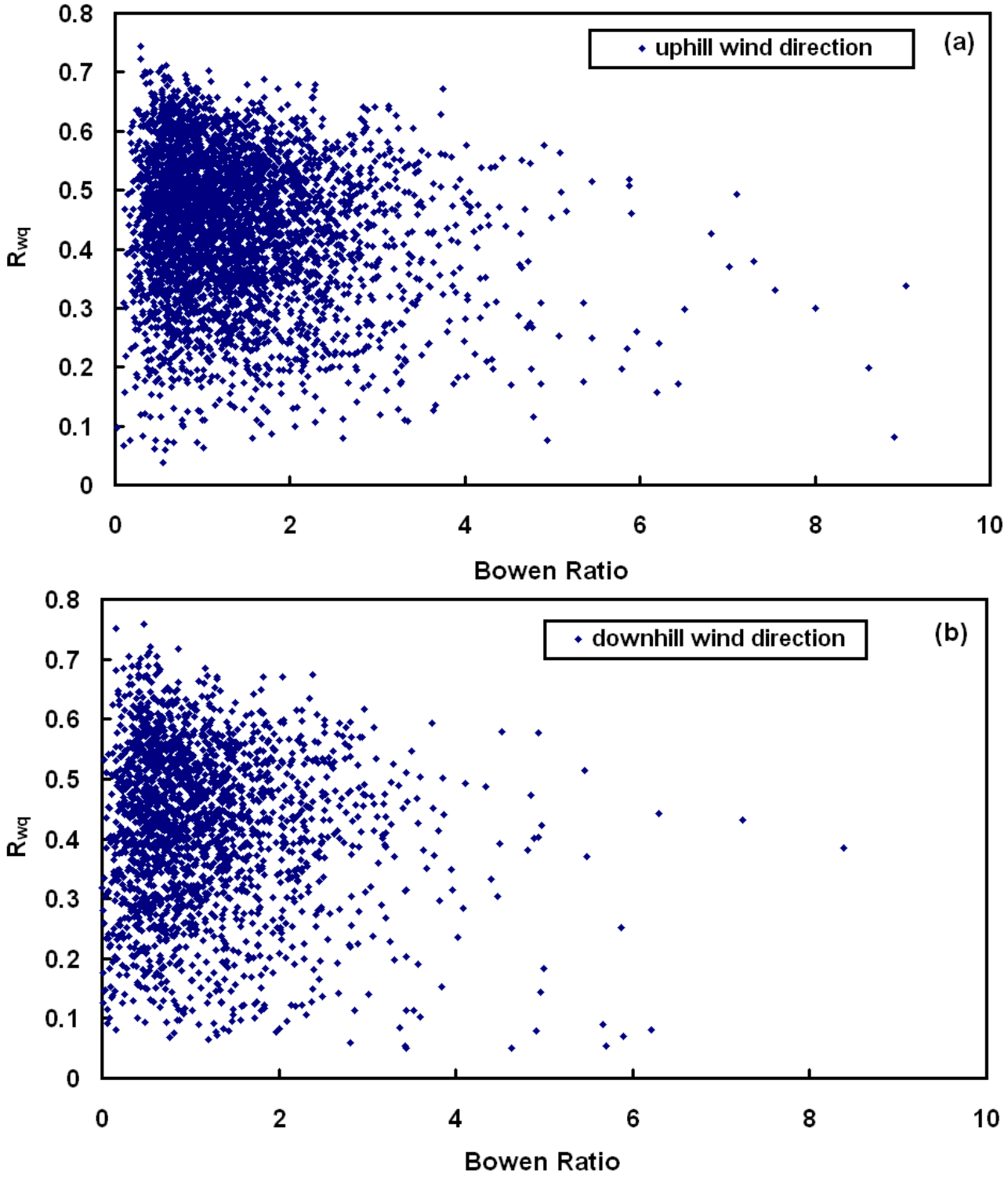

Figure 16. Correlation coefficients of vertical wind velocity and water vapor (R_{wq}) plotted against Bowen ratio in wind direction: (a) uphill and (b) downhill.

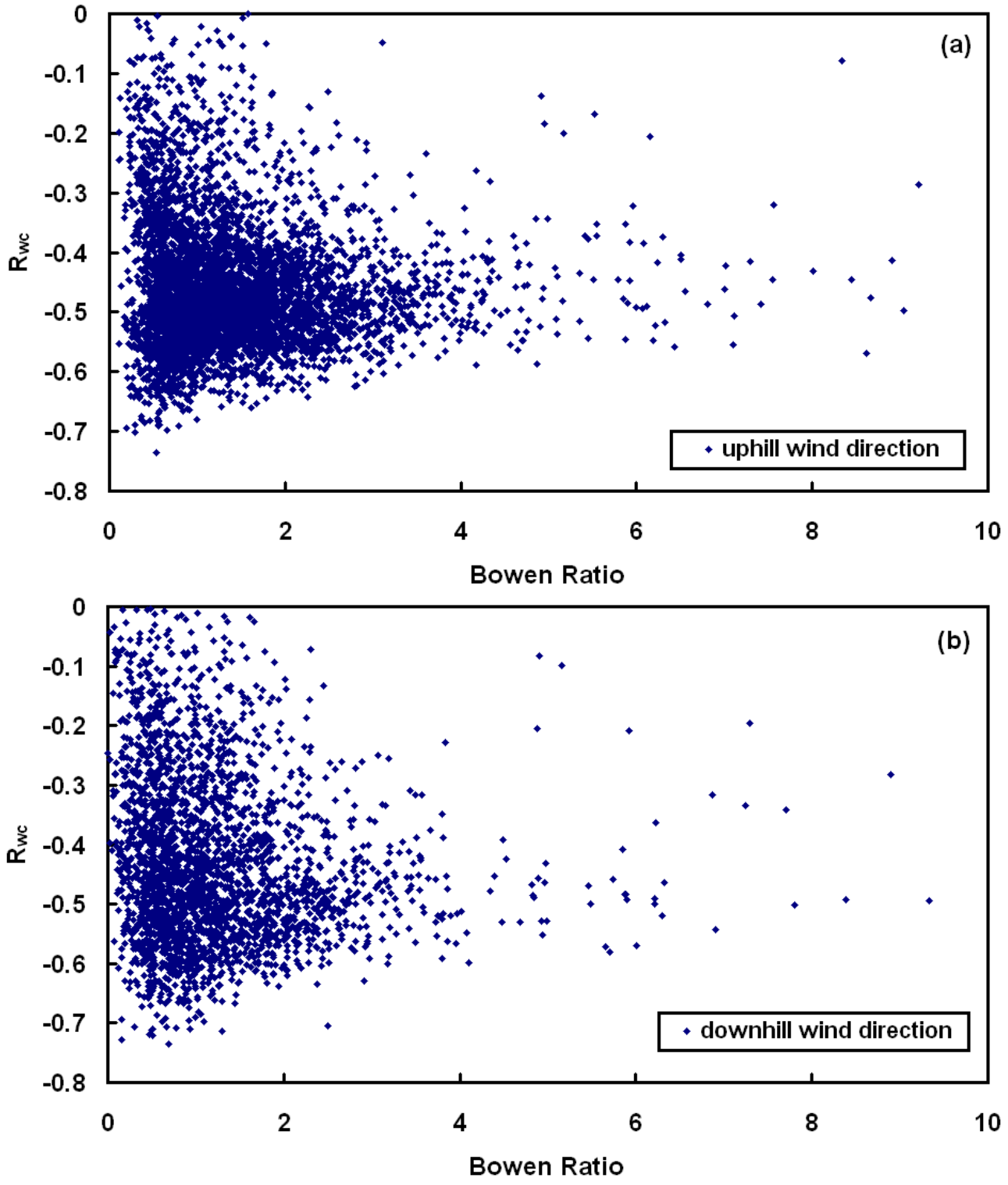

Figure 17. Correlation coefficients of vertical wind velocity and CO_2 (R_{wc}) plotted against Bowen ratio in wind direction: (a) uphill and (b) downhill.

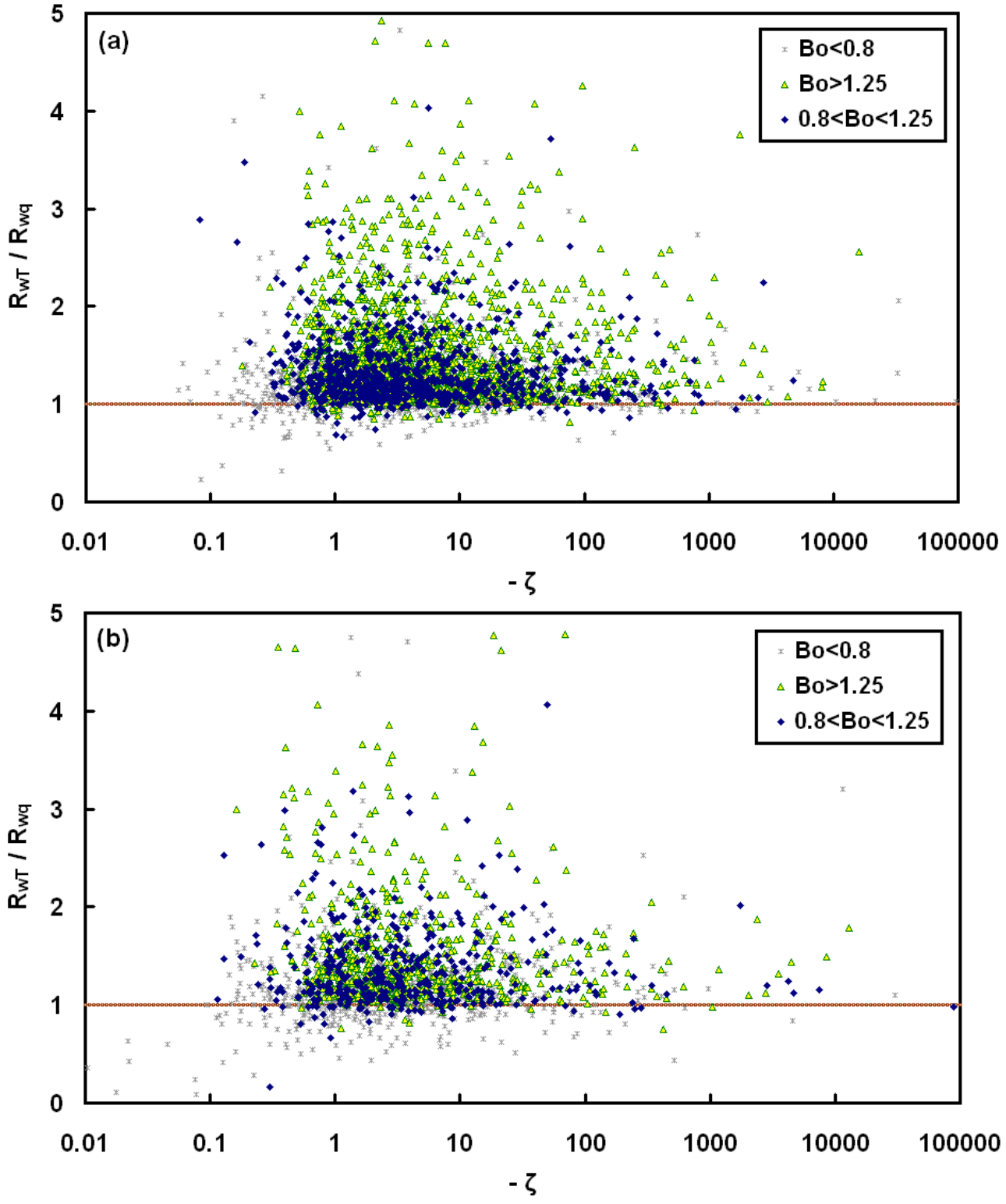

Figure 18. Relative transport efficiency between temperature and water vapor (λ_{Tq}) plotted against thermal stability in wind direction: (a) uphill and (b) downhill. With brown line $\lambda_{Tq} = 1$.

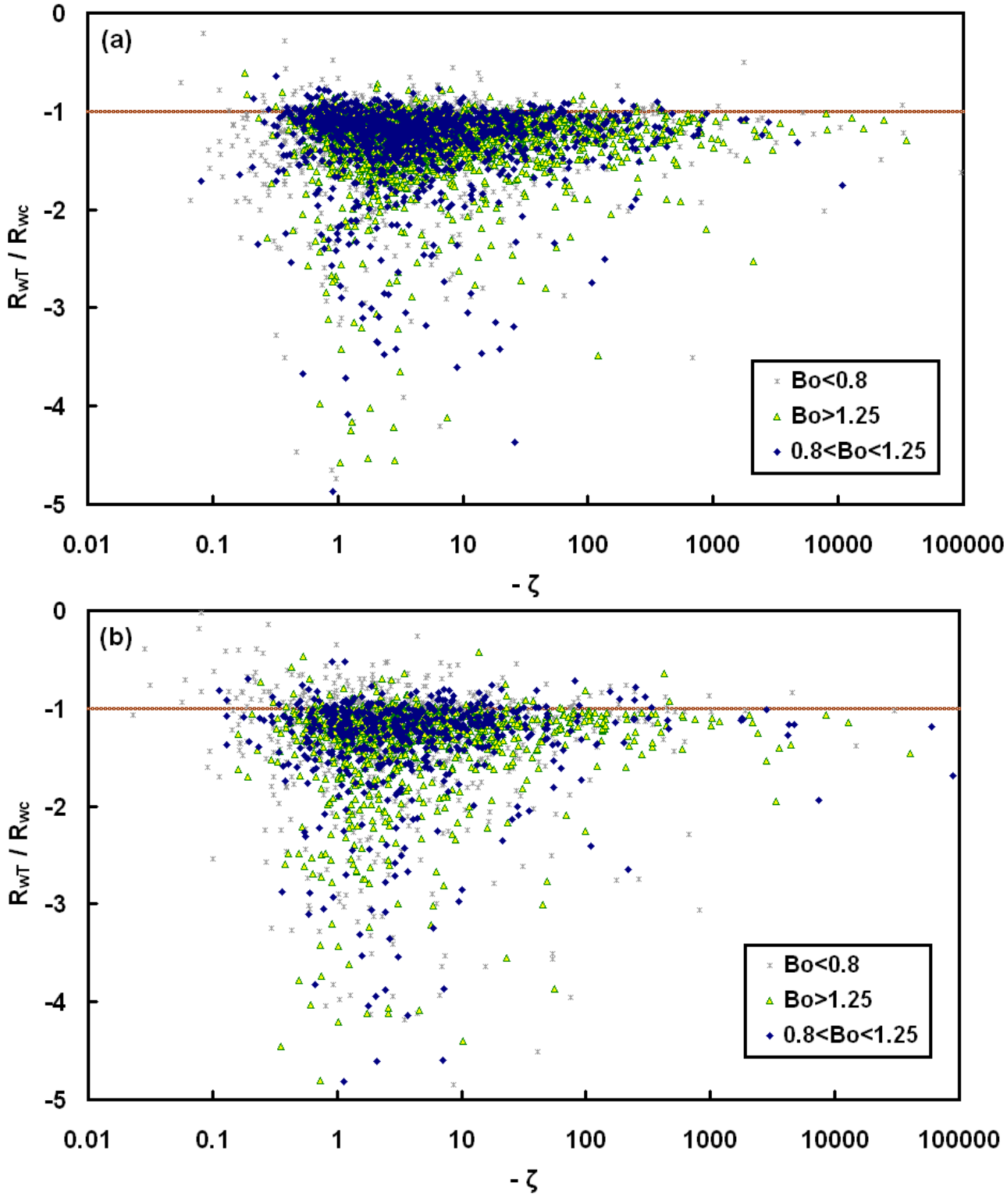

Figure 19. Relative transport efficiency between temperature and CO_2 (λ_{Tc}) plotted against thermal stability in wind direction: (a) uphill and (b) downhill. With brown line $\lambda_{Tc} = 1$.

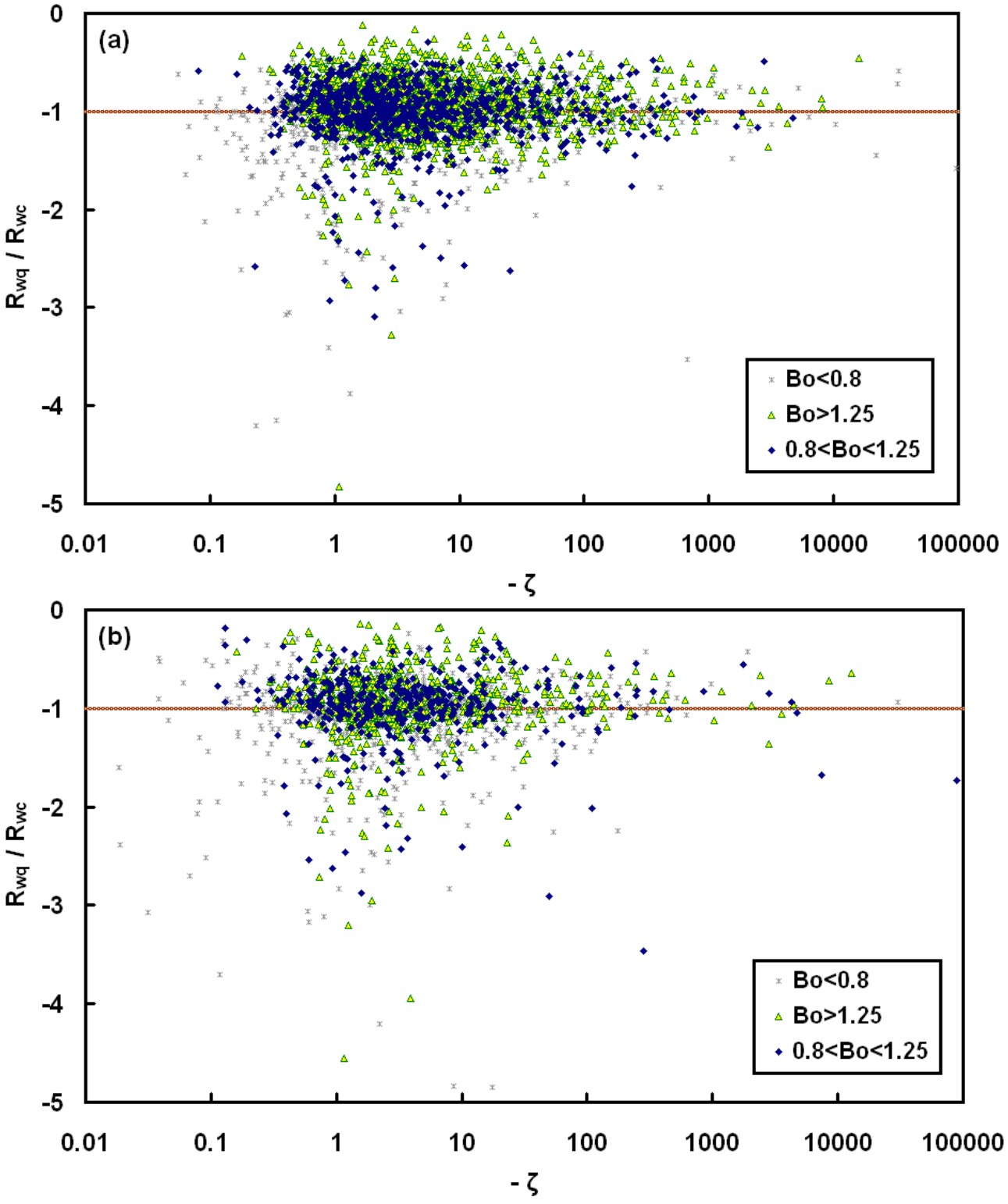

Figure 20. Relative transport efficiency between water vapor and CO_2 (λ_{qc}) plotted against thermal stability in wind direction: (a) uphill and (b) downhill. With brown line $\lambda_{qc} = 1$.

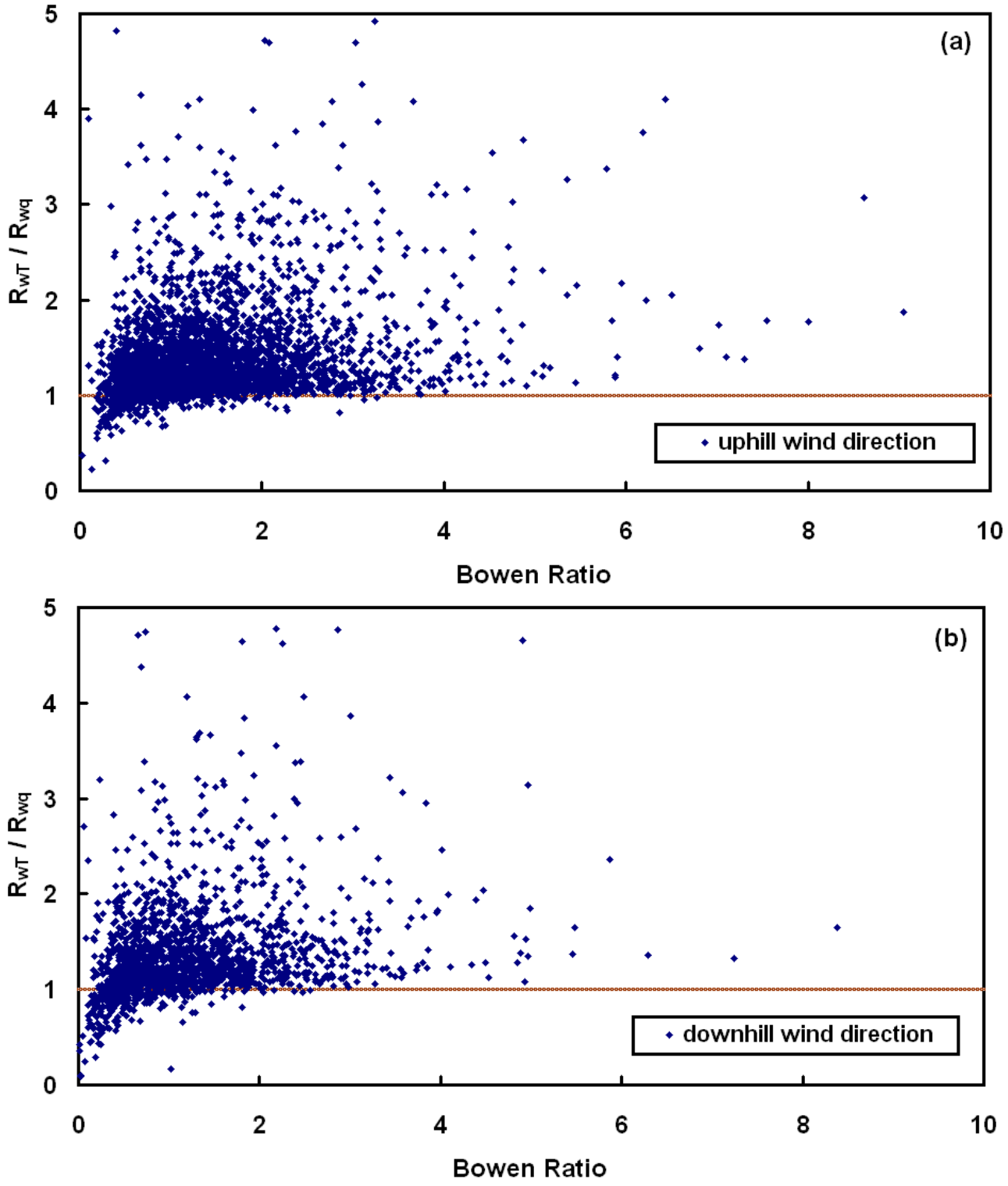

Figure 21. Relative transport efficiency between temperature and water vapor (λ_{Tq}) plotted against Bowen ratio in wind direction: (a) uphill and (b) downhill. With brown line $\lambda_{Tq} = 1$.

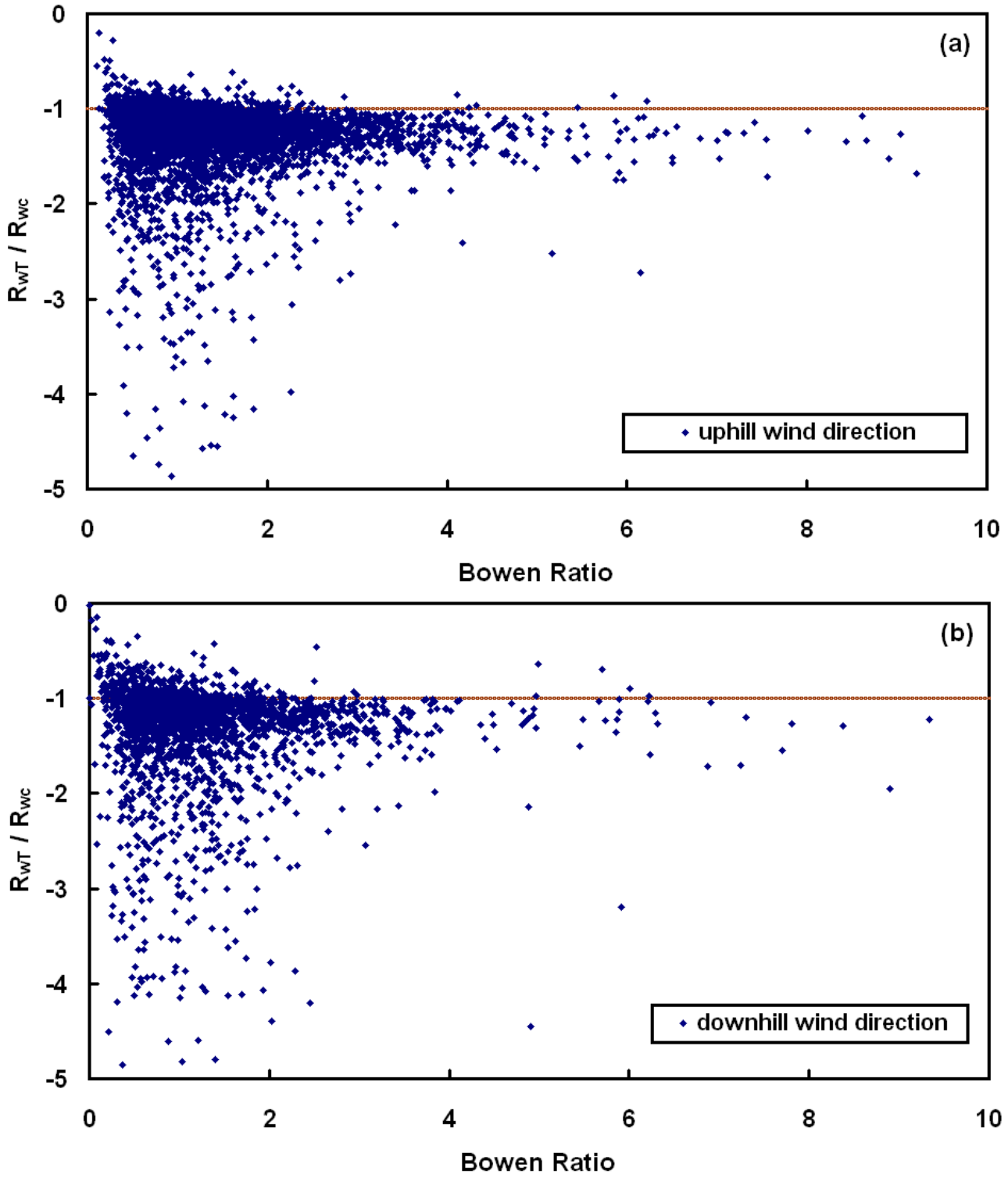

Figure 22. Relative transport efficiency between temperature and CO_2 (λ_{Tc}) plotted against Bowen ratio in wind direction: (a) uphill and (b) downhill. With brown line $\lambda_{Tc} = 1$.

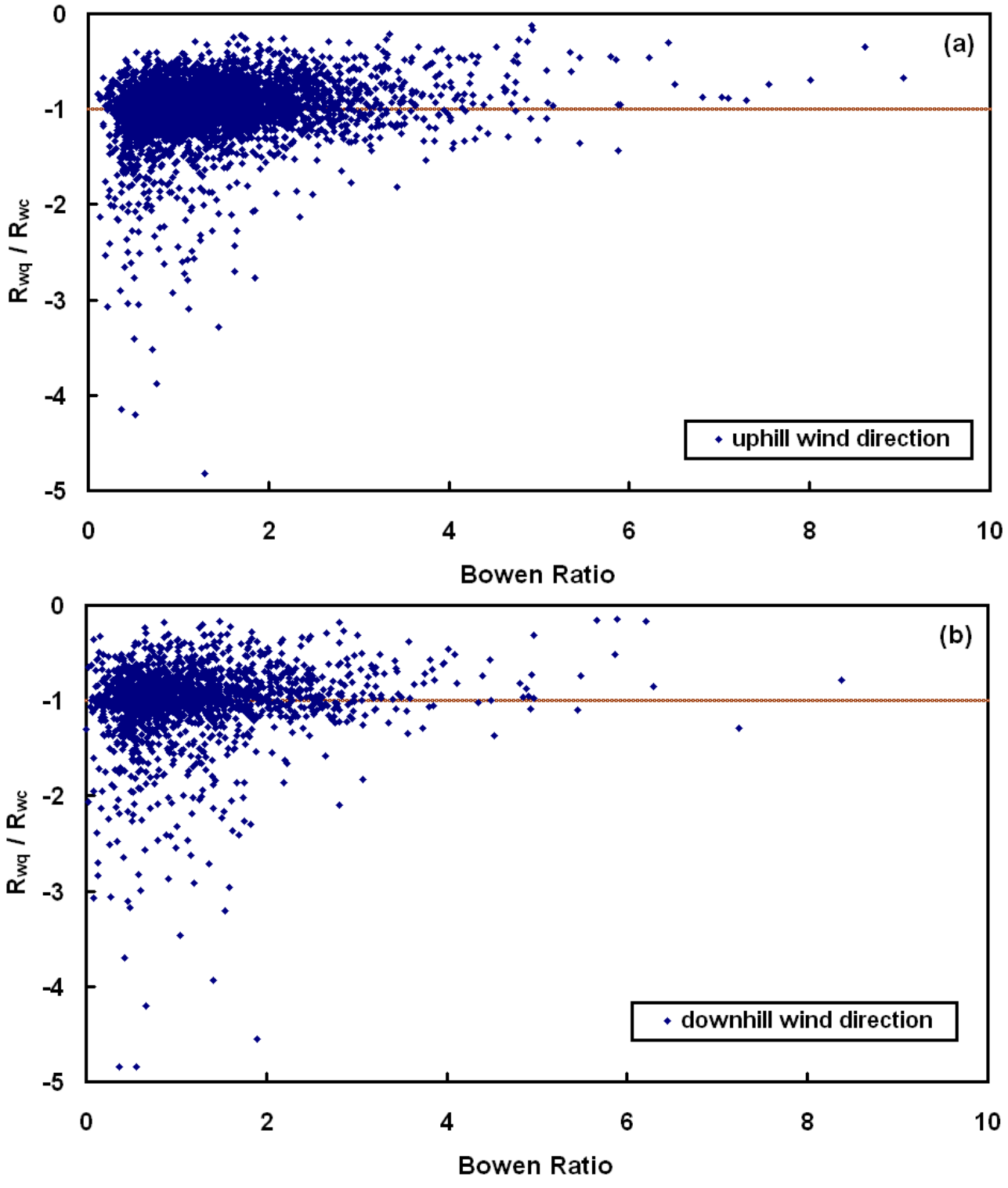

Figure 23. Relative transport efficiency between water vapor and CO_2 (λ_{qc}) plotted against Bowen ratio in wind direction: (a) uphill and (b) downhill. With brown line $\lambda_{qc} = 1$.

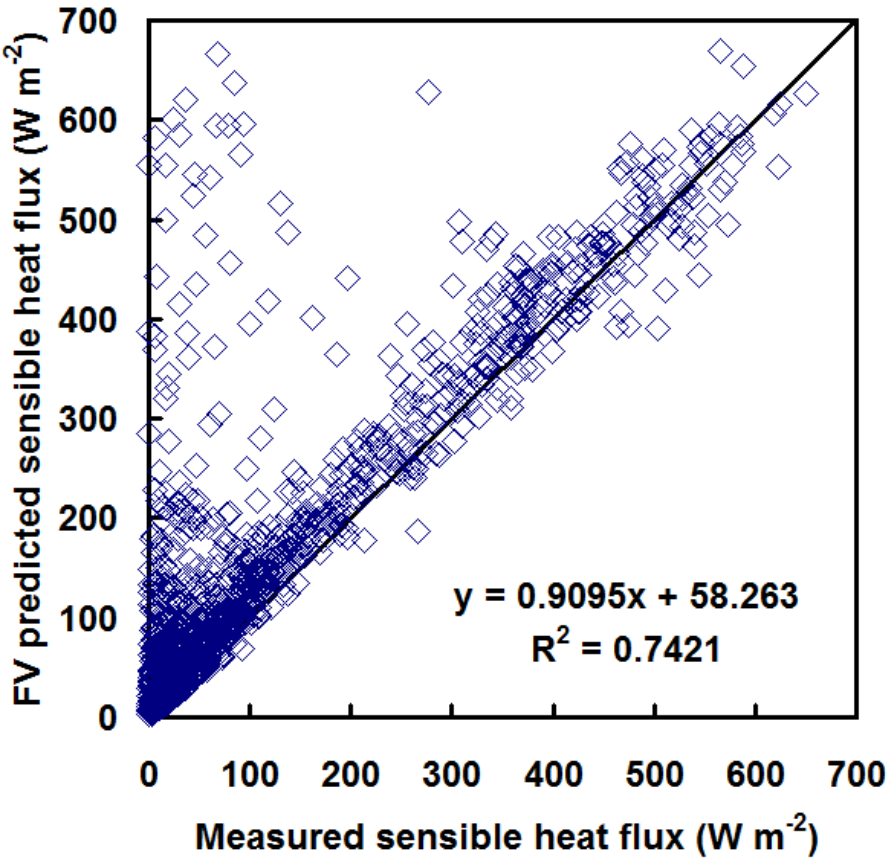

Figure 24. Comparison between measured and FV predicted sensible heat flux. The black line is the 1:1 line.

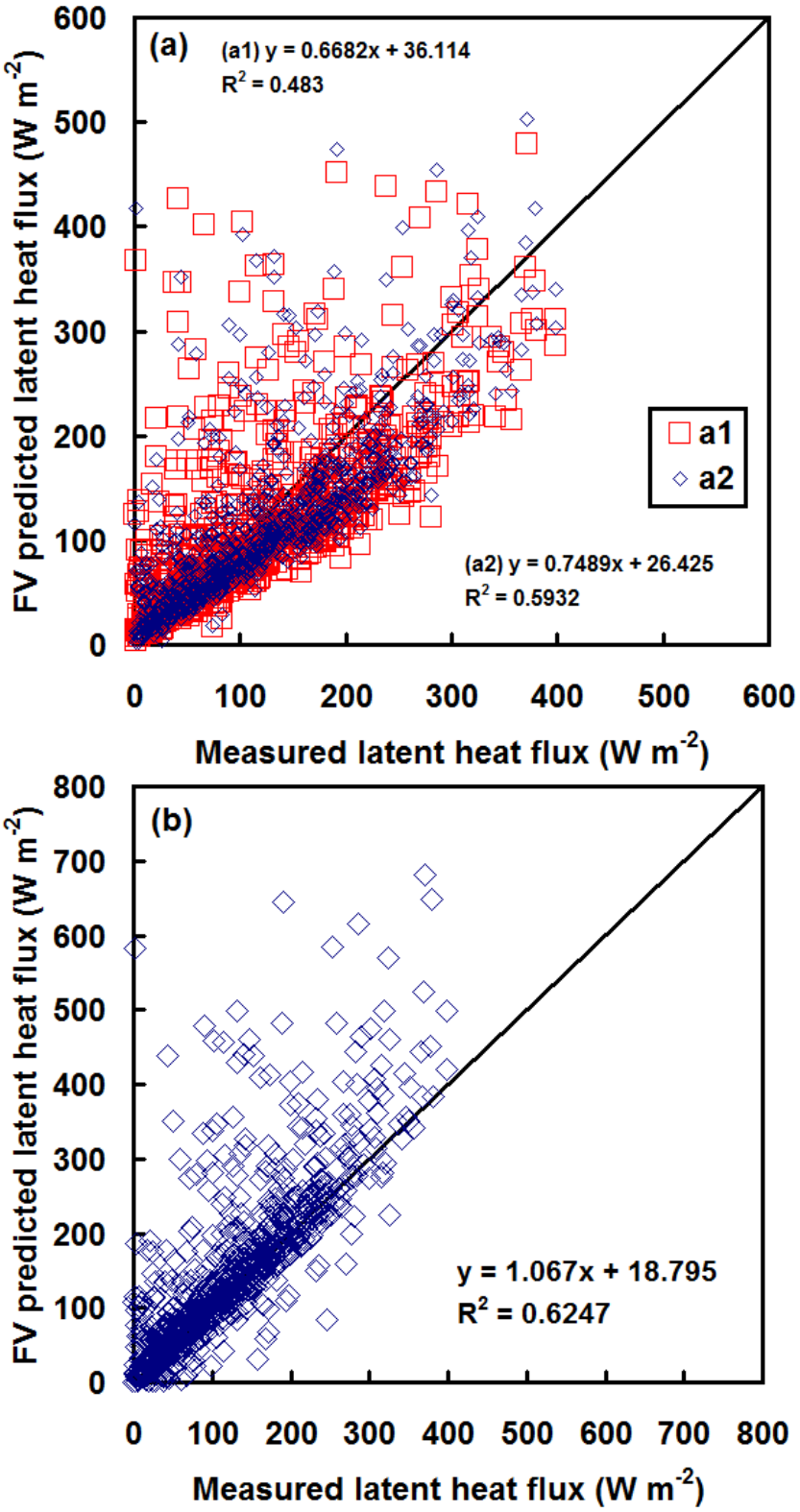

Figure 25. Comparison between measured and FV predicted latent heat flux: (a) functions in Hsieh et al. (2008) and (b) functions in Choi et al. (2004). The black line is the 1:1 line.

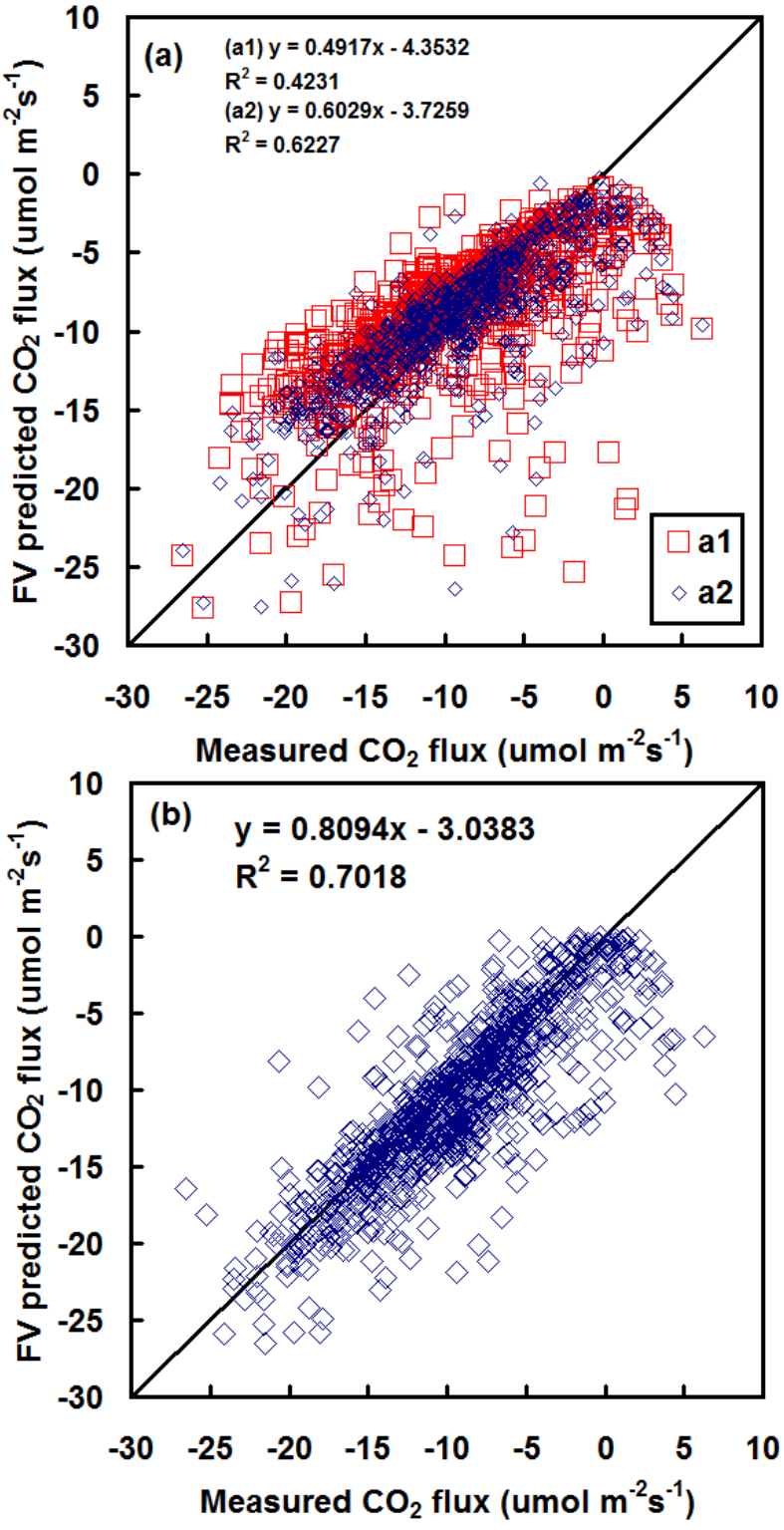

Figure 26. Comparison between measured and FV predicted CO_2 flux: (a) functions in Hsieh et al. (2008) and (b) functions in Choi et al. (2004). The black line is the 1:1 line.

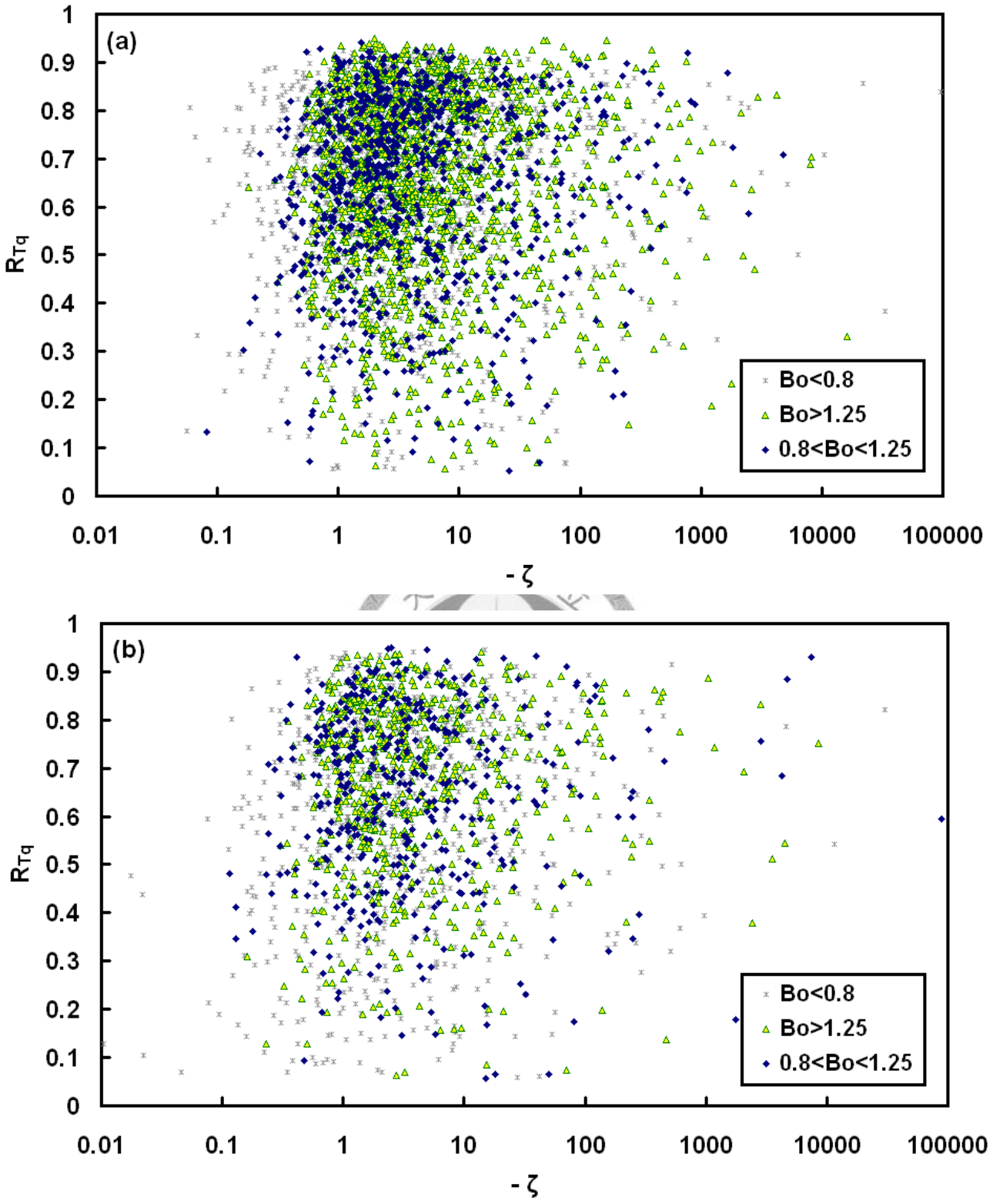

Figure 27. Correlation coefficients of temperature and water vapor (R_{Tq}) plotted against thermal stability in wind direction: (a) uphill and (b) downhill.

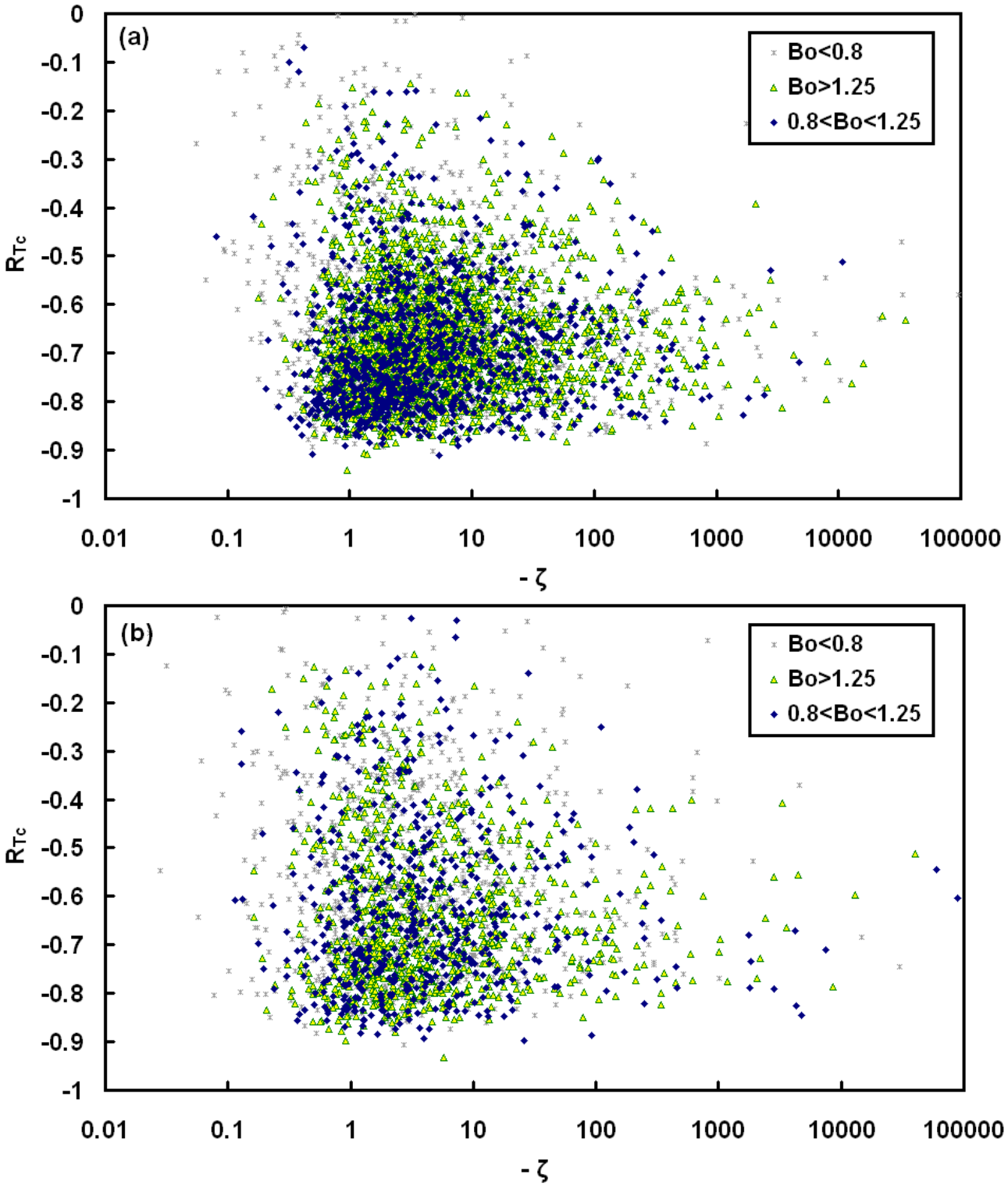

Figure 28. Correlation coefficients of temperature and CO_2 (R_{Tc}) plotted against thermal stability in wind direction: (a) uphill and (b) downhill.

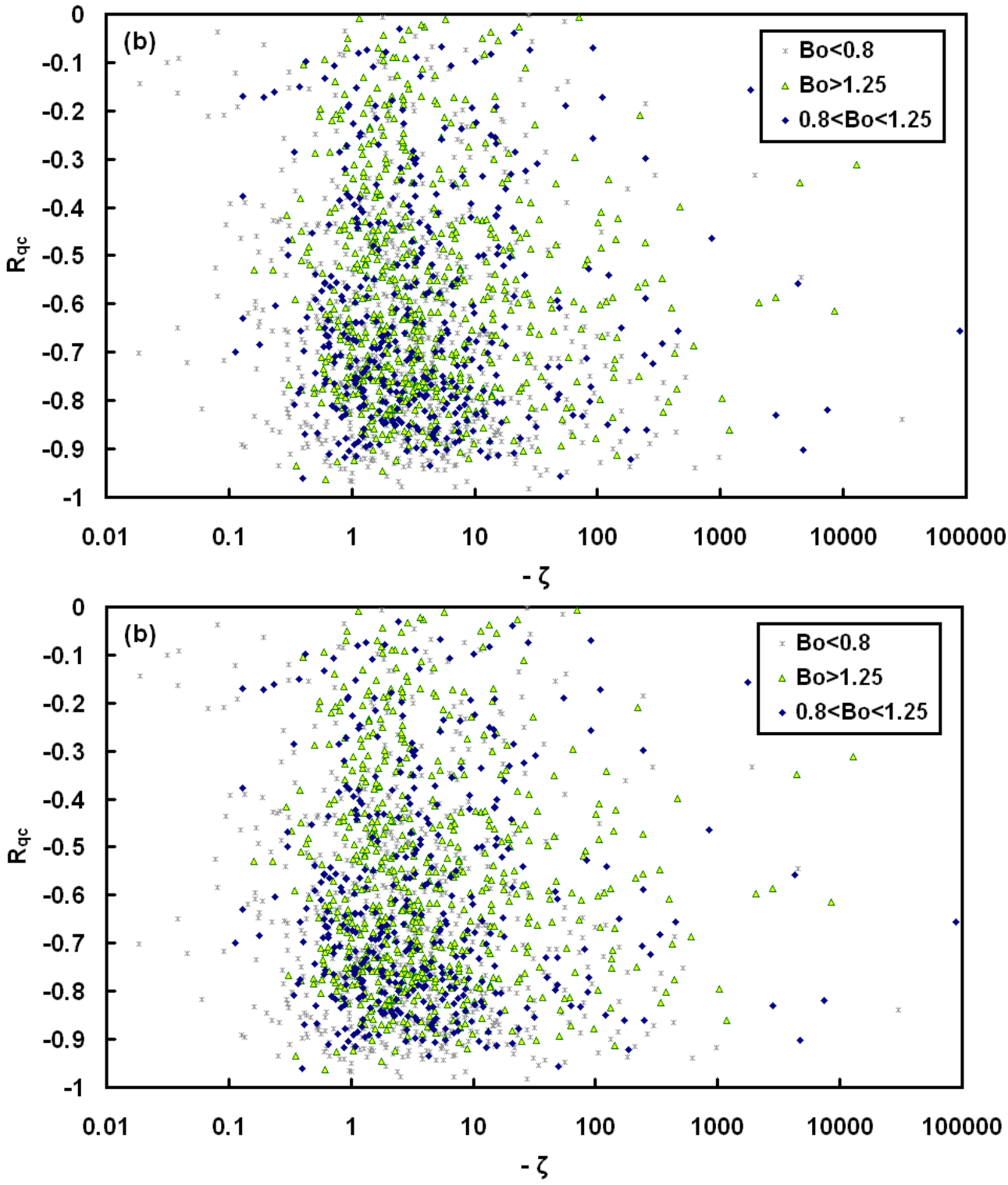

Figure 29. Correlation coefficients of water vapor and CO_2 (R_{qc}) plotted against thermal stability in wind direction: (a) uphill and (b) downhill.

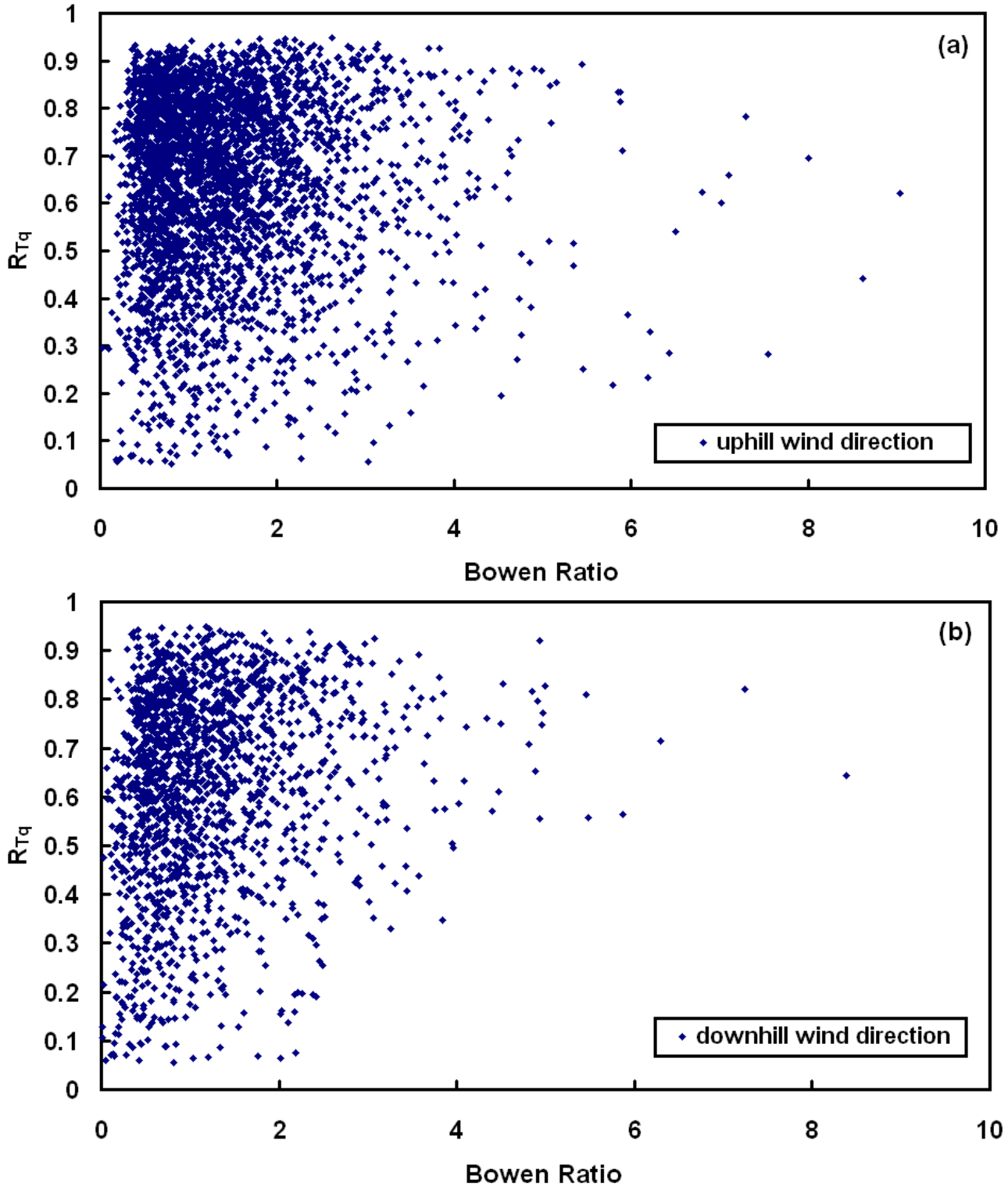

Figure 30. Correlation coefficients of temperature and water vapor (R_{Tq}) plotted against Bowen ratio in wind direction: (a) uphill and (b) downhill.

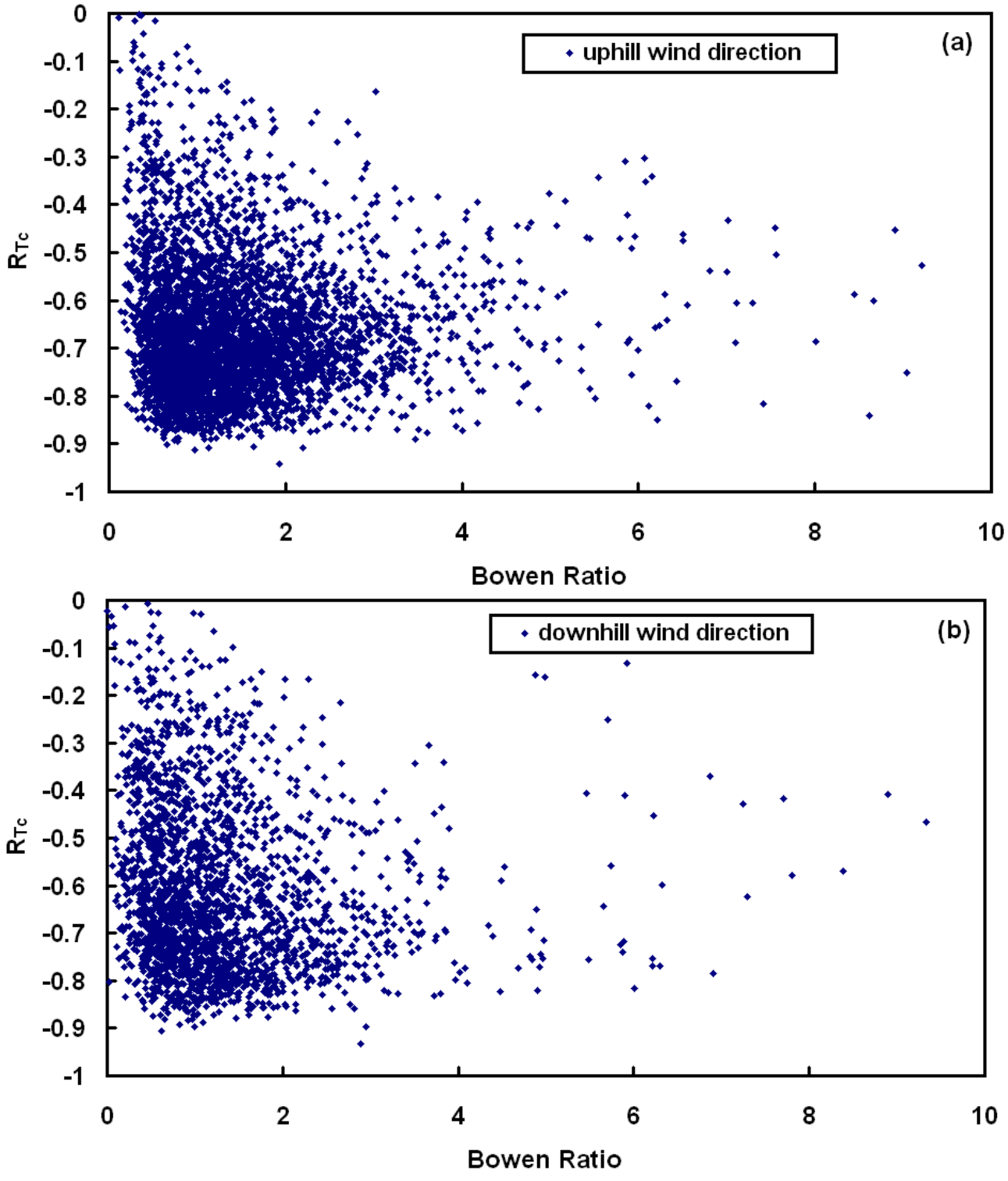

Figure 31. Correlation coefficients of temperature and CO_2 (R_{Tc}) plotted against Bowen ratio in wind direction: (a) uphill and (b) downhill.

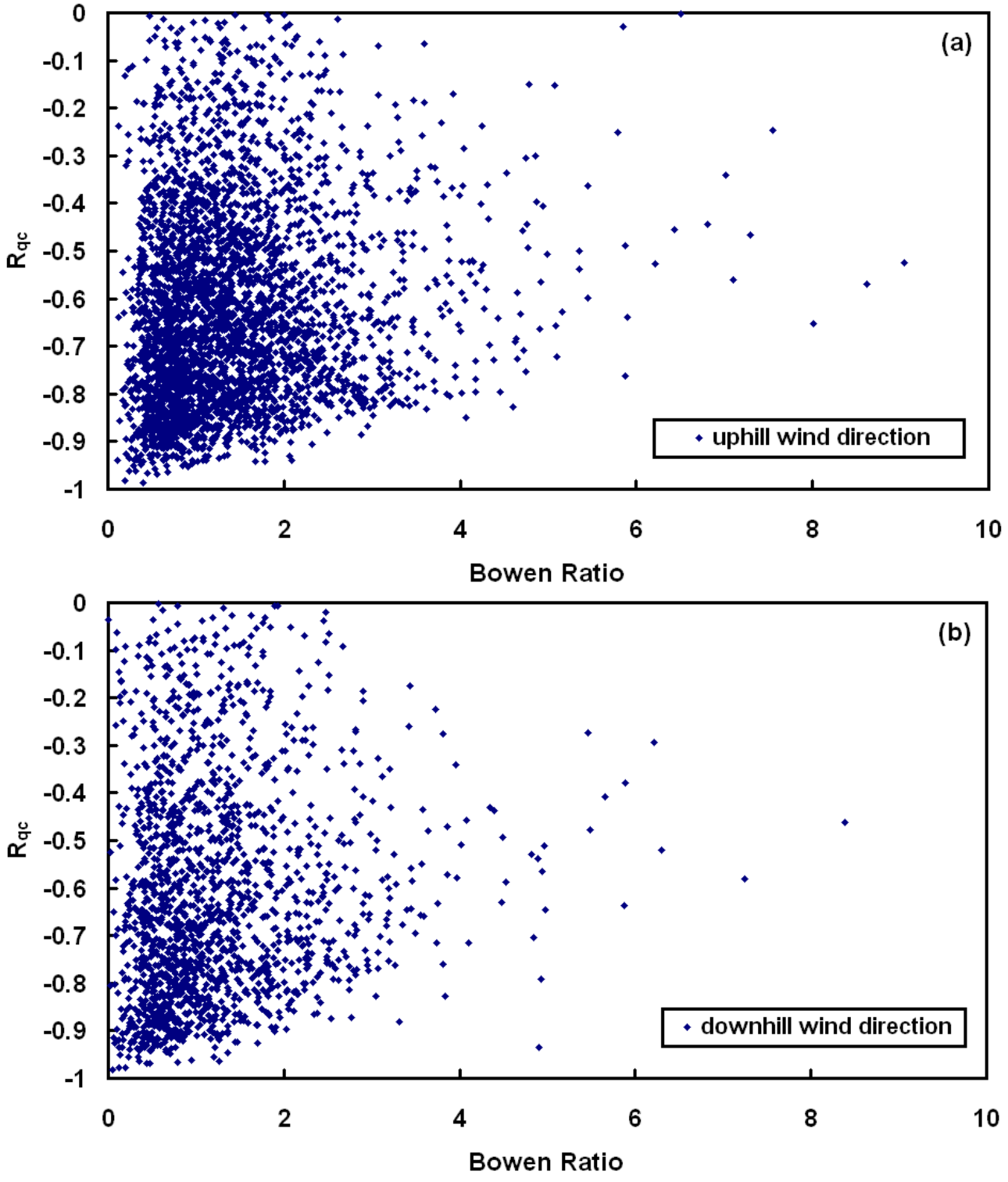

Figure 32. Correlation coefficients of water vapor and CO_2 (R_{qc}) plotted against Bowen ratio in wind direction: (a) uphill and (b) downhill.

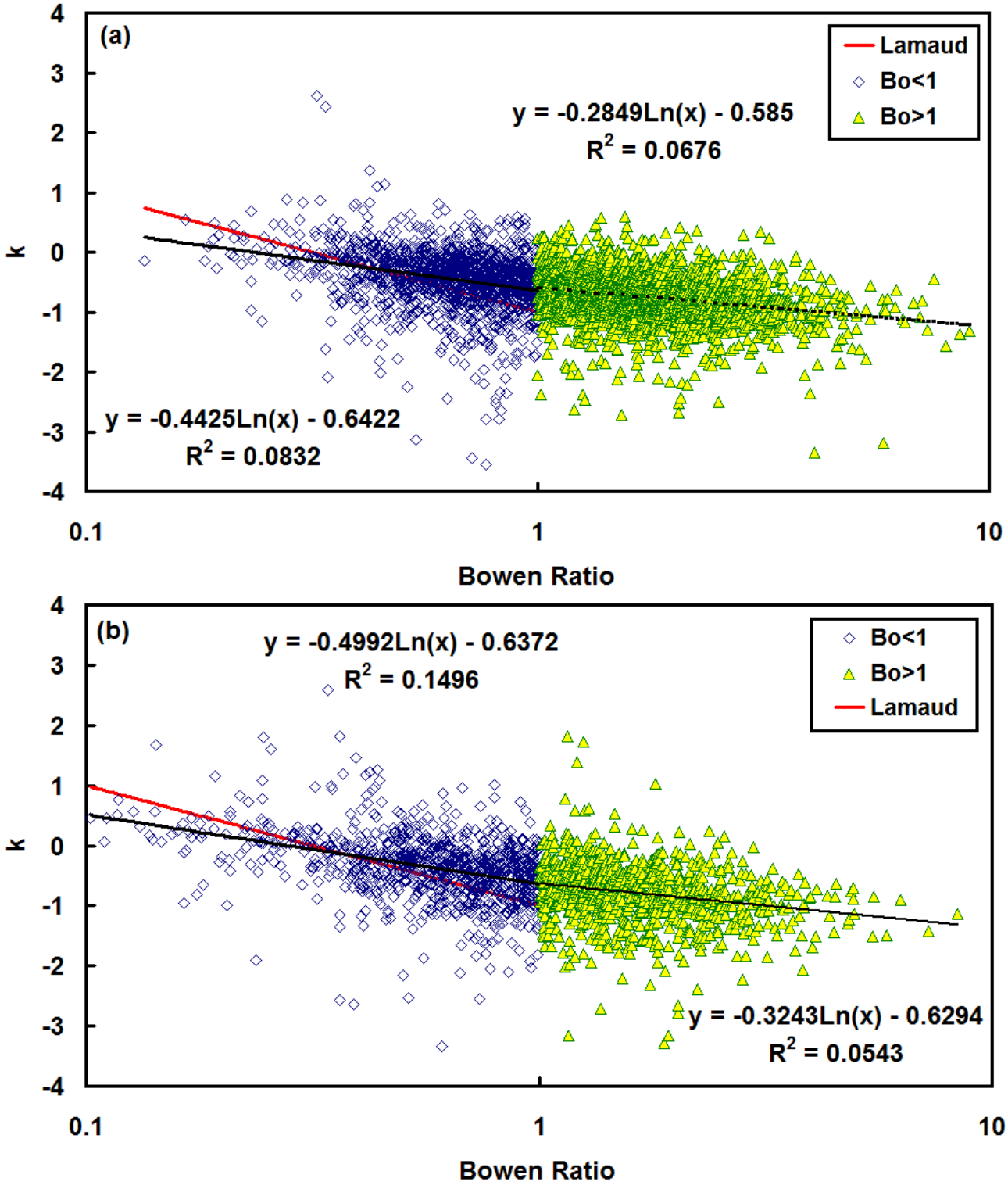

Figure 33. The determination of k in $\lambda_{Tq} = R_{Tq}^{\ k}$ as a function of Bowen ratio in wind direction: (a) uphill and (b) downhill. The red line is the suggested relation by Lamaud and Irvine (2006).

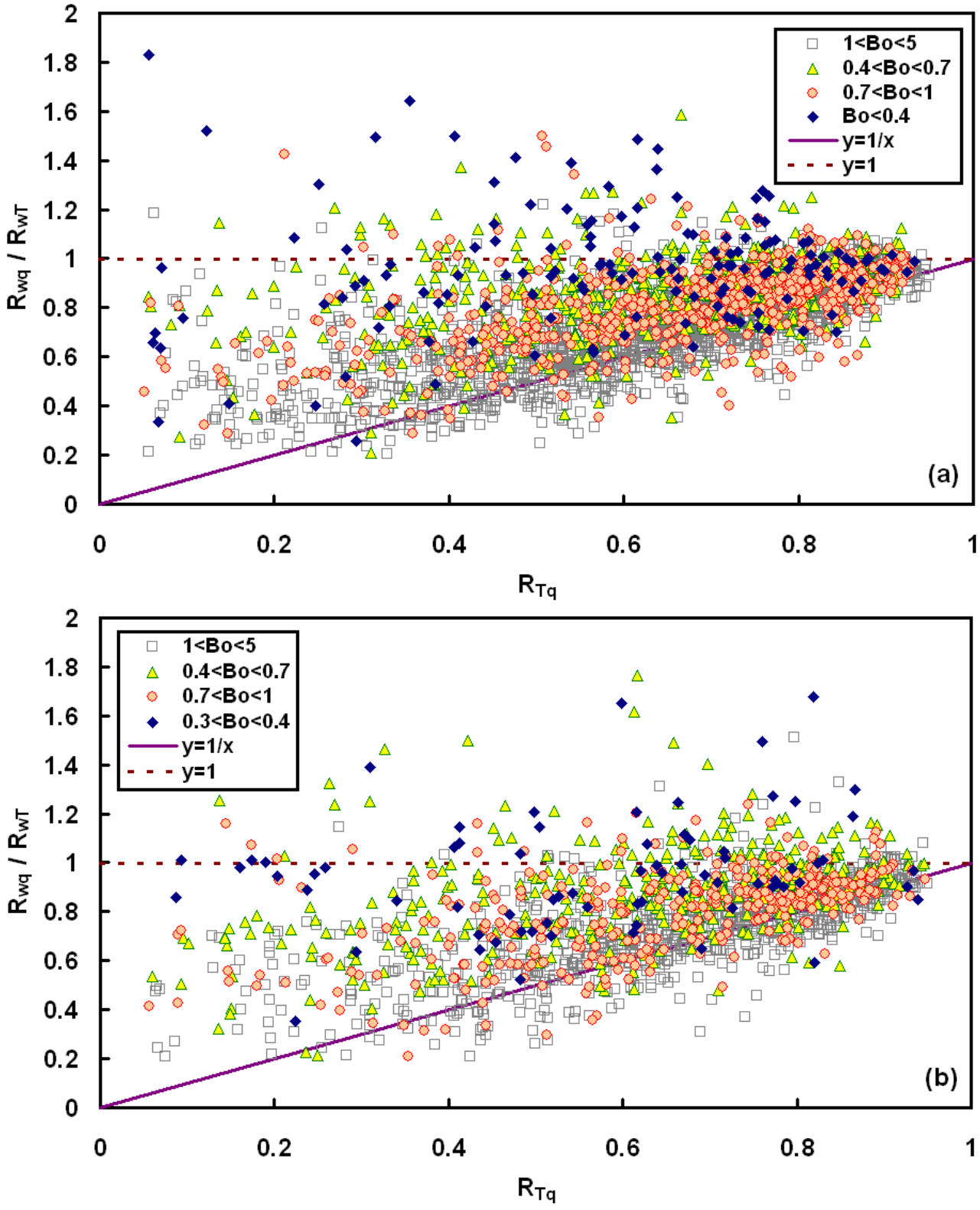

Figure 34. Relation between λ_{Tq}^{-1} and R_{Tq} in wind direction: (a) uphill and (b) downhill.

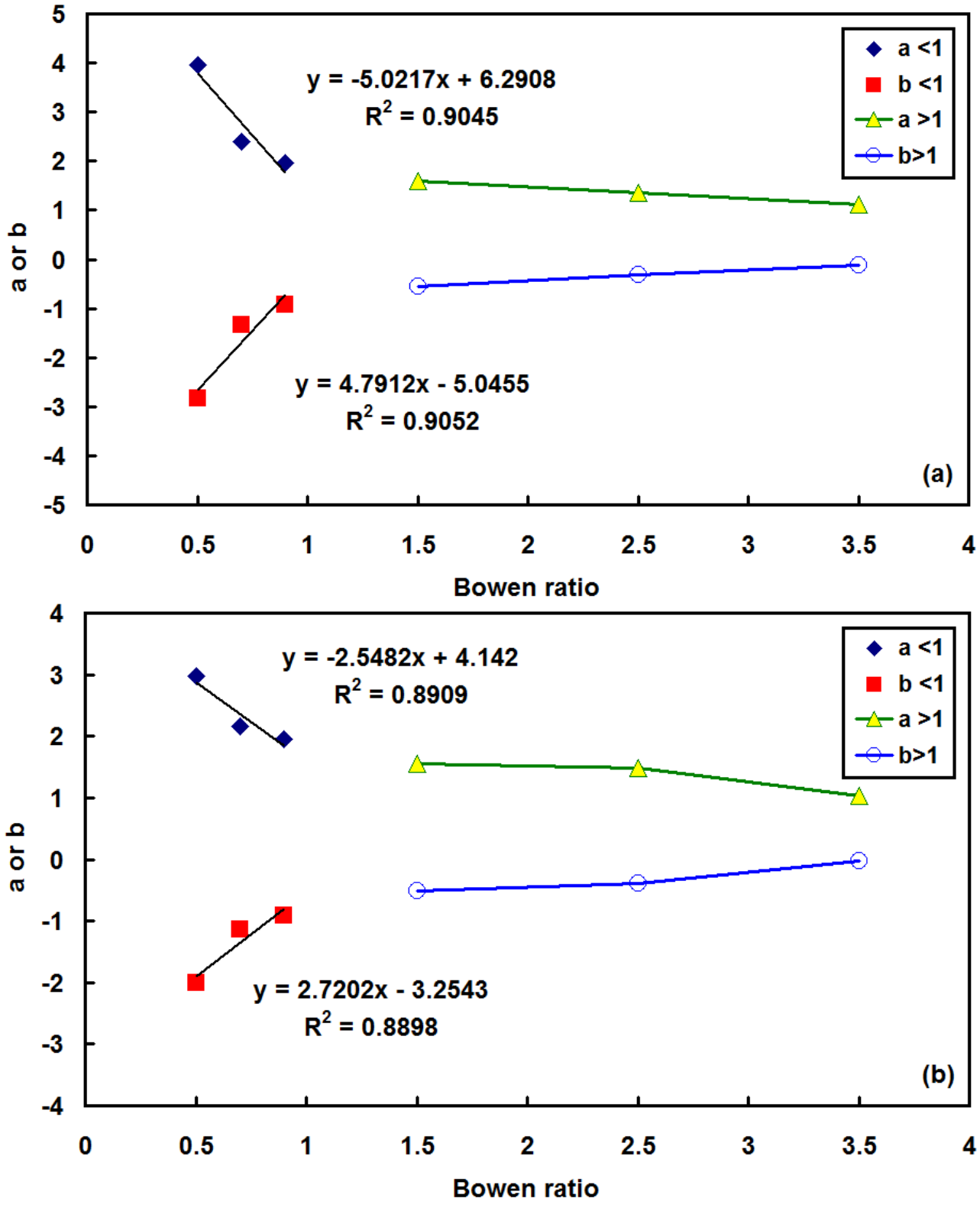

Figure 35. Regression results of a and b as a function of Bowen ratio for water vapor in wind direction: (a) uphill and (b) downhill.

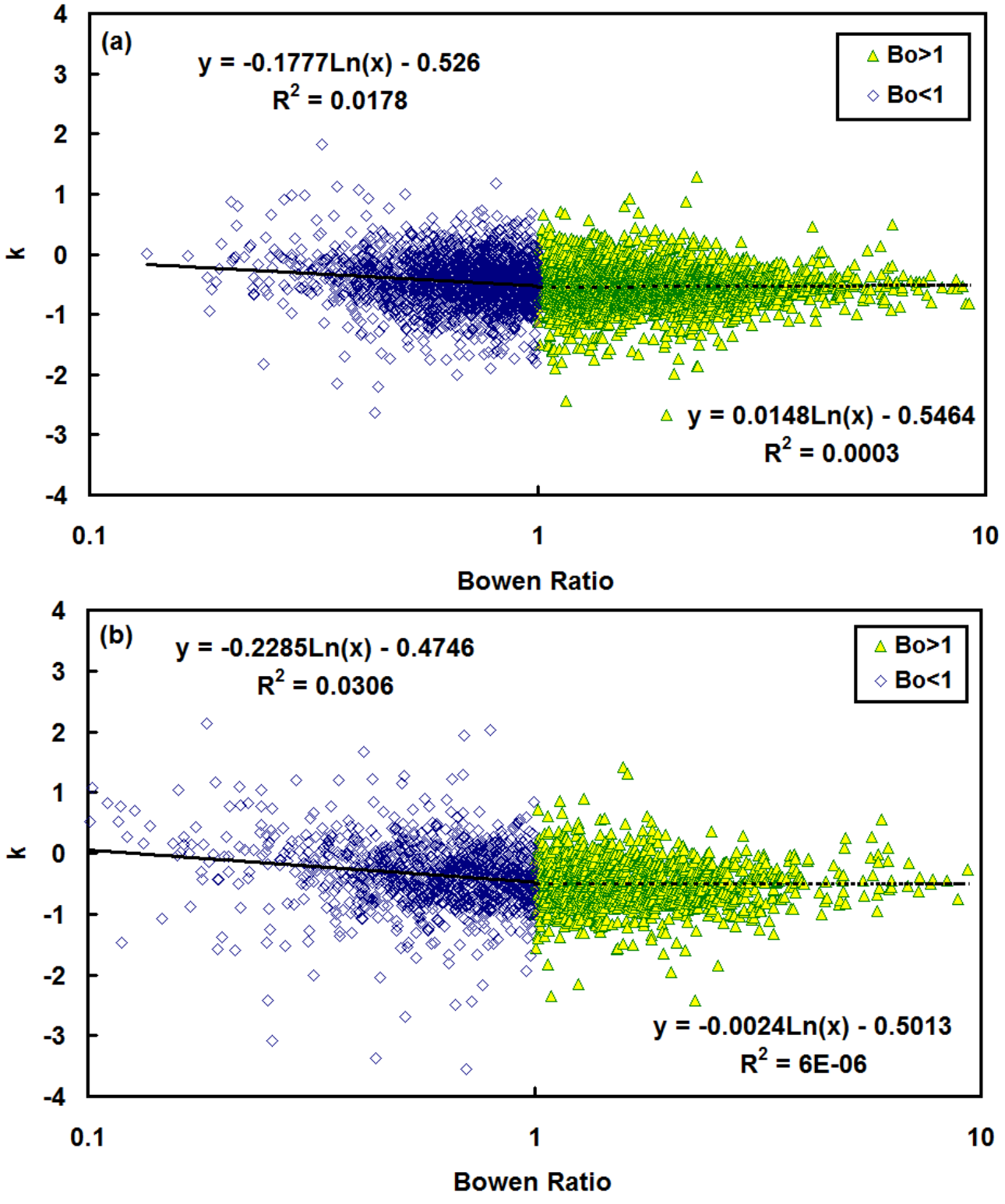

Figure 36. The determination of k in $\lambda_{Tc} = R_{Tc}{}^{k}$ as a function of Bowen ratio in wind direction: (a) uphill and (b) downhill.

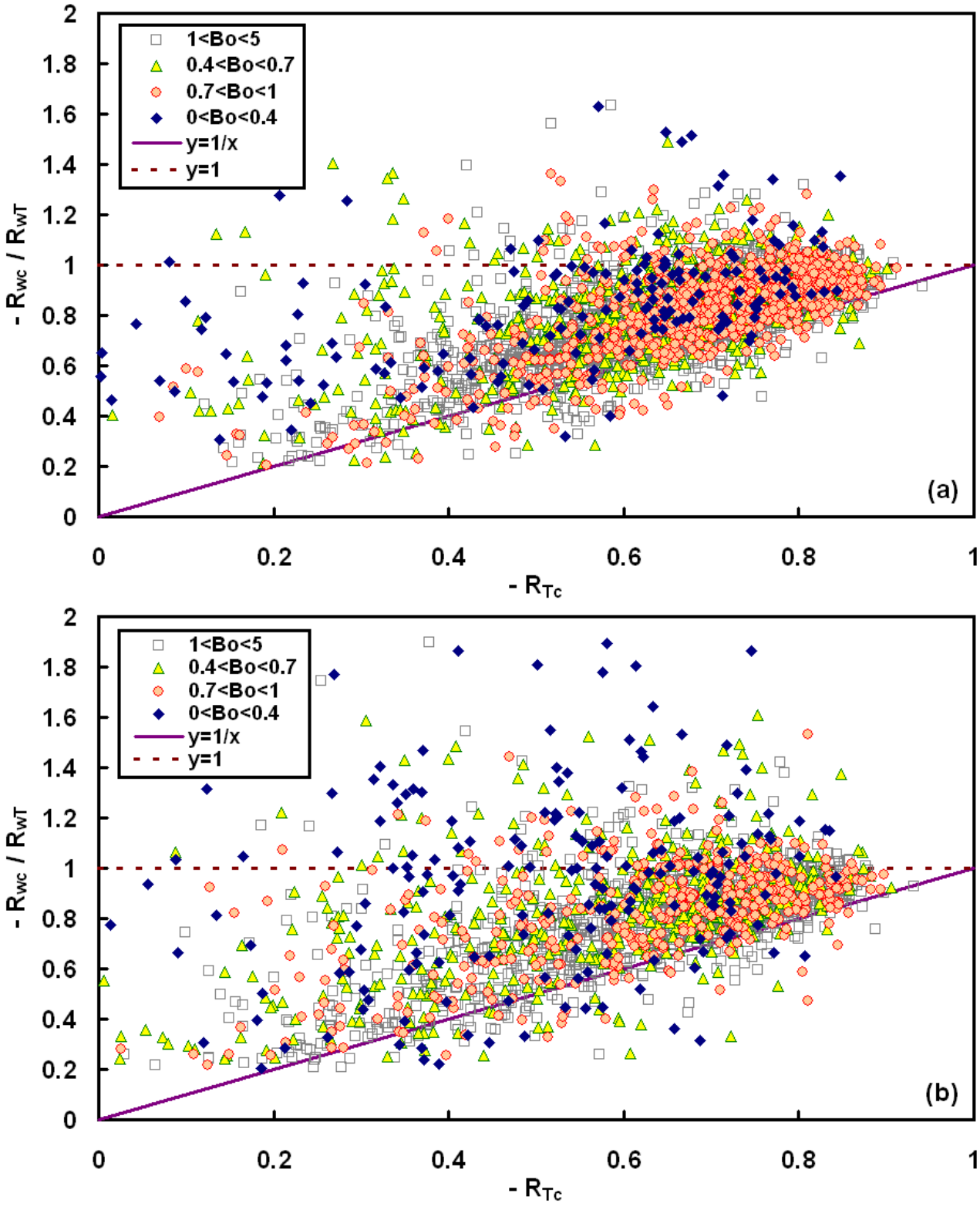

Figure 37. Relation between λ_{Tc}^{-1} and R_{Tc} in wind direction: (a) uphill and (b) downhill.

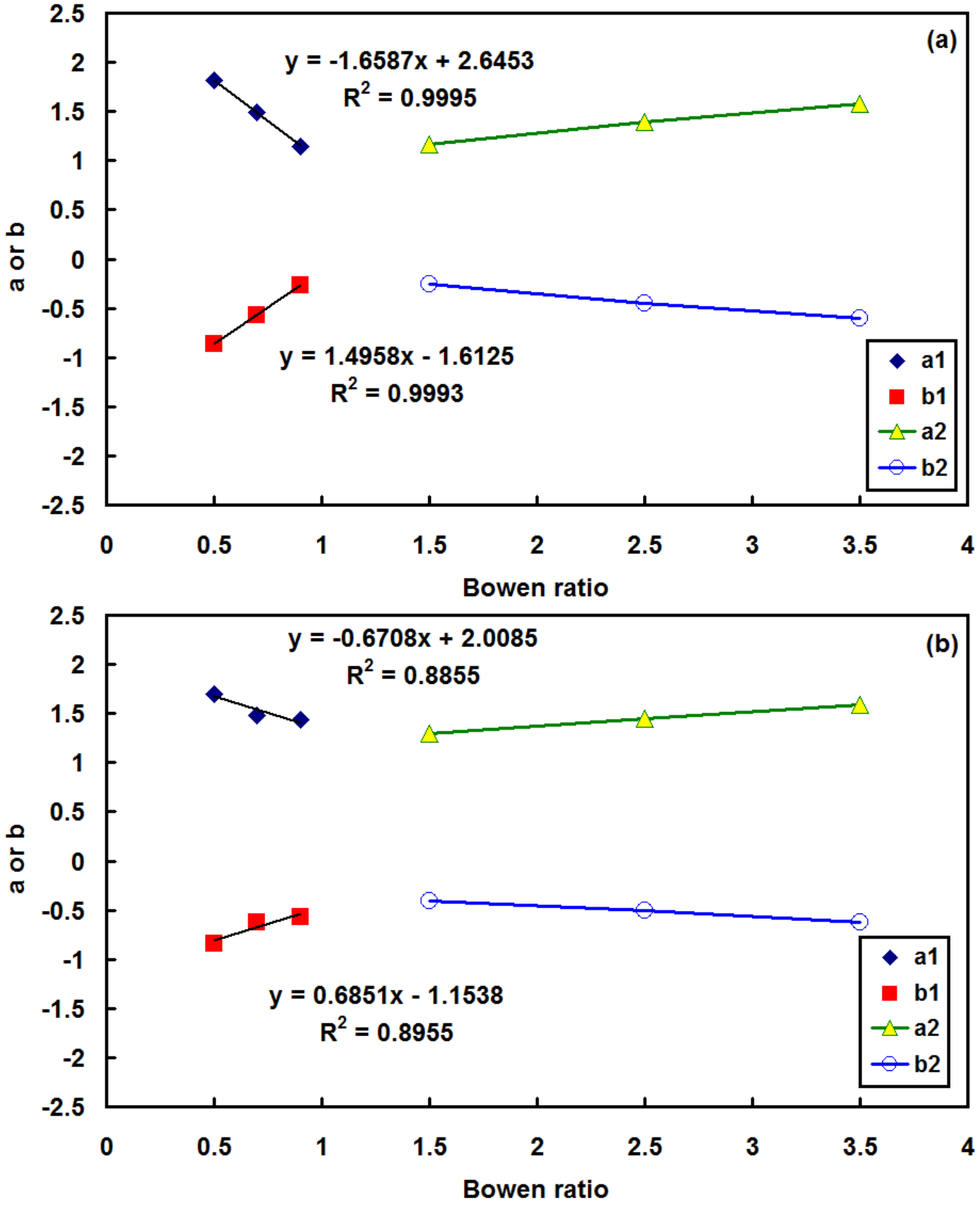

Figure 38. Regression results of a and b as a function of Bowen ratio for CO_2 in wind direction: (a) uphill and (b) downhill.

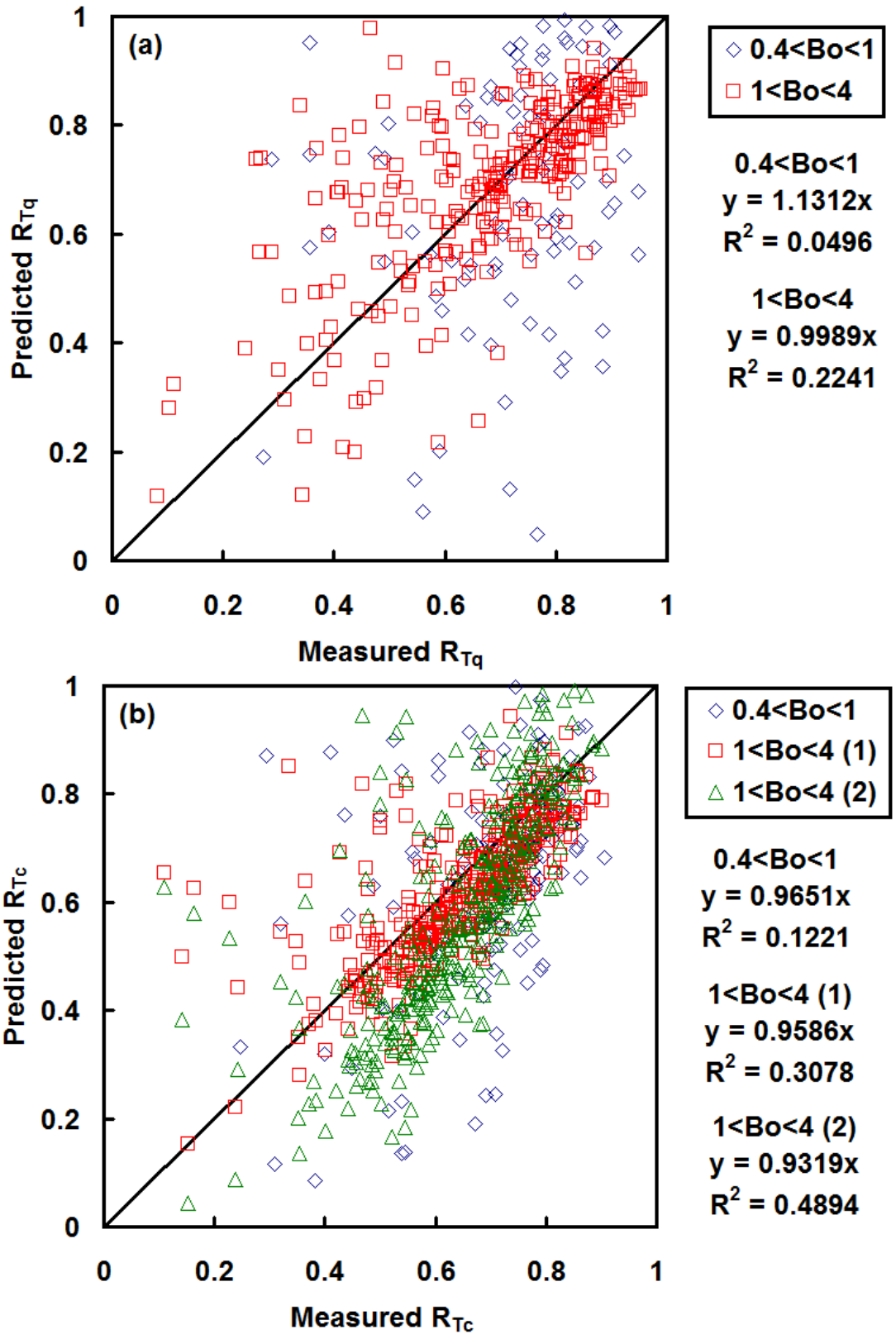

Figure 39. Checking on the regression value of k with records from April and May, 2009. The black line is the 1:1 line.

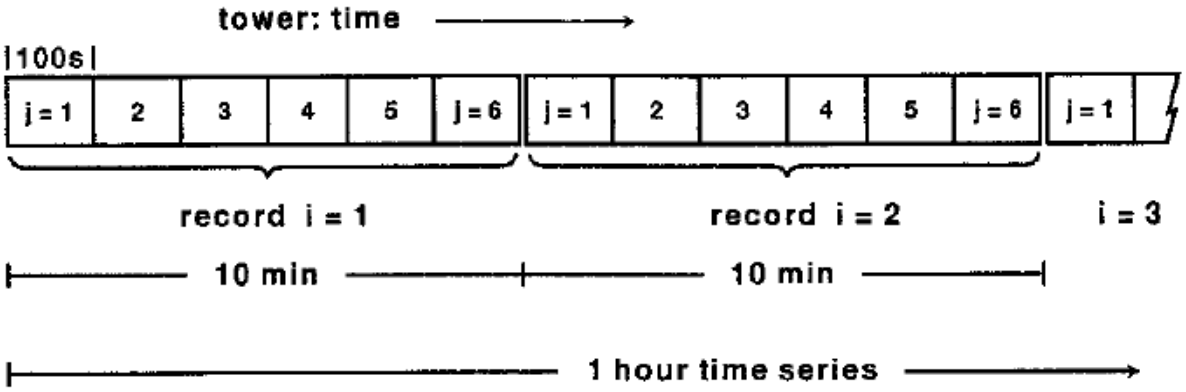

(a)

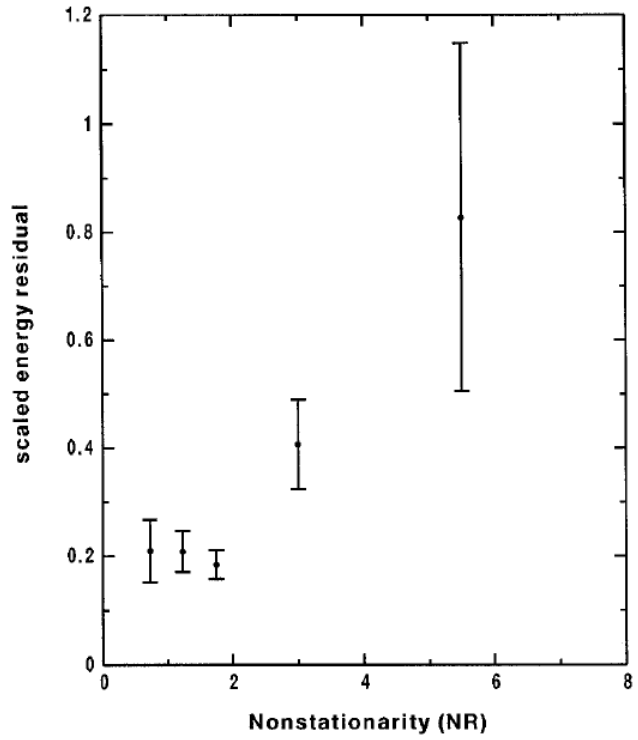

(b)

Figure A1. A way to examine the ratio of non-stationarity introduced by Mahrt: (a) block comparing diagram quoted from Fig. 5(a) of Mahrt, 1998, and (b) the threshold of the ratio found with the relation between its scaled energy residual (quoted from Fig. 6 of Mahrt, 1999).

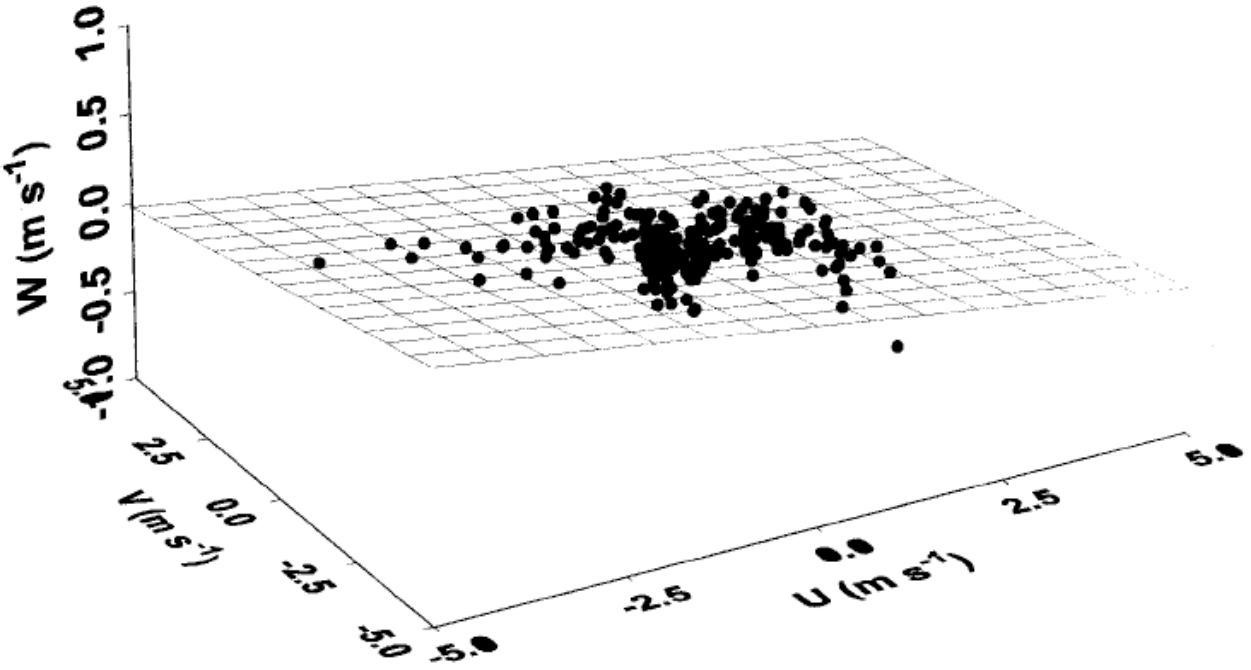

Figure A2. A diagram for the finding of a plane where events mostly fall on when doing the planar fit method (quoted from Fig. 5 of Paw U et al., 2000).